BRNO UNIVERSITY OF TECHNOLOGY
VYSOKÉ UČENÍ TECHNICKÉ V BRNĚ

FACULTY OF CHEMISTRY
FAKULTA CHEMICKÁ

INSTITUTE OF PHYSICAL AND APPLIED CHEMISTRY
ÚSTAV FYZIKÁLNÍ A SPOTŘEBNÍ CHEMIE

CONTROLLED RELEASE OF GROWTH FACTORS FROM A BIODEGRADABLE HYDROGEL HYBRID NETWORK
KONTROLOVANÉ UVOLŇOVÁNÍ RŮSTOVÝCH FAKTORŮ Z HYBRIDNÍ SÍTĚ BIODEGRADABILNÍHO HYDROGELU

MASTER'S THESIS
DIPLOMOVÁ PRÁCE

AUTHOR
AUTOR PRÁCE

Bc. Nikola Křivánková

SUPERVISOR
VEDOUCÍ PRÁCE

doc. Ing. Lucy Vojtová, Ph.D.

BRNO 2021

Specification Master's Thesis

Project no.:	FCH-DIP1504/2020	Academic year:	2020/21
Department:	Institute of Physical and Applied Chemistry		
Student:	**Bc. Nikola Křivánková**		
Study programme:	Chemistry for Medical Applications		
Study field:	Chemistry for Medical Applications		
Head of thesis:	**doc. Ing. Lucy Vojtová, Ph.D.**		

Title of Master's Thesis:

Controlled release of growth factors from a biodegradable hydrogel hybrid network

Master's Thesis:

1) literature search on the topic of hydrogels with a hybrid network and their characterization, growth factors and their release
2) preparation of a hybrid network of biodegradable copolymer and incorporation of growth factors
3) characterization of physico–chemical properties
4) spectroscopic monitoring of growth factor release
5) evaluation of results and data interpretation
6) conclusion

Deadline for Master's Thesis delivery: 30.7.2021:

Master's Thesis should be submitted to the institute’s secretariat in a number of copies as set by the dean This specification is part of Master's Thesis

Bc. Nikola Křivánková
Student

doc. Ing. Lucy Vojtová, Ph.D.
Head of thesis

prof. Ing. Miloslav Pekař, CSc.
Head of department

In Brno dated 1.2.2021

prof. Ing. Martin Weiter, Ph.D.
Dean

ABSTRACT

Temperature sensitive copolymers forming a hydrogel at body temperature are of high interest in the field of drug delivery. The hydrogel serves as a protection against hydrolysis and enzymatic degradation moreover it influences the drug release. Controlled gradual release results in an increased therapeutic activity compared to repetitive administration.

In this proposed master's thesis, a temperature and light sensitive block copolymer *α,ω*-itaconyl-PLGA-PEG-PLGA was used to form a hybrid hydrogel network. The amphiphilic copolymer forms a micellar network at body temperature, and due to the double bonds at the ends of the copolymer chain, a chemical network may be formed by photocrosslinking. The photocrosslinking and rheological properties of the resulting core-crosslinked micellar hydrogel were studied. Due to acidic pH of the UPW hydrogel and its instability in PBS solution, the carboxyl groups in the ABA/ITA copolymer were modified by butylamine thus preventing their dissociation.

The photocrosslinking and thermogelling properties of the novel *α,ω*-*N*-butylitaconamide-PLGA-PEG-PLGA were confirmed. The hydrogel was formed both in UPW and PBS and its hydrolytic stability was observed in PBS at physiological temperature. The UPW hydrogels exhibited higher hydrolytic stability, therefore, were chosen for the release study of a pro-healing protein.

The stabilized fibroblast growth factor 2 (FGF2-STAB®) enhances wound healing. The growth factor was incorporated to the hydrogel structure and its release was observed by the Bradford assay on UV-Vis spectrophotometer and by SDS-PAGE. Three types of hydrogel networks were formed: physical, hybrid, and chemical. Most of the released growth factor (25 %) was observed after 2 hours from the physical network. However, only 39 % of the incorporated FGF2-STAB® was detected after 22 days in total. The release from the hybrid network exhibited a two-phase, diffusion and degradation-controlled curve. The first detected growth factor released from the chemical network was after 6 days for samples irradiated for 5 min and after 14 days for hydrogels photocrosslinked for 30 min. The release curves from the chemical hydrogel network signify a delayed burst release. Unfortunately, the released proteins were unable to detect by SDS-PAGE.

The type and density of the hydrogel network influence the kinetics of the protein release. The formed hydrogel with incorporated FGF2-STAB® could be potentially applied as a wound dressing.

KEY WORDS

Hybrid network, wound healing, controlled release, fibroblast growth factor 2, PLGA-PEG-PLGA copolymer

ABSTRAKT

Termocitlivé kopolymery, které vykazují schopnost gelace při tělesné teplotě, představují velký potenciál v oblasti nosičů léčiv. Vzniklé hydrogely slouží jako ochrana proti hydrolýze a enzymatické degradaci, navíc mají vliv na uvolňování léčiv. Kontrolované postupné uvolňování vede ke zvýšení terapeutické aktivity v porovnání s opakovaným podáváním.

V této diplomové práci byl pro přípravu hybridní hydrogelové sítě použit blokový kopolymer *α,ω*-itakonyl-PLGA-PEG-PLGA, citlivý na světlo a změnu teploty. Amfifilní kopolymer tvoří při tělesné teplotě micelární síť, a díky dvojným vazbám na koncích kopolymerního řetězce může být vytvořena chemická síť pomocí fotochemického zesítění. Byly zkoumány reologické vlastnosti a chemické zesítění výsledného micelárního hydrogelu s kovalentně zesíťovanými jádry. Z důvodu kyselého pH vodného hydrogelu a jeho nestabilitě v PBS, byly karboxylové skupiny v ABA/ITA kopolymeru modifikovány butylaminem, čímž se zabránilo jejich disociaci.

Byly potvrzeny fotochemické zesítění a gelační vlastnosti nově připraveného *α,ω-N*-butylitaconamide-PLGA-PEG-PLGA kopolymer. Hydrogel byl vytvořen jak v ultra-čisté vodě, tak v PBS, a jejich hydrolytická stabilita byla sledována v PBS při fyziologické teplotě. UPW hydrogely vykazovaly vyšší hydrolytickou stabilitu, tudíž byly vybrány pro následné měření uvolňování pro-hojivého proteinu.

Stabilizovaný fibroblastový růstový faktor 2 (FGF2-STAB®) podporuje hojení ran. Růstový faktor byl zabudovaný do hydrogelové struktury a jeho uvolňování bylo pozorováno pomocí Bradfordovy metody na UV-Vis spektrofotometru a metodou SDS-PAGE. Byly vytvořeny tři typy hydrogelových sítí: fyzická, hybridní a chemická. Většina uvolněného růstového faktoru z fyzické sítě (25 %) byla pozorována už po dvou hodinách. Nicméně celkově bylo uvolněno pouze 39 % FGF2-STAB® po 22 dnech. Uvolňování z hybridní sítě vykazovalo dvoufázovou, difuzně a degradačně řízenou křivku. První detekované uvolnění růstového faktoru z chemické sítě bylo naměřeno po 6 dnech u vzorků ozařovaných po dobu pěti minut, a po 14 dnech u hydrogelů zesítěných po dobu půl hodiny. Křivky uvolňování z chemické hydrogelové sítě vykazovaly zpožděné nárazové uvolňování. Bohužel nebylo možné uvolněné proteiny detekovat metodou SDS-PAGE.

Typ a hustota hydrogelové sítě ovlivňuje kinetiku uvolňování proteinů. Připravený hydrogel se zabudovaným FGF2-STAB® by mohl být potenciálně využit jako kryt ran.

KLÍČOVÁ SLOVA

Hybridní síť, hojení ran, řízené uvolňování, fibroblastový růstový faktor 2, PLGA-PEG-PLGA kopolymer

KŘIVÁNKOVÁ, Nikola. *Kontrolované uvolňování růstových faktorů z hybridní sítě biodegradabilního hydrogelu*. Brno, 2021. Dostupné také z: https://www.vutbr.cz/studenti/zav-prace/detail/131942. Diplomová práce. Vysoké učení technické v Brně, Fakulta chemická, Ústav fyzikální a spotřební chemie. Vedoucí práce Lucy Vojtová.

DECLARATION

I declare that the master's thesis has been worked out by myself and all quotations from used literature sources are accurate and complete. The content of the master's thesis is the property of the Faculty of Chemistry of Brno University of Technology, and all commercial uses are allowed only if approved by both the supervisor and the dean of the Faculty of Chemistry, BUT.

…………………………..

student's signature

ACKNOWLEDGEMENT

I would like to express my gratitude to my supervisor assoc. prof. Ing. Lucy Vojtová, Ph.D. for her professional guidance and consultation. Furthermore, I would like to give my warmest thanks to my consultant Ing. Klára Lysáková for her patience, time, and mental support in the darkest times. I am also sending thanks to Ing. Jakub Palovčík, Ing. Kristýna Valová, Ing. Jana Dorazilová, Ing. Jana Brtníková, Ph.D, and Ing. Pawel Jewula, Ph.D. Last but not least, I would like to express appreciation to my family for supporting me during my studies.

TABLE OF CONTENTS

1 INTRODUCTION

With scientific advances, novel materials are created with specific properties adjusted according to the application. Materials for medicinal applications should ideally have properties comparable to the replaced tissue and be of course biocompatible. Hydrogel structures consist mostly of water content and are capable to mimic the extracellular matrix [1]. This research is focused on the preparation of a material for wound healing purposes. Ideal characteristics for wound care are following. The material should maintain high humidity, should not cause any immunogenic response, and should enable nontraumatic removal, preferably be biodegradable after a given time. Moreover, it should promote healing. These properties are achievable with hydrogel materials [2].

The goal of this thesis is to prepare a biocompatible and biodegradable material with gradual and well-controlled release of growth factors. A hybrid hydrogel stabilized with both physical and chemical network was chosen for this purpose. As a thermo-responsive copolymer is used, the physical micellar network was formed at physiological temperature due to hydrophobic interactions. Subsequently, the chemical network was prepared by photocrosslinking the ends of the polymer chains in the presence of a hydrophilic photoinitiator, resulting in a core-crosslinked micellar network. Chemical crosslinking of hydrogels increases the thermal and mechanical stability. Photocrosslinking may occur at physiological temperatures and produces minimal heat, therefore it may occur *in situ* [3].

Drug release from the hydrogel structure is based on a combination of diffusion and degradation mechanisms [4]. The influence of chemical network on the release kinetics of a growth factor incorporated in the hydrogel structure was studied.

2 THEORETICAL PART

2.1 Temperature-responsive polymers

Hydrogels are three-dimensional networks formed by natural or synthetic polymers. Due to their ability to absorb and hold large amounts of water, they are biocompatible and potentially capable of mimicking the properties of the extracellular matrix. They are categorized as physical and chemical hydrogels according to the type of hydrogel network. Physical, also called reversible hydrogels are stabilized by non-covalent interactions between the polymer chains, whereas chemical or irreversible networks are formed by covalent bonds between reactive groups of the polymer chain. [1]

Temperature-responsive polymers undergo spontaneous gelation with temperature change [5] (Figure 1). The sol-gel phase transition occurs at a critical gelation temperature which depends on the polymer concentration, its molecular weight, polydispersity [6], and chemical composition. [7] These thermo-responsive polymers are of an amphiphilic nature. In general, the hydrogel formation is driven by hydrophobic interactions and followed by partial dehydration triggered by temperature change. [8]

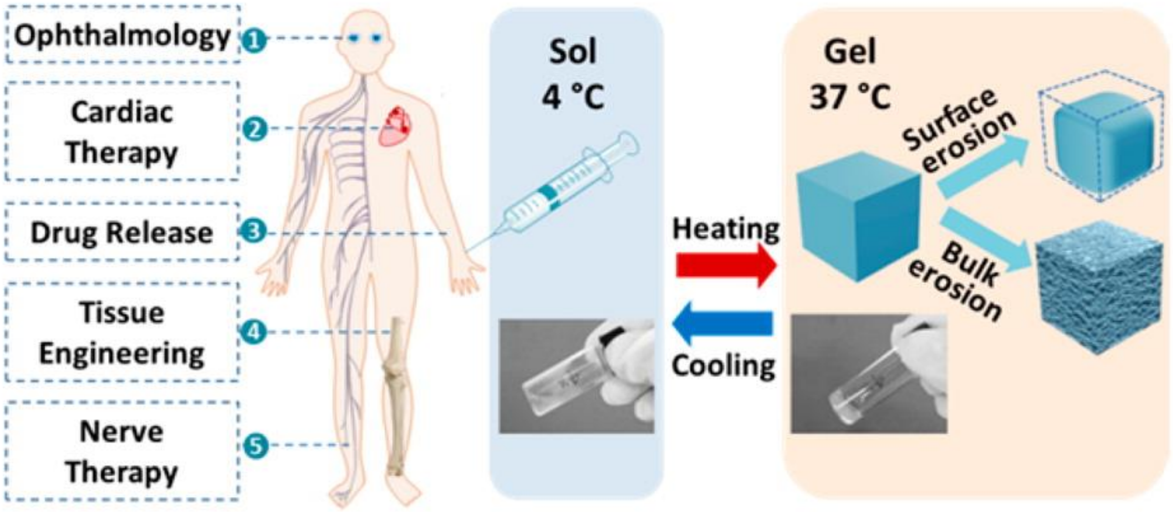

Figure 1: Temperature-responsive hydrogels. [9]

The temperature-responsive polymers have a wide variety of composition, however, biodegradable and biocompatible polymers with sol-gel transition close to body temperature are of high interest for biomedical and pharmaceutical applications. [9] Such hydrogels are applicable as drug or gene delivery systems or as scaffolds in tissue engineering. [8] The reversibility of the hydrogel network extends the use of sensors, switchable micro- and nanomaterials, enzyme immobilization, etc. [10]

When a certain concentration, called critical micellar concentration (CMC), is exceeded, the amphiphilic copolymers form micellar structures in aqueous solutions via self-assembly. The micelles have a hydrophilic shell and a hydrophobic core. The shell provides stability and reduces nonspecific phagocytosis thus prolonging blood circulation. The hydrophobic core enables the solubility of hydrophobic drugs. [11]

2.1.1 PLGA–PEG–PLGA

The triblock copolymer poly(D,L-lactic acid-*co*-glycolic acid)-*b*-poly(ethylene glycol)-*b*-poly(D,L-lactic acid-*co*-glycolic acid) (PLGA-PEG-PLGA) is composed of two hydrophobic blocks PLGA with a hydrophilic PEG in the middle (Figure 2A). The PEG segment provides biocompatibility whereas the hydrolysable ester bonds in PLGA blocks render the biodegradable characteristics. [12] Due to its amphiphilic properties, the copolymer forms core-shell micelles in aqueous solutions above the critical micellar concentration (CMC) (Figure 2B). [13] PLGA-PEG-PLGA gradually degrades to PEG, lactic and glycolic acids. All of them are classified as safe materials by FDA. [14] When in the body, both glycolic and lactic acids are metabolised in the Krebs cycle [15], whereas the hydrophilic PEG is eliminated via kidney. [16]

The copolymer exhibits thermo-responsive properties. PLGA-PEG-PLGA with the appropriate composition is soluble in water at room temperature and lower. When the temperature is increased, the physical hydrogel is formed, exhibiting the lower critical solution temperature (LCST). At lower temperatures, the hydrogen bonding between the PEG parts and water molecules prevails, resulting in dissolution. However, with the increasing temperature, the hydrogen bonding weakens, and hydrophobic interactions become stronger. PLGA blocks migrate between the individual micelles, forming bridges and leading to the sol-gel transition (Figure 2C). [17][18]

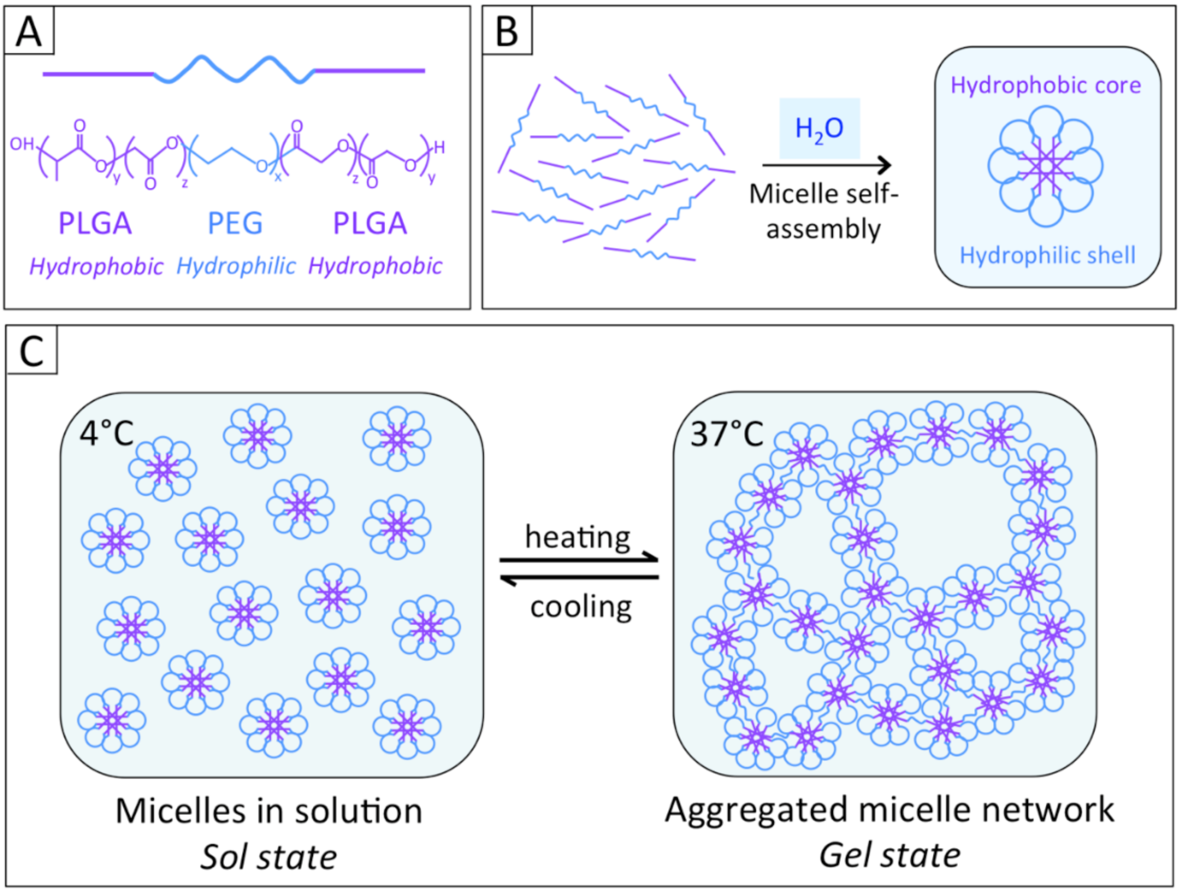

Figure 2: The PLGA-PEG-PLGA polymer chain (A), the self-assembly of the copolymer in aqueous solutions (B), the sol-gel transition properties and formation of a micellar network (C). [19]

The degradation rate of the formed hydrogel is adjustable with the change in copolymer composition, specifically with molecular weight and the D,L-lactide (LA) to glycolide (GA) ratio. In general, with the increasing content of GA, the degradation is fastened except for the 50/50 ratio which degrades the fastest. [17] LA is more hydrophobic compared to GA. The hydrogel with higher LA to GA ratio proved to be more stable due to stronger hydrophobic interactions between the copolymer blocks. Moreover, the sol-gel transition temperature decreases with the increasing LA to GA ratio. The stability of the copolymer can be tailored up to 6 weeks. [20] The effect of PEG molecular weight has also been studied. [7] The copolymer with PEG_{1500} underwent gelation at higher temperatures compared to the copolymer with PEG_{1000}. Furthermore, the shape of PEG_{1000} structure above CMC was rather asymmetric (ellipsoid). On the contrary, the PLGA-PEG_{1500}-PLGA assembled into spherical core-shell micelles. [14]

The properties stated above indicate a great potential for a controlled-release drug delivery system. The amphiphilic properties allow the solubility of both hydrophilic and hydrophobic drugs. The copolymer is commercially available for gradual release of insulin over two weeks under the name ReGel™. [21] OncoGel™ exploits the hydrophobic core micelle structure to solvate a hydrophobic paclitaxel used for cancer treatment. The drug depot also demonstrated targeted delivery of the drug. [22] There are several other studies on controlled release from the PLGA-PEG-PLGA hydrogel structure for both hydrophilic (exenatide [23], lysozyme [24], or 5-fluorouracil [20]) and hydrophobic (doxorubicin [25], indomethacin [20], and docetaxel [26]) drugs.

2.1.1.1 α,ω-itaconyl-PLGA-PEG-PLGA

In order to improve the properties of the copolymer, new functional groups may be introduced to the ends of the copolymer chain. Depending on the purpose, amino, hydroxyl, carboxyl groups or double bonds may be added. The end-capping may affect solubility, degradation rate as well as the thermo-responsive properties. [27]

In 2010, a copolymer PLGA-PEG-PLGA functionalized with itaconic anhydride (ITA) was presented by our group. [28] ITA is produced by filamentous fungi, mostly by *Aspergillus terreus,* via fermentation of polysaccharides. This unsaturated cyclic anhydride is metabolised in the Krebs cycle. [29] The copolymer modification proceeded in a one-pot polymerization through ring-opening reaction resulting in bonded itaconic acid at the ends of the copolymer chains (Figure 3). [28] As the itaconic acid contains a carboxyl group and an unreacted double bond, novel crosslinking approaches are enabled.

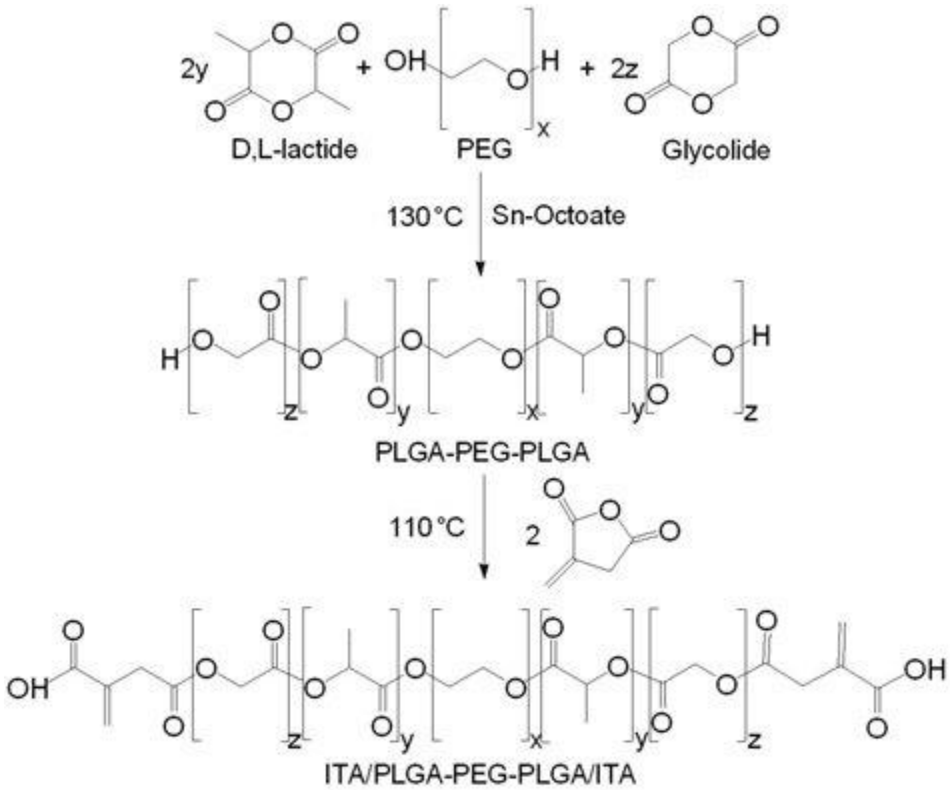

Figure 3: One-pot modification by ITA resulting in ITA/PLGA-PEG-PLGA/ITA copolymer. [8]

Physical crosslinking induced by temperature change is preserved. However, the novel functional groups influence the physical gel. It was observed that the functionalization increased the gel stiffness and that the temperature when the gel exhibits the highest stiffness shifted closed to the physiological temperature. [30] Moreover, the hydrolytic stability in ultra-pure water (UPW) was increased with the increasing amount of bonded ITA. However, the degradation rate is strongly affected by the medium and its pH. When in acidic pH (4.2), the carboxyl groups in the modified copolymer create hydrogen bonds, stabilizing the structure and resulting in slower degradation compared to PLGA-PEG-PLGA copolymer. Nevertheless, when in a medium with physiological pH (7.4), the ITA/PLGA-PEG-PLGA/ITA copolymer degrades significantly faster due to dissociated carboxyl groups that increase the copolymer hydrophilicity. [8]

As carboxyl groups are present at the ends of the copolymer chains, another type of physical network may be formed. When polyvalent cations are added (for example Ca^{2+}), crosslinks between them and dissociated carboxyl groups are established due to electrostatic interactions. Carboxyl groups are suitable for bonding bioactive compounds as well. [31]

Introducing a chemical network is enabled by the presence of double bonds in the functionalized copolymer. End-linked hydrogels from ITA/PLGA-PEG-PLGA/ITA were prepared by Michlovská et al. in 2016 by photocrosslinking. The hydrolytic stability and swelling were observed, confirming a longer life-time for hydrogels with longer crosslinking time. [32] As stated in part 2.3, Zahoranova et al. exploited the thermo-responsive and photocrosslinkable properties and created a hybrid hydrogel (being a part of my bachelor thesis).

2.2 *In situ* chemical crosslinking

The formation of hydrogels at the site (*in situ*) is a great advantage. The *in situ* crosslinkable materials possess the ability of simple drug encapsulation, and to copy the exact shape of the defect, they are easy to handle and require minimal invasiveness. [33] The possible approaches for *in situ* gelation are either through physical interactions (hydrophobic or electrostatic) or chemical crosslinking. [34] Physical gelation via hydrophobic effect is discussed above (2.1).

Chemical crosslinking *in situ* may be achieved by Michael addition, click chemistry, Shiff base crosslinking, photocrosslinking or enzymatic-mediated gelation. [35]

2.2.1 Photocrosslinking

Photopolymerization is a process of *in situ* crosslinking of monomers or macromers by irradiation with ultraviolet or visible light. This method is industrially applied in solvent-free paints, for 3D printing materials, in optoelectronics, adhesives, and varnishes. In the biomedical field, the application may be divided into main sectors: dentistry, tissue engineering, bioimaging, drug delivery systems, and medical devices. [36]

Two mechanisms of photopolymerization according to the used monomers and initiating systems are distinguished. The reaction commonly used for biomedical purposes is a free-radical photopolymerization. It follows three stages. Firstly, radicals are generated from photoinitiators by light illumination. Then the radicals attack the specific functional groups of the macromer, resulting in the formation of new covalent crosslinks between the polymer chains. Lastly, when all radicals are consumed, the reaction is terminated. [37] The polymerization process is however inhibited by atmospheric oxygen. The presence of oxygen causes to quench the excited state of initiators, thus diminishing the efficiency. [36]

The other mechanism of photopolymerization is cationic photopolymerization. Compared to the free-radical reaction, it is more effective due to its living nature, meaning that it continues to run even after the removal of the light sources. It is becoming more popular for industrial purposes. However, due to its sensitivity to moisture and generation of acidic compounds negatively affecting the cell culture, it is inapplicable in the biomedical field. [36]

In order to generate radicals, compounds called photoinitiators have to be included in the process. Photoinitiators exhibit high absorption of light with specific wavelengths. Ideally the photoinitiator would be biocompatible and water soluble. Since the breakthrough of introducing a water-soluble Irgacure 2595, another hydrophilic photoinitiators were presented, e.g., based on monoacylphosphine oxide (MAPO) or bisacylphosphine oxide (BAPO). [38]

Lithium phenyl-2,4,6-trimethylbenzoylphosphinate (LiTPO, Figure 4) is a photoinitiator widely used in hydrogel preparation for example on poly(ethylene glycol) diacrylate (PEGDA) [38] or gelatin-methacryloyl (GelMA). [39] LiTPO absorbs light with wavelengths in the 380–420 nm range. It exhibits good solubility in water (47 g/dm^3) and toxicity around LC_{50} 3.1 mmol/dm^3. [36]

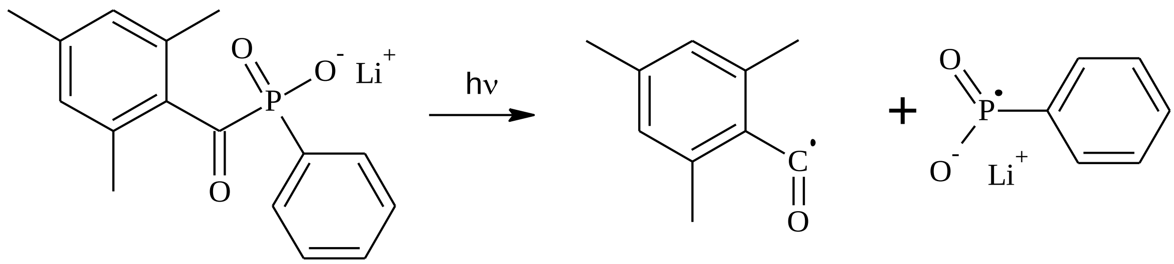

Figure 4: The production of radicals by LiTPO photocleavage. [40]

The reaction may be precisely controlled by the choice of photoinitiator, light source and dosages, as well as by the irradiation time. [41]

2.3 Hybrid hydrogels

Conventionally, hydrogels are stabilized by one network. Covalent networks are formed in permanent shapes usually with low mechanical strength due to the poor ability of energy dissipation. However, the mechanical properties could be altered by changing the crosslink density of the hydrogel network. [42] In this case, the crosslinked hydrogels behave similarly to typical thermosetting polymers. With increasing crosslink density, the hydrogel exhibits higher moduli and brittleness. [43] On the other hand, physical networks demonstrate an energy dissipative mechanism due to their reversibility according to external stimuli (stress, temperature, pH, or ionic strength) thus possibly resulting in high mechanical strength. The drawback of physical hydrogels is the transient nature of their network that could lead to an unacceptable creep in dimensions of the sample. [42]

The mechanical properties of a hydrogel are crucial for their applications. [43] In order to improve the mechanical strength of chemical networks, an additional network capable of energy dissipation can be introduced. Such a network could be stabilized by weak physical crosslinks capable of reversible break, i.e., hydrogen bonding, electrostatic and hydrophobic interactions, crystallization, and interpolymer complexation. [44] One-component systems stabilized simultaneously by physical and chemical networks are identified as hybrid hydrogels. Such hydrogels are often prepared from modified macromolecules or biopolymers. [45]

Che et al. prepared a redox-responsive hydrogel based either on poly(*N*-isopropylacrylamide) or poly(acrylamide). The network consisted of reversible and permanent crosslinks (Figure 5). The reversible disulfide bonds between *N,N'*-bis(acryloyl)cystamine influenced the swelling or deswelling behaviour according to the changes in crosslinking density dependent on the redox environment. The permanent links provided with *N,N'*-methylenebisacrylamide always secured an intact hydrogel structure. Such hydrogels may be applicable for chemical sensing and microfluidics. [46]

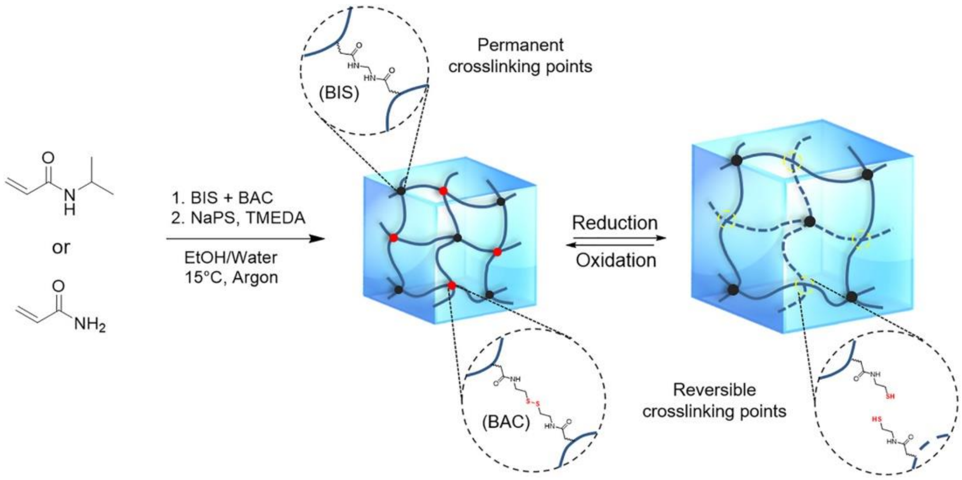

Figure 5: A scheme of the redox-responsive hydrogel. [46]

Szabó et al. developed a hybrid hydrogel derived from sodium alginate and poly(ethylene glycol) (PEG) stabilized by ionic and covalent bonds. The presence of a chemical network led to an improvement of mechanical resistance compared to a hydrogel stabilized purely with ionic interactions. The chemical network was formed by photocrosslinking PEG and methacrylate residues. Such hydrogel is a promising candidate for cell encapsulation (Figure 6). [47]

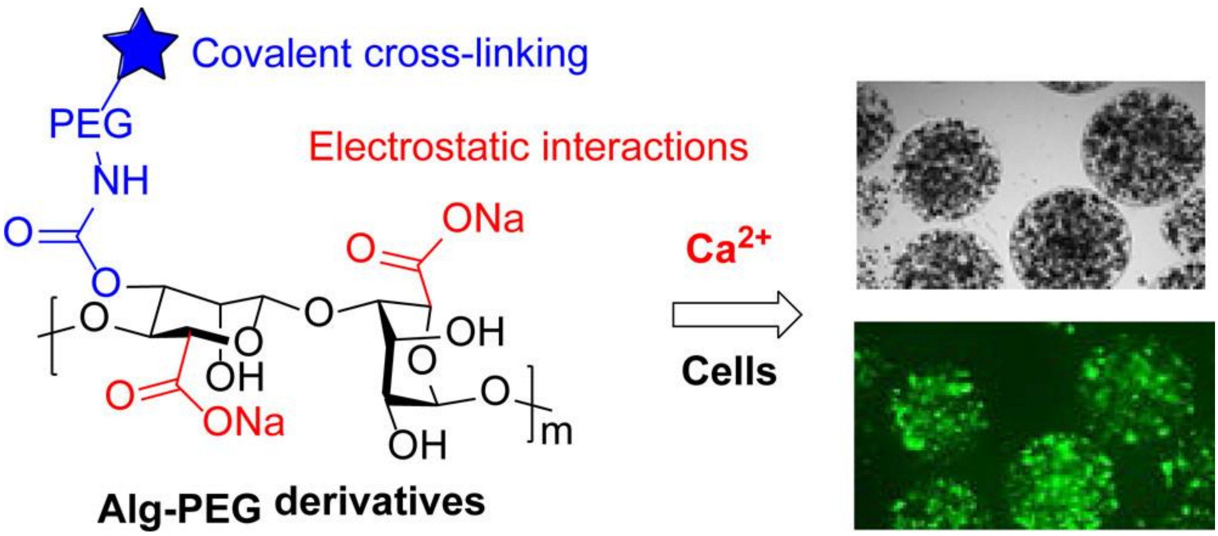

Figure 6: Crosslinking possibilities of PEGylated alginate. [48]

Another type of hybrid hydrogel was prepared by Li et al. An acrylamide was polymerized with a star-shaped multifunctional crosslinker resulting in a steady chemical network. The reversible physical network originates from entanglements between dangling chains. Li et al conclude to have prepared a viscoelastic hydrogel capable of full recovery under compression. Furthermore, a mechanical properties tunability arises from the adjustability of the number of double bonds in the crosslinker. [44]

A hybrid hydrogel formed from *α,ω*-itaconyl-PLGA-PEG-PLGA was introduced by Zahoranova et al. The presented hydrogel was firstly heated to physiological temperature so the physical network would form due to hydrophobic interactions. Subsequently, it was photocrosslinked by visible light, thus a chemical network was made. As the copolymer exhibits amphiphilic properties and the whole preparation process occurred in an aqueous environment, the resulting structure was in the form of micellar networks with covalently crosslinked cores. Zahoranova et al. observed increased storage moduli after covalent crosslinking of the copolymer. [40]

2.4 Release from hydrogel structure

The unacceptable side effects during drug treatment are limiting the possibilities for therapy. Drug delivery systems have the ability to control the drug release, and in some cases also the location of it. [49] The goal of the delivery system is to release the drug at the rate needed to maintain the drug concentration within the so-called therapeutic window. At this concentration range, the drug induces the therapeutic response. Above the window, the drug causes toxic responses whereas below the therapeutic window, it produces no effect. [50] Ideally, the release kinetics of the drug would proceed at the zero-order kinetics to ensure the maximal pharmacological effect (Figure 7). [51] The instant or burst release refers to a fast release of a high amount of drug. This case is unsuitable for long-term therapy as frequent dosing would be required. Moreover, burst release may result in adverse drug effects due to high concentrations. [52]

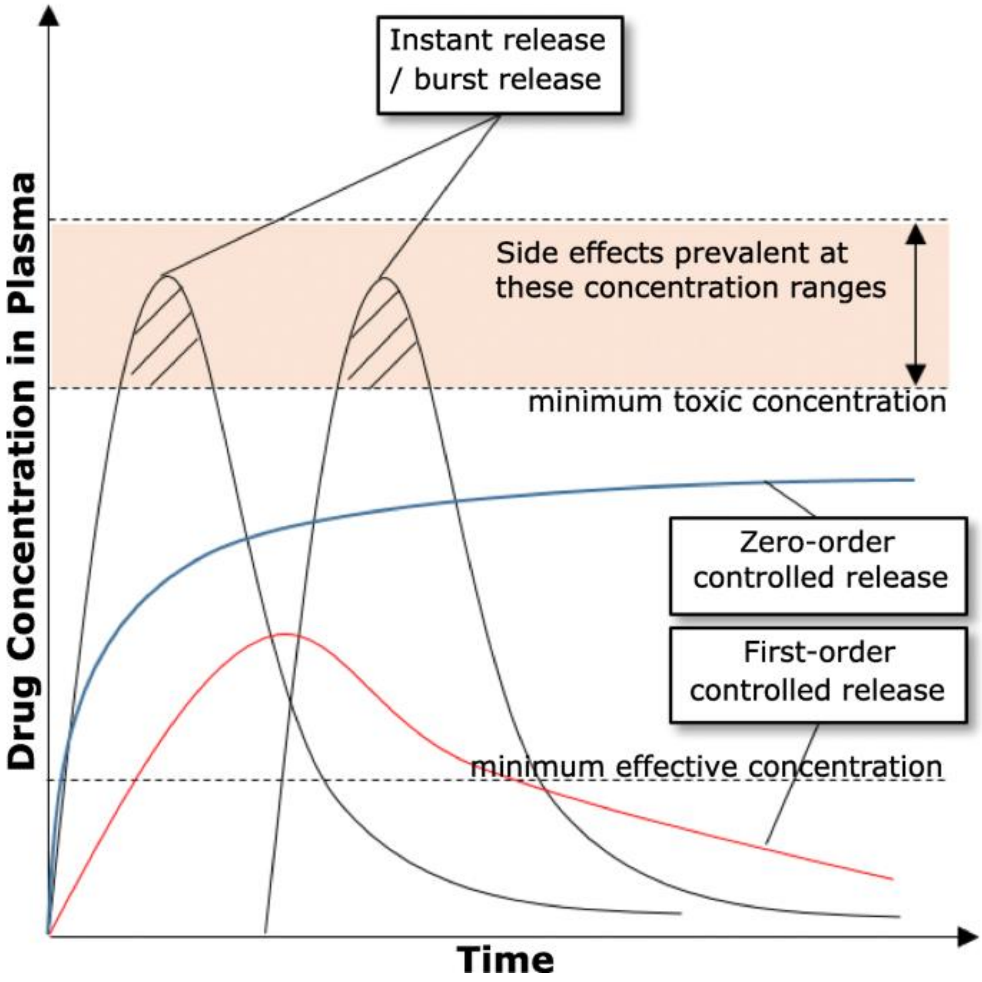

Figure 7: Comparison of burst release with zero and first-order controlled release. [53]

The physical and chemical properties of the hydrogel influence the drug release. The pore size of the polymeric network, the structure and diameter affect the rate of diffusion. [54] The release mechanisms may be diffusion- or solvent-controlled, as well as a response to chemical or environmental stimuli, i.e., degradation or deformation (Figure 8). [53]

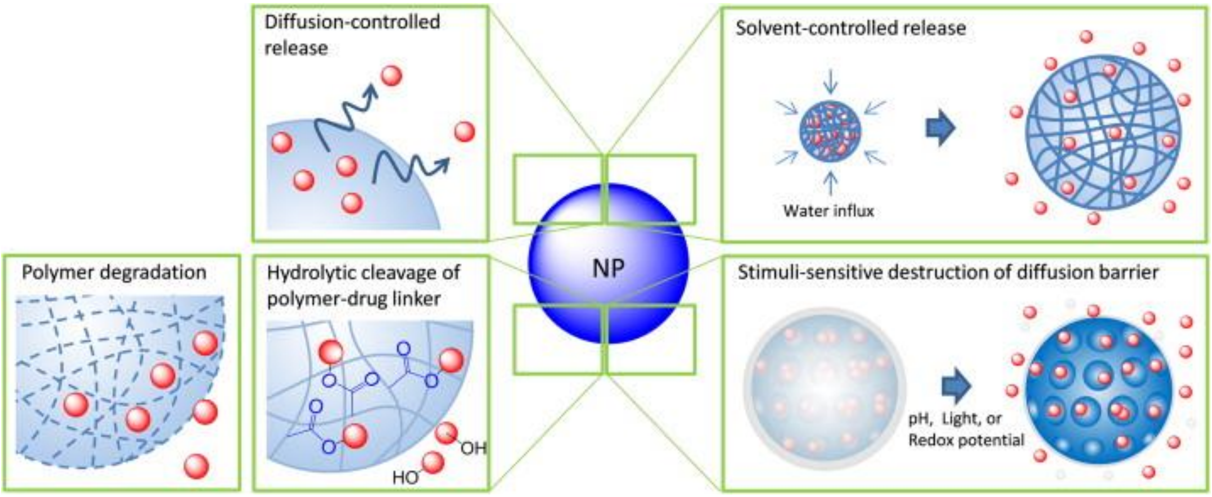

Figure 8: Examples of release mechanisms. [55]

2.4.1 Diffusion-controlled release

This mechanism is driven by the concentration differences between the carrier and the surroundings. The release rate depends on the polymer’s mesh size and porosity, the drug size, and on the affinity of the drug to the polymer. [53] The diffusion is inhibited by the polymer chains. [56]

2.4.2 Solvent-controlled release

This mechanism includes osmosis- and swelling-controlled release. Swelling occurs in glassy hydrophilic polymers while placed in aqueous solution. With water entering the hydrogel network, the hydrogel swells and the encapsulated drugs diffuse through the network. The rate is determined by the diffusion rate of water and the polymer chain relaxation. [55][56]

2.4.3 Degradation-controlled release

In biomedical applications, biodegradable polymers represent a major advantage. When exposed to certain enzymes, water, microbes, or chemicals, they degrade to biocompatible products that are eliminated or metabolised in the body. Two types of degradation may be distinguished. When the degradation rate is faster than water diffusion, the hydrogel undergoes surface erosion. Whereas, when the diffusion of water molecules is faster, the hydrogel degrades homogeneously with a bulk erosion process (Figure 9). [57] The drug release rate depends on the degradation rate of the hydrogel network. The degradation rate may be tailored by introducing labile groups to the polymer composition, such as esters, anhydrides, carbonates, orthoesters, or amides. The drug may also be chemically linked to the polymer chain. The drug release kinetics is in this case controlled by the rate of hydrolytic or enzymatic cleavage. [58]

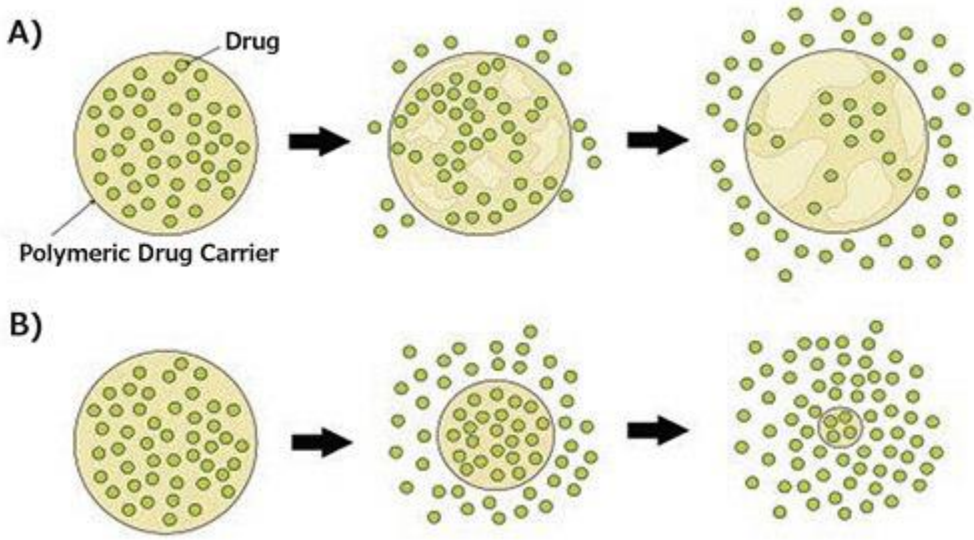

Figure 9: Degradation mechanisms of hydrogel carriers – bulk erosion (A), surface erosion (B). [59]

2.4.4 Stimuli-controlled release

The concept of drug release in these systems lies in internal or external stimuli such as temperature, pH, ionic strength, and electric or magnetic fields. These carriers have been employed for targeted drug delivery. [55]

2.4.5 Release profiles

As several factors influence the release rate from the hydrogel structure, pluri-phasic release profiles are widespread. For example, in the tri-phasic release profile, the first phase is usually caused by the burst release of non-encapsulated drugs on the surface or of drug particles close to the surface. Afterwards, a phase of slow release follows. During this phase, the drug molecules diffuse through the hydrogel structure, while the polymer undergoes degradation and hydration. The third phase usually exhibits a fast release, sometimes referred to as the second burst, due to the onset of erosion. [60]

The explained profile is just an example of possible release phases that may occur. The release profile depends on complex factors, i.e., the physical and chemical properties of the material as well as of the drug. In Figure 10 several examples of release profiles are displayed. [60]

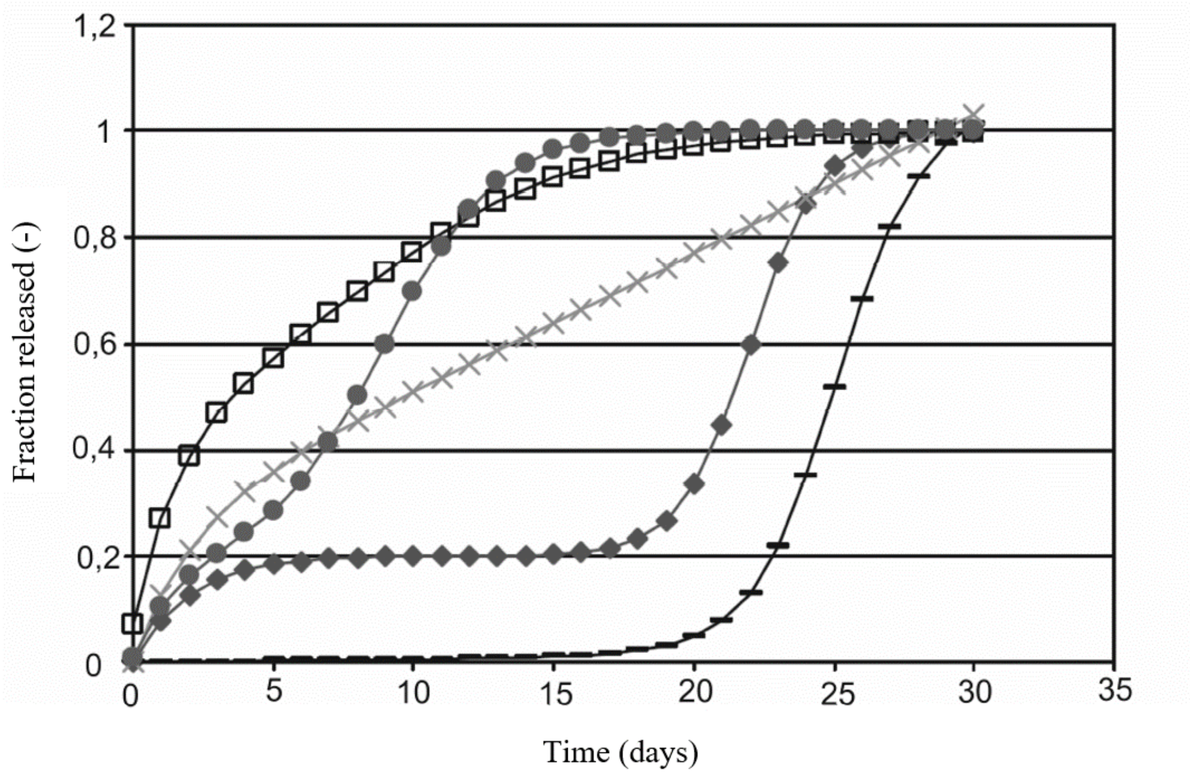

Figure 10: Release profiles – burst with a rapid second phase (□), tri-phasic release with a short second phase (●), zero-order profile with burst release (×), tri-phasic profile (♦) and bi-phasic profile without burst release (▬). [60]

2.5 Growth factors

The process of wound healing is complex. It involves several steps leading to tissue remodelling. Firstly, upon skin disruption, interleukin-1 is released from keratinocytes alerting the neighbouring cells to barrier the wound. The clotting cascade is activated. The hemostasis is secured and the formed clot serves as a matrix for inflammatory cells. Alpha granules are released from degranulating platelets and secreting growth factors such as epidermal growth factor (EGF), platelet-derived growth factor (PDGF) and transforming growth factor-beta (TGF-β). The purpose of TGF-β at the site is to convert monocytes to macrophages that increase the inflammatory reaction by releasing proinflammatory cytokines. Moreover, they secrete EGF, PDGF, TGF-β, and fibroblast growth factors (FGF). Each family of growth factors have their given function and are secreted by different cell types. [61] The overview is shown in Table 1.

Table 1: Major families of growth factors, their functions and secretion cell types. [61]

Growth factors	Cells	Function
EGF	Platelets Macrophages Fibroblasts	Reepithelialisation
FGF-2	Keratinocytes Mast cells Fibroblasts Endothelial cells Smooth muscle cells Chondrocytes	Granulation tissue formation Reepithelialisation Matrix formation and remodelling
TGF-β	Platelets Keratinocytes Macrophages Lymphocytes Fibroblasts	Inflammation Granulation tissue formation Reepithelialisation Matrix formation and remodelling
PDGF	Platelets Keratinocytes Macrophages Endothelial cells Fibroblasts	Inflammation Granulation tissue formation Reepithelialisation Matrix formation and remodelling

2.5.1 Fibroblast growth factor 2 (FGF-2)

FGF-2, also known as basic FGF, affects angiogenesis, normal wound healing, and tissue development. Its role is to activate high affinity transmembrane receptors. The receptors consist of an extracellular ligand-binding site, a transmembrane domain, and an intracellular tyrosine kinase part. When FGF is bound to the receptor, receptor dimerization occurs, and kinase activity is increased. Thus, resulting in controlled phosphorylation of tyrosine residues found on the receptor. Tyrosine residues then activate several signalling pathways that control cell proliferation, migration, and survival. [62] The receptor activation is conditional on binding of FGF-2 to heparin or heparan sulfate. Another regulatory mechanisms depend on the receptor's intrinsic tyrosine kinase activity and on second messengers, e.g., mitogen activated protein kinases. [63]

Concerning the structure, several forms of FGF-2 have been confirmed with molecular weights 18, 22, 22.5, 24 and 34 kDa. It contains a large number of basic residues, resulting in a p*I* of 9.6. Moreover, FGF-2 has two sites for kinase A phosphorylation (Ser 64 and Thr 112). It folds into twelve antiparallel *β*-sheet structures. [64][65]

The wild type FGF-2 exhibits quite low stability, as the half-life at 37 °C is around nine hours. This fact quite limits the applicability. During a treatment, at least daily uptake of fresh FGF-2 would be in need. In my work, a stabilized FGF-2 (FGF2-STAB®) composed of 155 amino acids was used. The FGF2-STAB® was introduced by the company Enantis. They promise a biologically active FGF-2 even after twenty days at physiological temperature. [66]

3 MAIN GOAL OF THE WORK

The goal of this work is to synthesize and characterize a thermo- and photo-sensitive *α,ω*-itaconyl-PLGA-PEG-PLGA copolymer. The aim is to form a hybrid hydrogel network by photocrosslinking a physically stabilized micellar network, thus creating a core-crosslinked micellar hydrogel network. Furthermore, the work is also focused on the incorporation and release of fibroblast growth factor.

- Synthesis and characterization of *α,ω*-itaconyl-PLGA-PEG-PLGA via ring-opening polymerization
- Preparation of a hybrid hydrogel by photocrosslinking physically stabilized hydrogel with visible light in the presence of a hydrophilic and biocompatible photoinitiator
- Characterization of prepared hydrogels
- Measurement of FGF2-STAB® release from different types of hydrogel networks: physical, chemical, and hybrid

4 EXPERIMENTAL PART

4.1 Chemicals

- Acrylamide/Bis-acrylamide, 30% solution, Sigma-Aldrich (USA)
- Bradford Reagent (for 0.1–1.4 mg/ml protein), Sigma-Aldrich (USA)
- Butylamine (99.5%), Sigma-Aldrich (China)
- Chloroform-d (99.8 atom % D), Sigma-Aldrich (Switzerland)
- Coomassie Brilliant Blue R ($C_{45}H_{44}N_3NaO_7S_2$), Sigma-Aldrich (USA)
- N-(3-Dimethylaminopropyl)-N'-ethylcarbodiimide hydrochloride (EDC, commercial grade), Sigma-Aldrich (Japan)
- D,L-lactide (LA, 99.9%), Polysciences, Inc. (Pennsylvania)
- Di-sodium hydrogen phosphate dodecahydrate (≥ 98%), Lach-Ner, L.t.d. (Czech Republic)
- Glycolide (GA, 99.9%), Polysciences, Inc. (Pennsylvania)
- N-Hydroxysuccinimide (NHS, 98%), Sigma-Aldrich (Japan)
- Itaconic anhydride (98%) flushed with nitrogen, Acros Organics
- Liquid nitrogen, Linde Gas, a.s. (Czech Republic)
- Lithium phenyl-2,4,6-trimethylbenzoylphosphinate (LiTPO, ≥95%), Sigma-Aldrich (USA)
- 2-Mercaptoethanol (≥99.0%), Sigma-Aldrich (USA)
- Physiological solution (0.9% NaCl), B. Braun (Germany)
- Poly(ethylene glycol) (PEG, M_n = 1500 g/mol), Fluka (Germany)
- Potassium chloride (≥ 99%), Sigma-Aldrich (USA)
- Potassium dihydrogen phosphate (≥ 99%), Lach-Ner, L.t.d. (Czech Republic)
- Sodium chloride (≥ 99.5%), Lach-Ner, L.t.d. (Czech Republic)
- Sodium dodecyl sulfate (SDS, ≥ 98.5%), Sigma-Aldrich (China)
- Stabilized fibroblast growth factor (FGF2-STAB®), Enantis, L.t.d. (Czech Republic)
- Tetrahydrofuran (THF, p.a.), PENTA (Czech Republic)
- N,N,N',N'-Tetramethylethylenediamine (TEMED, ~99%), Sigma-Aldrich (China)
- Tin octanoate (SnII-ethylhexanoate, 95%), Sigma-Aldrich (USA)
- Tris(hydroxymethyl)aminomethane (Tris, ≥ 99.8%), Sigma-Aldrich (USA)
- Ultra-pure water type I was prepared on a water purification system Milipore Direct-Q® 3 UV equipped at CEITEC BUT
- Unstained Protein Molecular Weight Marker (REF 26610), Thermo Fisher (Lithuania)

4.2 Equipment

- Common laboratory equipment and glassware, e.g., spatulas, vials, flasks, etc.
- OHAUS Adventurer Pro, analytical scales (Switzerland)
- All glass high-vacuum line (hand-made at CEITEC BUT)
- CHRIST Epsilon 2-10D LSCplus, lyophilizator (Germany)
- Thermoblock HLC (DITABIS AG, Germany)
- Rheometer TA Instruments AR-2 (TA Instruments, USA)
- GPC/SEC 1260 Infinity (Agilent, USA) with Multi-angle light scattering photometer HELEOS-II and refractometer Optilab T-rEX (Wyatt Technology)

- Incubator CO2cell (MMM group, Germany)
- 500 MHz NMR spectrometer Bruker Avance NEO
- ATR-FTIR, Vertex 70v (Bruker Co., Germany)
- UV-Vis Spectrophotometer V-730 (Jasco, Japan)
- Raman confocal microscope SOL Nanofinder II with 633 nm laser
- Irradiation chamber with 395–405 nm LED (hand-made at CEITEC BUT)
- PowerPac™ Basic Power Supply (Bio-Rad, Czech Republic) with Mini-PROTEAN® Tetra Vertical Electrophoresis Cell (Bio-Rad, Czech Republic)
- Discovery TGA, TA Instruments, Nicolet iS10, Thermo Fisher Scientific

4.3 Sample preparation

4.3.1 Synthesis of *α,ω*-itaconyl-PLGA-PEG-PLGA

The thermo- and light-sensitive *α,ω*-itaconyl-PLGA-PEG-PLGA copolymer with D,L-LA/GA molar ratio of 3 and PLGA/PEG weight ratio of 2.5 was prepared via living ring-opening polymerization following the instructions given by Michlovská (2009). [18] The synthesis of PLGA-PEG-PLGA was carried out under nitrogen atmosphere and Sn(II) 2-ethylhexanoate catalysis for 3 hours at 130 °C. Subsequently to the polymerization, itaconic anhydride was added to the reaction flask against a nitrogen flow. The functionalization of the copolymer occurred under intense stirring and nitrogen atmosphere at 110 °C for one hour.

The prepared copolymer was purified from the unreacted monomers by repeated dissolution in ultra-pure water (UPW) with subsequent copolymer precipitation at 80 °C. The decantation was repeated three times. The purified functionalized copolymer was freeze-dried at -35 °C under 1 mBar for 15 hours followed by a secondary drying process at 25 °C under 0.01 mBar until decreasing Δp (the change in pressure was up to 10 %).

4.3.2 Carboxyl group masking

In order to mask the carboxyl groups at the ends of the copolymer chains, butylamine was bonded to the carboxyl groups via activation with 1-ethyl-3-(3-dimethyl-aminopropyl)-1-carbodiimide hydrochloride (EDC) and *N*-hydroxysulfosuccinimide (NHS) thus forming an amide bond. The copolymer batch was firstly dissolved in UPW at 12 °C. Afterwards, the solution was tempered to room temperature. Calculated amounts of NHS and EDC were added to the solution and stirred for one hour at 400 rpm. The amount of NHS was calculated in a molar ratio of 2.0 per carboxyl group. The molar ratio of EDC was 1.0 per carboxyl group. Butylamine in a molar ratio of 2.0 to carboxyl groups was then pipetted to the solution and the reaction proceeded for two hours while stirred (400 rpm) at room temperature. The modified copolymer was precipitated at 80 °C, decantated and freeze-dried as described above.

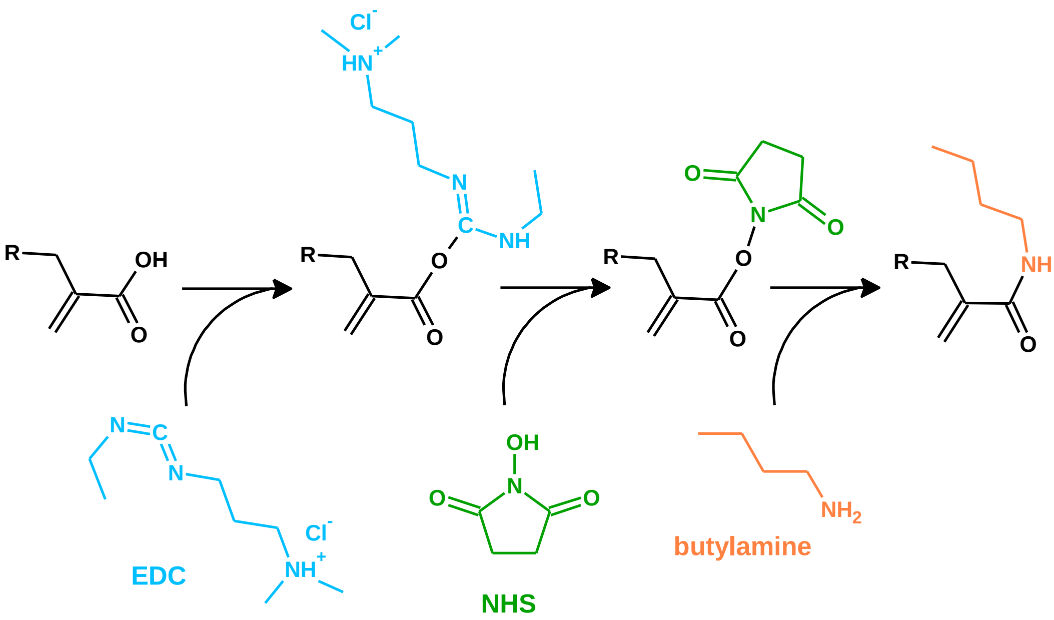

Figure 11: The process of masking carboxyl groups with butylamine via EDC/NHS activation

4.3.3 Preparation of copolymer solutions

The 20 wt.% copolymer solutions were prepared. The copolymer was weighed into a vial and calculated volume of UPW or PBS was pipetted to the vial. It was then stirred for 4-6 days at 12 °C.

4.3.4 Preparation of photocrosslinked samples

First, copolymer solutions were prepared according to 4.3.3. When the copolymer was completely dissolved, the water-soluble photoinitiator LiTPO was added to the solution (1 wt.% per raw copolymer). As from now on, the solutions were photo-sensitive therefore they were kept wrapped in aluminium foil and all manipulations occurred in a yellow lab.

The sample was loaded to a small Petri dish or an insert depending on the method. The loaded volume was always calculated according to the diameter of the container to ensure similar sample thickness. The sample was then left at 37 °C for 30 to 60 minutes to form a physical network. Subsequently, the physically stabilized hydrogel was irradiated for the appropriate time with light in the 395–405 nm range while maintaining the physiological temperature. For several methods, the prepared samples had to be freeze-dried.

4.3.5 Preparation of hydrogels loaded with FGF2-STAB® for release study

The release process of FGF2-STAB® was studied from different types of hydrogel networks: physical, chemical, and hybrid. All samples consisted of the α,ω-itaconyl-PLGA-PEG-PLGA (ABA/ITA) copolymer with masked carboxyl groups by butylamine (butyl-ABA/ITA). The 20 wt.% solutions were prepared as stated in 4.3.3 with PBS as the solution.

4.3.5.1 Release from the physical hydrogel network

In the case of release from physical hydrogel, the FGF2-STAB® was added to the solution in concentration 100 µg/ml. The sample was stirred for 30 min at room temperature. Afterwards, the solution was poured into the insert and left at 37 °C for 30 to 60 min to gel. The insert was then put to the PBS-containing pan. The sample was left in the incubator at 37 °C. The PBS diffused to the hydrogel through the insert while the protein diffused to the outer pan. At certain time intervals, the PBS solution from the pan was removed and replaced with a new PBS solution. The removed solution was analysed to determine the concentration of the released protein. The steps are shown in Figure 12.

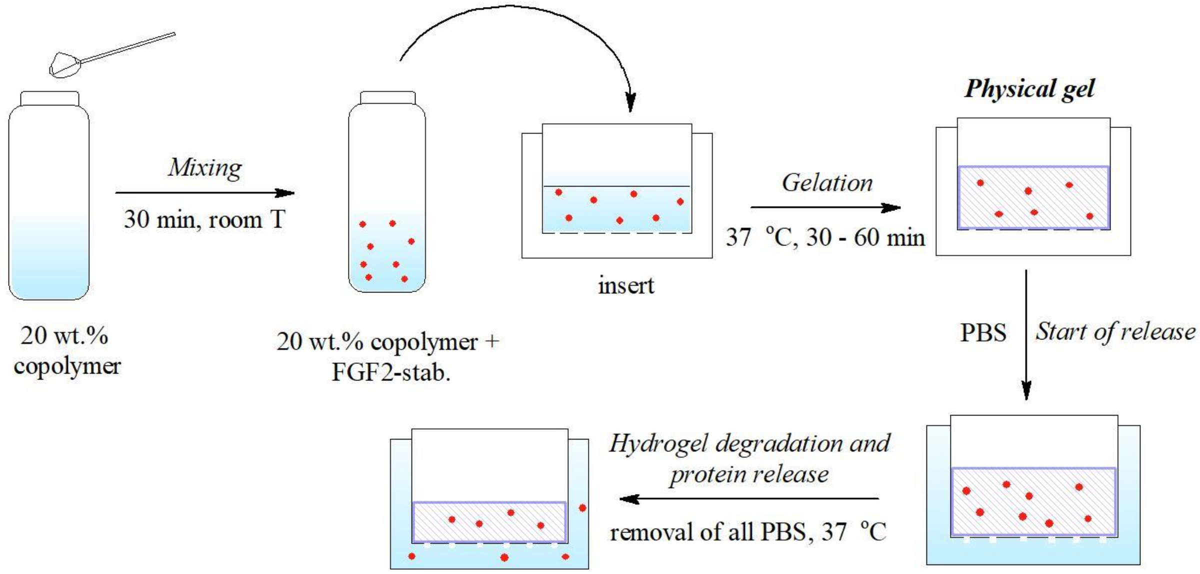

Figure 12: The sample preparation of physically stabilized hydrogel for FGF2-STAB® release.

4.3.5.2 Release from the chemical hydrogel network

The samples stabilized with a chemical network were prepared as follows (Figure 13). Together with FGF2-STAB®, the hydrophilic photoinitiator LiTPO (1 wt.% per copolymer) was added to the PBS solution of butyl-ABA/ITA and stirred for 30 min at room temperature. From this moment, the sample was either covered in aluminium foil or handled in a yellow lab. The solution was transferred to the insert and irradiated for either 5 or 30 min at room temperature. The sample was then put into the PBS-filled pan. The following steps were the same as for the samples with physical hydrogel.

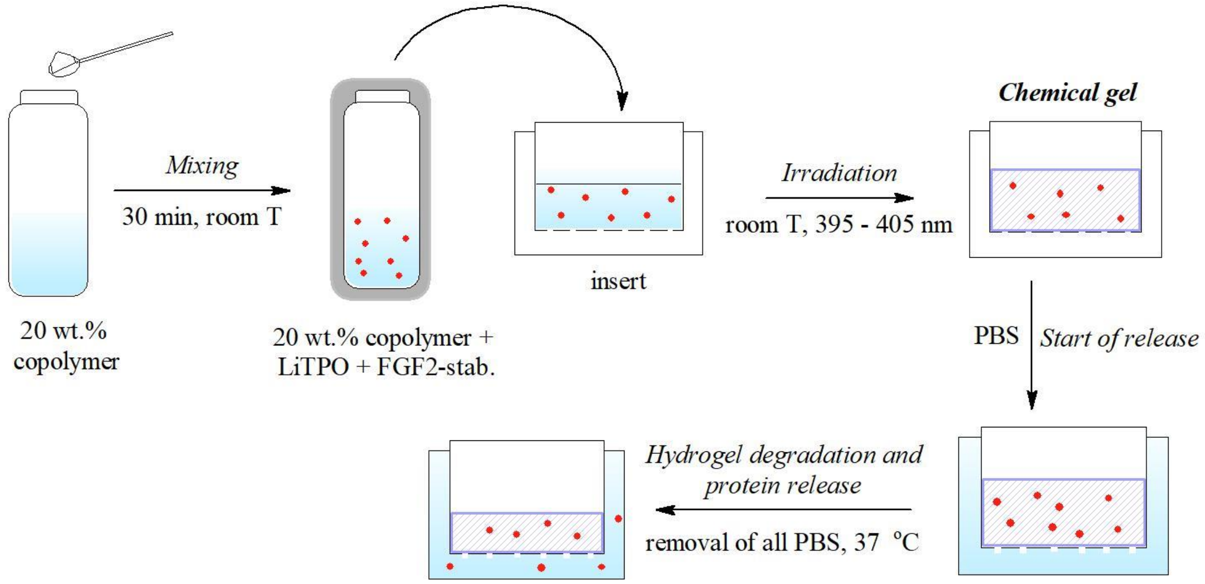

Figure 13: Preparation of chemical hydrogel for FGF2-STAB® release.

4.3.5.3 Release from the hybrid hydrogel network

For the preparation of hybrid hydrogel samples, the initial steps were similar as for the samples with chemical hydrogel. However, before irradiation, the samples were left at 37 °C for 30 to 60 min to form a physical network. The micellar hydrogel was subsequently irradiated for either 5 or 30 min while maintaining the physiological temperature, thus preparing the hybrid hydrogel. Afterwards, the procedure was the same as for the above-mentioned samples. The preparation steps are shown in Figure 14.

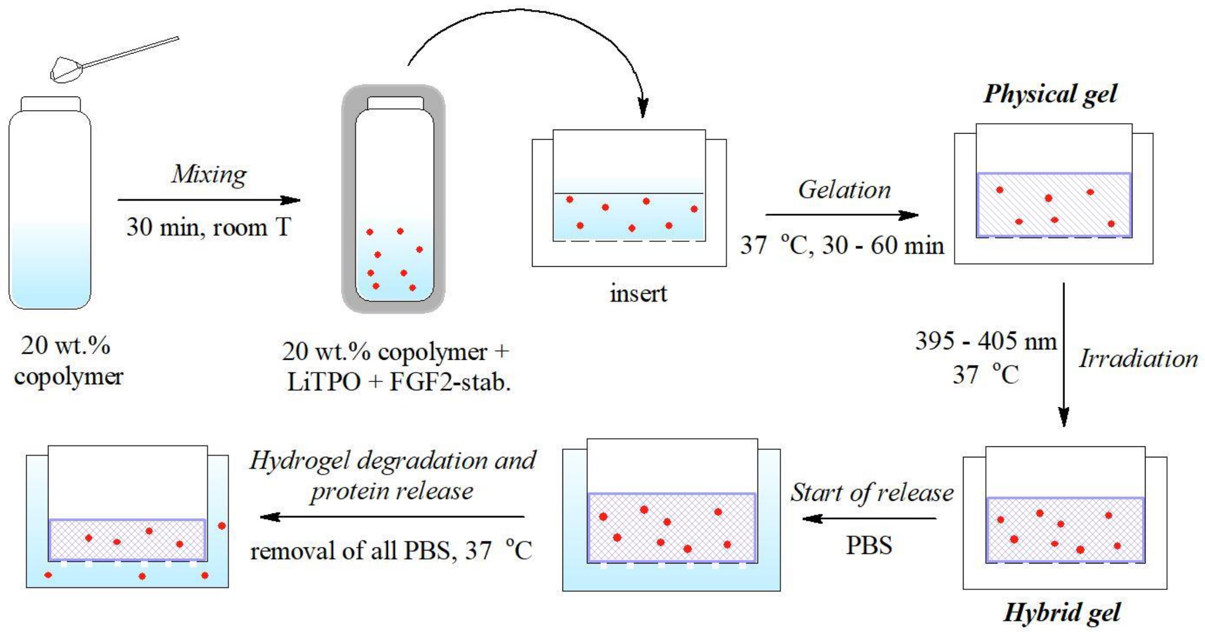

Figure 14: The preparation of hybrid hydrogel samples for FGF2-STAB® release.

4.4 Methods

4.4.1 Gel Permeation Chromatography (GPC)

The number average molecular weight (M_n) and polydispersity index (M_w/M_n) of the synthesized copolymers were measured by GPC. The samples were dissolved in tetrahydrofuran (THF) with the concentration of 15 mg/ml. The injected samples were separated using two columns PLgel 5 µm Mixed-C with THF as a mobile phase and a flow rate of 1 ml/min against a polystyrene standard (M_w = 30 000 g/mol, polydispersity index 1.06). The data was detected by multi-angle light scattering photometer HELEOS-II and a refractive index detector Optilab T-rEX (Wyatt Technology, Germany). The measurements were performed by dr. Brtníková from CEITEC BUT. The data were evaluated by Astra software.

4.4.2 Proton Nuclear Magnetic Resonance (^{1}H NMR)

The PLGA/PEG, LA/GA ratios, the degree of functionalization by ITA and molecular weight of the synthesized copolymer were determined by ^{1}H NMR spectroscopy on 500 MHz Bruker Avance NEO instrument with 128 scans at 25 °C. Deuterated chloroform was used as a solvent. The measurement was provided by dr. Pawel Jewula from CEITEC BUT, Brno. Data were evaluated using the ACD/1D NMR Processor.

4.4.3 Dynamic Rheological Analyses

The viscoelastic properties of the synthesized copolymers and the influence of different solvents were studied using the TA Instruments AR-G2. All experiments were performed by Ing. Valová from CEITEC BUT.

To determine the gelation properties of the copolymers, the storage and loss moduli were measured using a cone-plate geometry with a 60 µm gap. The copolymer solution was transferred to the Peltier by syringe and covered by a solvent trap to prevent solvent evaporation. The measurements were carried out with increasing temperature from 20 to 50 °C at 0.5 °C/min rate and at a constant frequency of 1 rad/s.

To compare the viscoelastic properties of photocrosslinked hydrogels, a stress sweep measurement was performed using plate-plate geometry with a 500 µm gap (37 °C, frequency of 1 Hz). The oscillation stress was increased from 0.001 to 1500 Pa. The samples were prepared as stated in 4.3.4.

4.4.4 UV-Vis spectrophotometry

The absorbance range of the photoinitiator LiTPO and the influence of the copolymer was determined by UV-Vis spectrophotometer. The data were collected from 900 to 200 nm using deuterium and halogen lamps on V-730 Jasco. The photoinitiator was either dissolved in UPW or in 20 wt.% aqueous solution of the copolymer at concentration 1 wt.%.

4.4.5 Attenuated Total Reflectance Fourier Transformed Infrared Spectroscopy (ATR-FTIR)

The modification by butylamine was confirmed by the ATR-FTIR method on Vertex 70/70v Bruker spectrometer. Freeze-dried samples of copolymers before and after butylamine modification were transferred to a Germanium crystal and the spectra were recorded using 128 scans from 600 to 4500 cm^{-1} at resolution 1 cm^{-1}. The spectra were normalized and evaluated using Origin software. The measurement was performed by Ing. Valová (CEITEC BUT).

4.4.6 Raman spectroscopy

In order to study the double bond conversion during photocrosslinking, the freeze-dried samples before and after irradiation were studied under the Raman confocal microscope SOL Nanofinder II with 633 nm laser. The samples were prepared according to the steps in 4.3.4. The lens magnification was set to 51x, grid to either 150/500 or 600 and time of measurement to 60 or 120 s. Data were obtained from two different places for all samples and evaluated in Origin software. The measurement was provided by Ing. Palovčík (FCH BUT).

4.4.7 Thermogravimetric analysis (TGA)

The thermal stability experiments were performed on TA Instruments, Nicolet iS10. Nitrogen was used as a purge gas with a flow rate of 60 ml/min. The temperature increased from ambient temperature to 500 °C at the rate of 5 °C/min followed by faster heating (25 °C/min) to 650 °C. The samples were freeze-dried and prepared according to 4.3.4. The measurement was performed by Ing. Dorazilová (CEITEC BUT). Data were evaluated using TRIOS software.

4.4.8 Hydrolytic stability

The hydrolytic stability of both physical and hybrid hydrogels was observed at 37 °C in physiological solution or PBS. The samples were prepared in inserts as stated in 4.3.4. Each insert was immersed in the given solution and left in the incubator at 37 °C. The solution diffused through the membrane (0.4 μm pores) to the hydrogel and the degradation products diffused to the solution. At certain time intervals the solution from the external pan was removed. The insert with the hydrogel was weighed and the pH value of the solution was measured. The same volume of new solution was then dosed to the external pan.

4.4.9 Protein detection by Bradford method using UV-Vis spectrophotometry

To determine the amount of released FGF2-STAB® from the hydrogel structure, the colorimetric Bradford assay was applied. The Bradford reagent interacts with certain amino acids in proteins – arginine, lysine, and histidine. This results in an absorbance shift. The values were collected at 595 nm. The samples and reagent were pipetted to quartz cuvettes according to the expected amount of released protein (Table 2). The volumes were adopted from the master's thesis of Lysáková. [64] The concentration of the released protein was then calculated from the appropriate calibration curves.

Table 2: The volumes of Bradford reagent and sample according to the expected amount of released protein.

	Bradford reagent [µl]	Sample [µl]
lower concentration (10–100 µg/ml)	800	200
higher concentration (50–750 µg/ml)	1 000	30

4.4.10 Sodium dodecylsulphate-poly(acrylamide) gel electrophoresis (SDS-PAGE)

To identify the proteins in the removed PBS samples, PAGE electrophoresis was used with the SDS detergent. The SDS binds non-covalently to proteins giving them a uniform negative charge, thus ensuring separation based solely on protein size. 23 µl of samples were mixed with 5 µl of SDS dye containing, among others, the reducing agent mercaproethanol and Coomassie Brilliant Blue dye. The solution was heated at 95 °C for 5 min. The samples were loaded on the prepared separation gel. The 15 and 10% gels were used for the experiments with the composition stated in Table 3. The voltage was set to 120 V.

Table 3: Composition of the electrophoresis gels. The volumes stated in the table are for the preparation of 2 gels.

Stacking gel		**Resolving gel**		
5%			10%	15%
Stacking buffer	1 ml	Resolving buffer	2.6 ml	2.88 ml
30% acryl-bisacrylamide mix	0.54 ml	30% acryl-bisacrylamide mix	3.4 ml	5.63 ml
UPW	2 ml	UPW	3.8 ml	2.5 ml
10% APS	60 µl	10% APS	100 µl	113 µl
10% SDS	40 µl	10% SDS	100 µl	113 µl
TEMED	5 µl	TEMED	4 µl	9 µl

5 RESULTS AND DISCUSSION

5.1 Synthesis and characterization of *α,ω*-itaconyl-PLGA-PEG-PLGA

The thermo- and photo-sensitive copolymer *α,ω*-itaconyl-PLGA-PEG-PLGA (ABA/ITA) was synthesized on high-vacuum line apparatus via living ring-opening polymerization. The copolymer was characterized by GPC and NMR to confirm the structure. Three batches of the copolymer were produced. The average values of all batches are shown in Table 4 together with the theoretical values. The number average molecular weight (M_n) obtained from GPC was a bit higher however the M_n calculated from the NMR spectrum was in good agreement with the theoretical value. The synthesized copolymers exhibited an acceptable index of polydispersity (PDI) as well as the PLGA/PEG and LA/GA ratios. The degree of modification by ITA was in average 64 mol.%.

Table 4: Average values of ABA/ITA received from GPC (^{a}) and NMR (^{b}) compared to the theoretical values.

	M_n [g/mol]		PDI	PLGA/PEG [wt./wt.]	LA/GA [mol/mol]	ITA [mol.%]
theoretical values	5 250		-	2.50	3.00	-
measured values	5 878 ± 88^a	5473 ± 52^b	1.12 ± 0.01^a	2.64 ± 0.04^b	2.92 ± 0.04^b	64.0 ± 2.5^b

The received spectrum from ^1H NMR of ABA/ITA copolymer is shown in Figure 15. The peaks in the graph are assigned to the appropriate proton in the structure. The protons in the $=CH_2$ group (a, b) in ITA exhibit different chemical shifts due to different functional groups in *cis* and *trans* positions. The proton with the carboxyl group in the *cis* position is less shielded due to decreased electron density around the proton, resulting in a higher chemical shift (6.31 ppm) compared to the proton with the carboxyl group in the *trans* position (5.73 ppm). The LA block is represented by the peak at 5.17 ppm (c) belonging to the CH group, and by the 1.59 ppm peak (g) of the CH_3 group. The CH_2 group in GA can be found in the 4.9 – 4.5 ppm range (d). Between LA and PEG, a CH_2 group with a characteristic peak at 4.33 ppm (e) can be found in the copolymer structure. The peak at 3.65 ppm (f) stands for PEG. The two singlet peaks at around 3.44 ppm (h) represent the two protons in CH_2 group in ITA. [67]

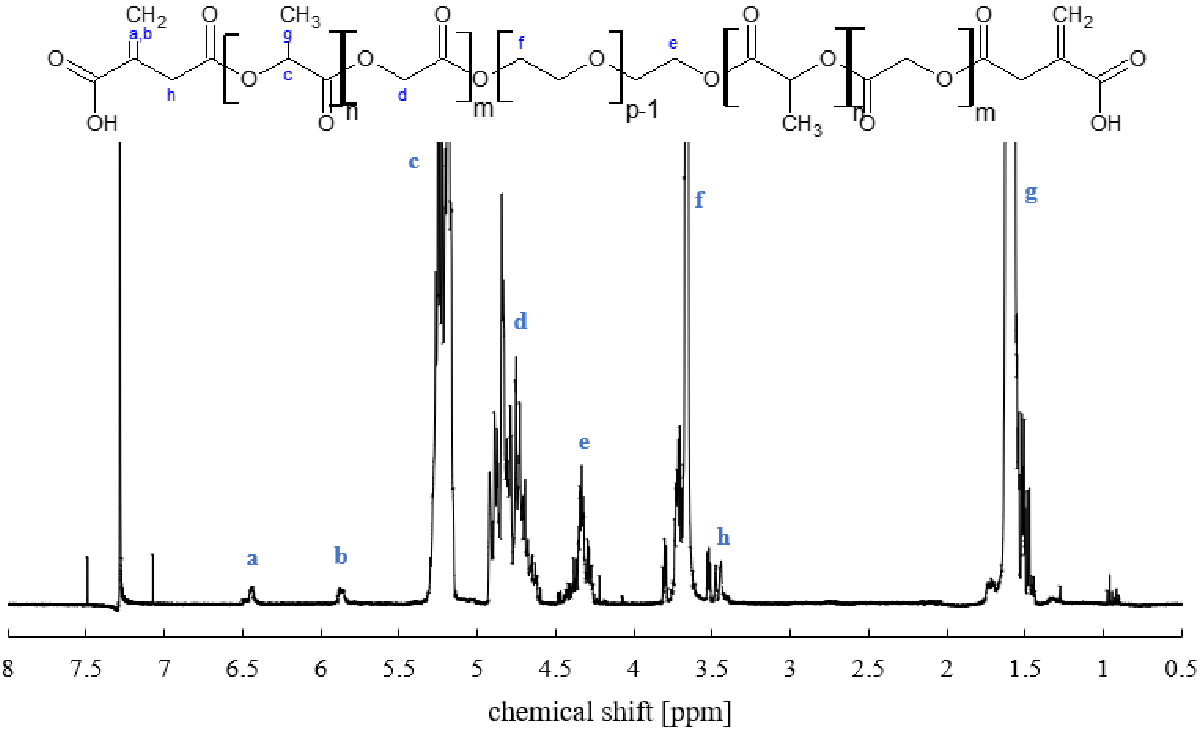

Figure 15: The ^{1}H NMR spectrum of ABA/ITA.

5.2 Crosslinking of *α,ω*-itaconyl-PLGA-PEG-PLGA

5.2.1 Physical network

The gelation properties of aqueous solutions of ABA/ITA were confirmed with rheometer (Figure 17). The copolymer is of an amphiphilic nature therefore, when a certain concentration, known as CMC, is exceeded, the copolymer chains form flower-like micelles. When the temperature of the copolymer solution is raised above the gelation temperature, a sol-gel transition occurs, resulting in a micellar hydrogel (Figure 16). The sol-gel transition is determined by the first crosslink of storage (G') and loss (G'') moduli (Figure 17, point 1), 32.8 °C. The copolymer forms a physical network at physiological temperature due to hydrophobic interactions between the PLGA blocks. The temperature at which the hydrogel exhibits the highest strength is when the G' reaches maximum. In this case of 20 wt.% aqueous solution of ABA/ITA, the maximum is at 37 °C. The second cross-point of G' and G'' (at 39 °C) is caused by the decrease of the elastic modulus below the loss modulus, indicating the decay of the hydrogel network into a precipitate.

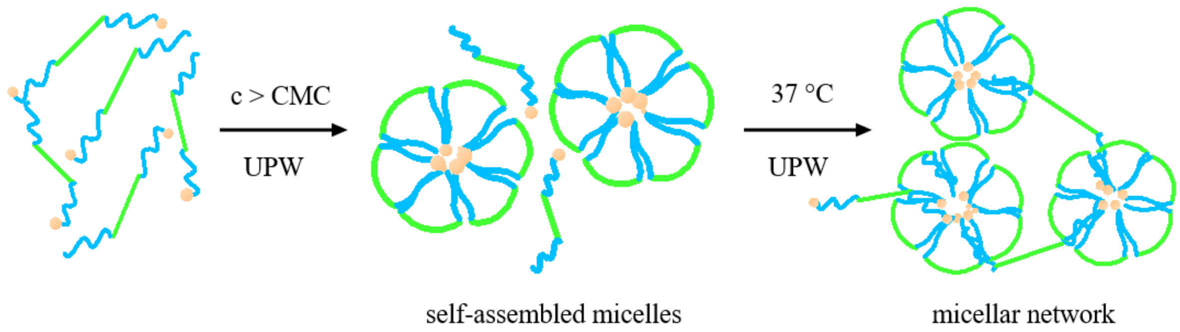

Figure 16: Graphical illustration of the formation of micellar network.

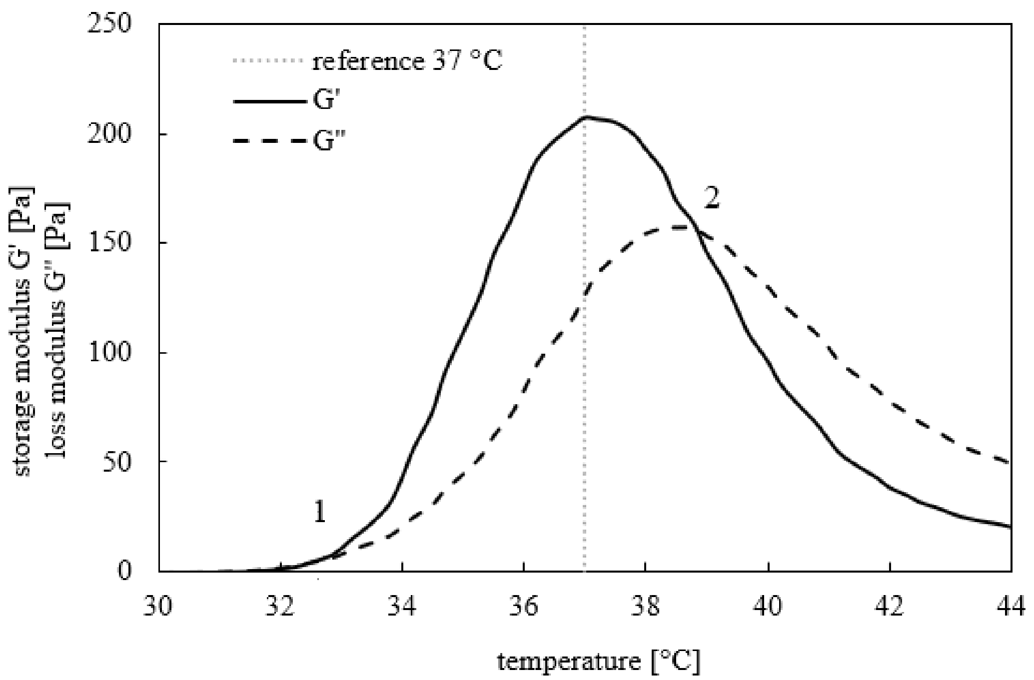

Figure 17: Rheological properties of 20 wt.% aqueous solution of ABA/ITA.

The properties and formation of the physical network have been stated. The copolymer was also photocrosslinked in order to form a hybrid hydrogel. The proof of photocrosslinking has already been confirmed by Zahoranova et al. [40] However, the degree of chemical crosslinking has not been very well studied.

5.2.2 Chemical network

Due to the presence of double bonds at the ends of the copolymer chains, the copolymer may be chemically crosslinked in the presence of a photoinitiator. In this work, a hydrophilic and biocompatible photoinitiator LiTPO was used. This photoinitiator absorbs light with wavelengths below 405 nm (Figure 18) thus producing radicals. Such radicals attack the double bonds and novel covalent bonds are formed (Figure 19). As the micellar physical network needed to be preserved, the temperature of the sample was always kept at 37 °C. The resulting hydrogel consisted of core-crosslinked micellar network. Several methods were used in order to determine the degree of crosslinking.

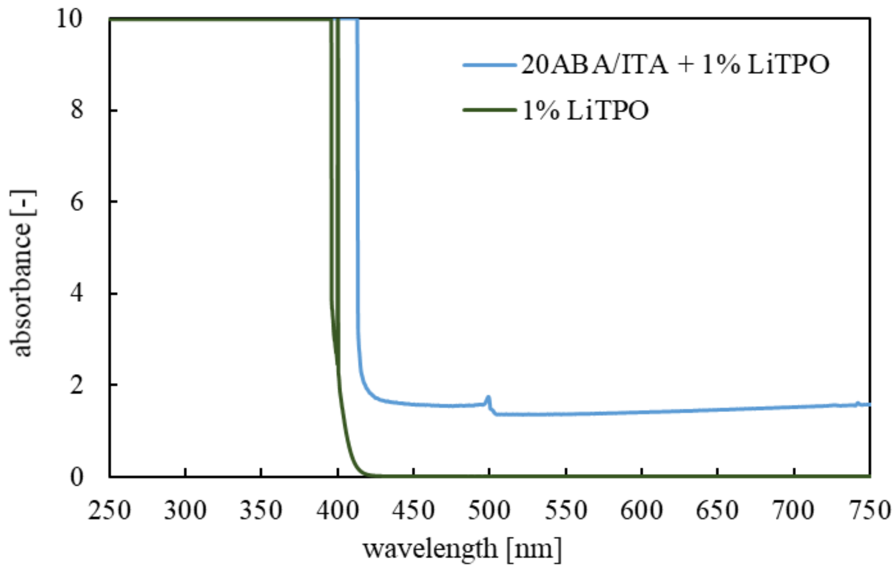

Figure 18: Absorbance of 1 wt.% aqueous solution of LiTPO compared to a sample including the 1 wt.% LiTPO and 20 wt.% aqueous solution of ABA/ITA.

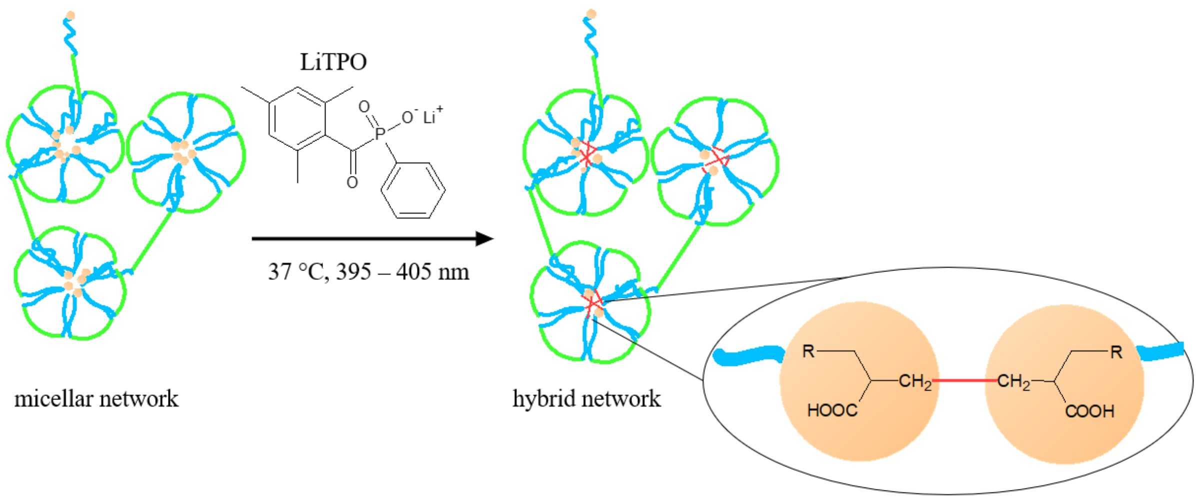

Figure 19: Graphical illustration of the formation of hybrid core-crosslinked micellar network.

5.2.2.1 Raman and IR spectroscopy

As the double bonds are symmetric functional groups, they have a strong intensity band in the Raman spectrum. While infrared spectroscopy is based on dipole moment changes, Raman spectroscopy works on the principle of change in the polarizability of molecular bonds due to photon interactions. Even though liquid samples in general may be analysed by Raman spectroscopy, the hydrogel samples of ABA/ITA were probably not concentrated enough as the microscope detected only the plastic Petri dish below it. Therefore, freeze-dried samples of irradiated and non-irradiated hydrogels were prepared. Different grids were applied during the measurement. Figure 20 shows a freeze-dried ABA/ITA copolymer measured with a 150/500 grid. The double bonds have a characteristic band around 1640 cm^{-1}. In the spectrum measured with a 150/500 grid, the characteristic band for double bonds is not very distinguishable. A comparison of raw data and smoothed data is shown in the zoomed part of the spectrum. Another grid has been applied in order to detect the band. In the spectrum with grid 600 (Figure 21), the 1640 cm^{-1} peak is slightly stronger, however, when compared to the raw data, it seems as if during the smoothing of the spectrum a ‘fake’ peak was formed. The double bonds might not be visible due to the low molar ratio compared to the whole copolymer structure. However, the carboxyl groups in ITA are represented by a weak 1389 cm^{-1} band. In Table 5 the bands are assigned to the appropriate functional groups.

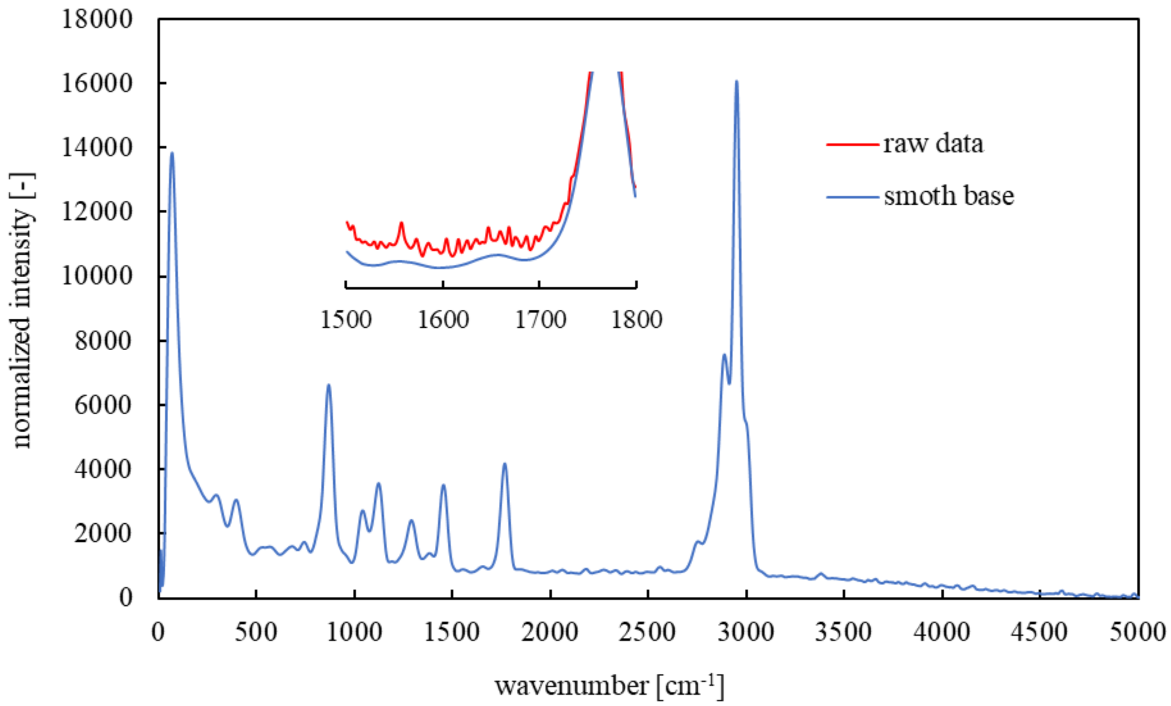

Figure 20: Freeze-dried ABA/ITA with grid 150/500.

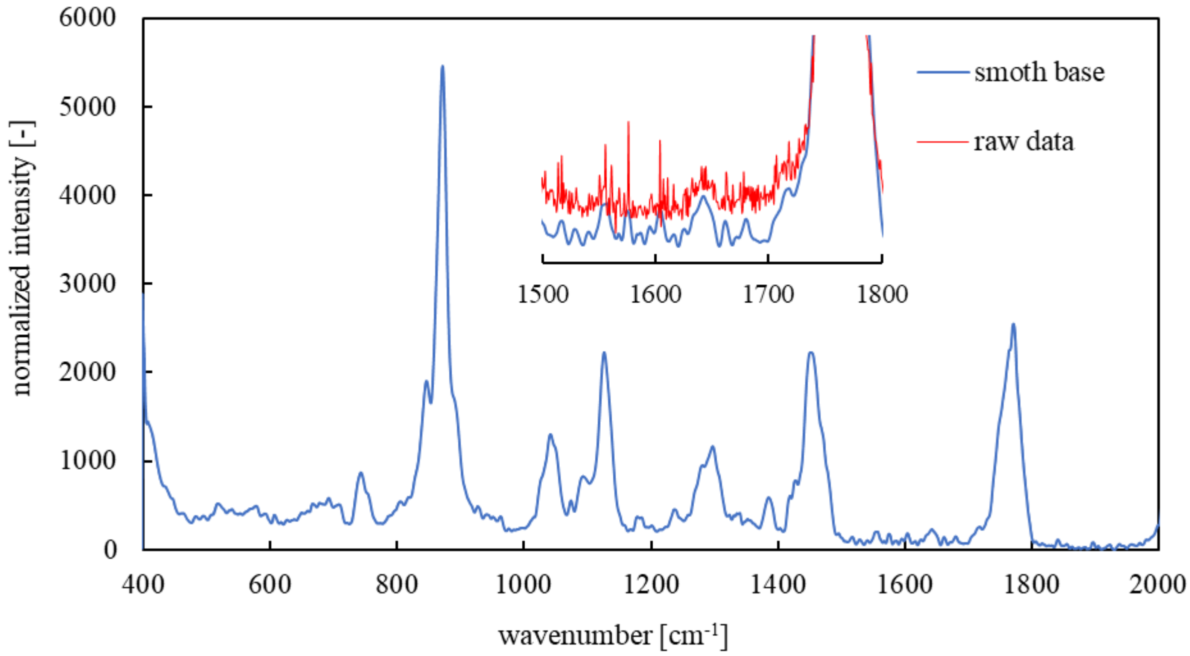

Figure 21: Freeze-dried ABA/ITA with 600 grid.

Table 5: Assigned functional groups to the wavenumbers in Raman spectra. [68]

wavenumber [cm^{-1}]	**functional group**
746	C-C aliphatic chain
845	C-O-C (PEG)
872	-C-C(=O)-O- (LA)
1044, 1073	rocking symmetric CH_2
1092, 1126	C-O-C (PEG)
1299	twist CH_2 (PEG)
1389	$R\text{-}CO_2^-$
1455	bend CH_2 (PEG)
1645	$-C{=}CH_2$
1775	stretch C=O
2887	CH stretch (LA)
2950	CH_3 stretch (LA)

Even though the double bonds did not produce a strong peak in the spectrum, there should theoretically be visible also other changes in the spectrum after photocrosslinking. After irradiation, the peak in the 1640 cm^{-1} area, belonging to double bonds, should reduce in intensity. Moreover, the intensity of the 795 cm^{-1} band should increase as it represents newly formed covalent bonds (RRC-CHR). As in the case of ABA/ITA, the new bonds are in a proximity to carboxyl groups therefore they should be visible also in the 2965 cm^{-1} area.

The Raman spectra of irradiated and non-irradiated gels are shown on Figure 22. Both freeze-dried samples contain 20 wt.% ABA/ITA and 1 wt.% LiTPO so that they could be comparable. The sample called 5 min was irradiated by light of 395 – 405 nm for five minutes whereas the other one was not irradiated at all. On Figure 22 there are also zoomed parts of the spectra containing the crucial areas where the changes were supposed to occur. As it is obvious from the graphs, there are not any noticeable changes in the spectra after irradiation.

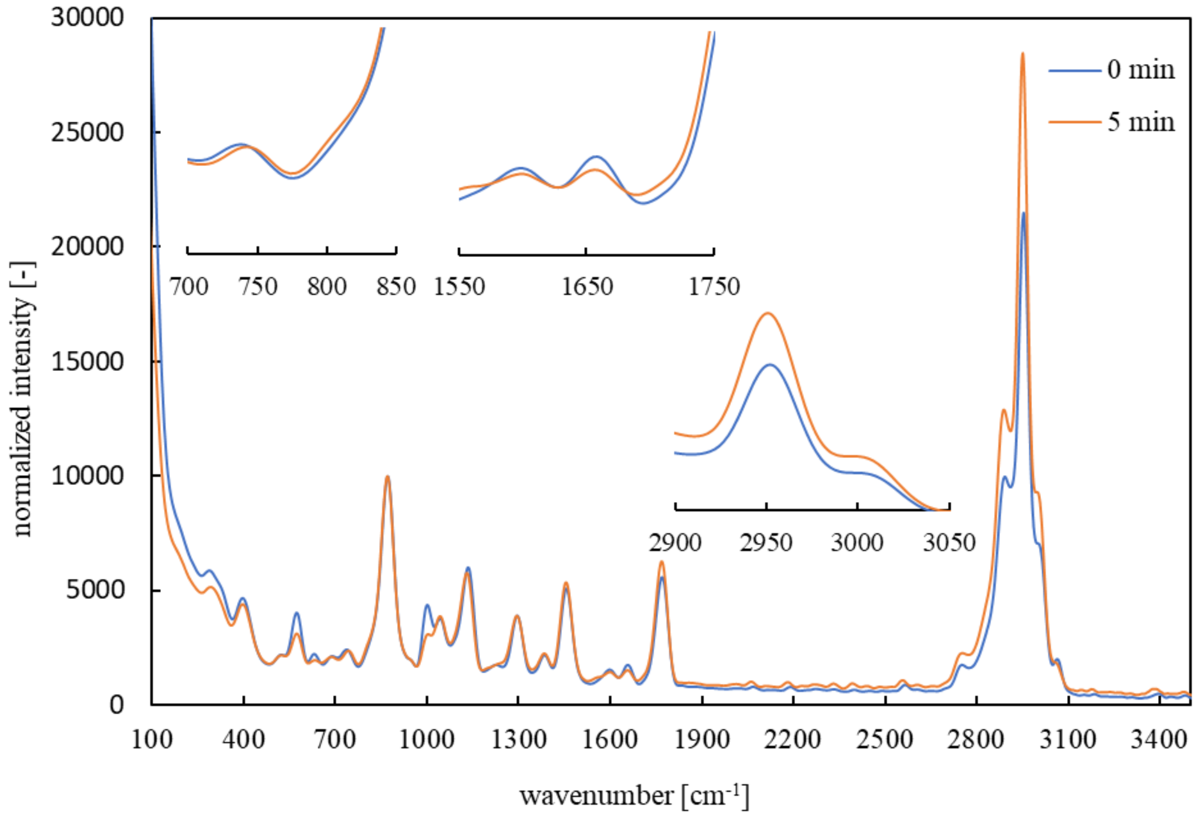

Figure 22: Comparison of Raman spectra before and after irradiation of ABA/ITA with LiTPO.

In order to complete the spectral bands, an IR measurement of ABA/ITA was performed. As the double bonds are close to the carboxyl groups, the COOH group affects the polarity of the double bond. It was then assumed that the band might be also visible in the IR spectrum. The obtained data is shown in Figure 23. Unfortunately, the intensity in the 1640 cm^{-1} band was weak.

The carboxyl groups are represented by the 3500 cm^{-1} band. The 2950 – 2800 cm^{-1} range stands for the CH_2 groups in the polymer chain. The sharp peak at 1755 cm^{-1} is characteristic for carbonyl groups. -O-CH_2- groups are in the 1350 cm^{-1} area. The peak at 1100 cm^{-1} stands for R-CO-R group.

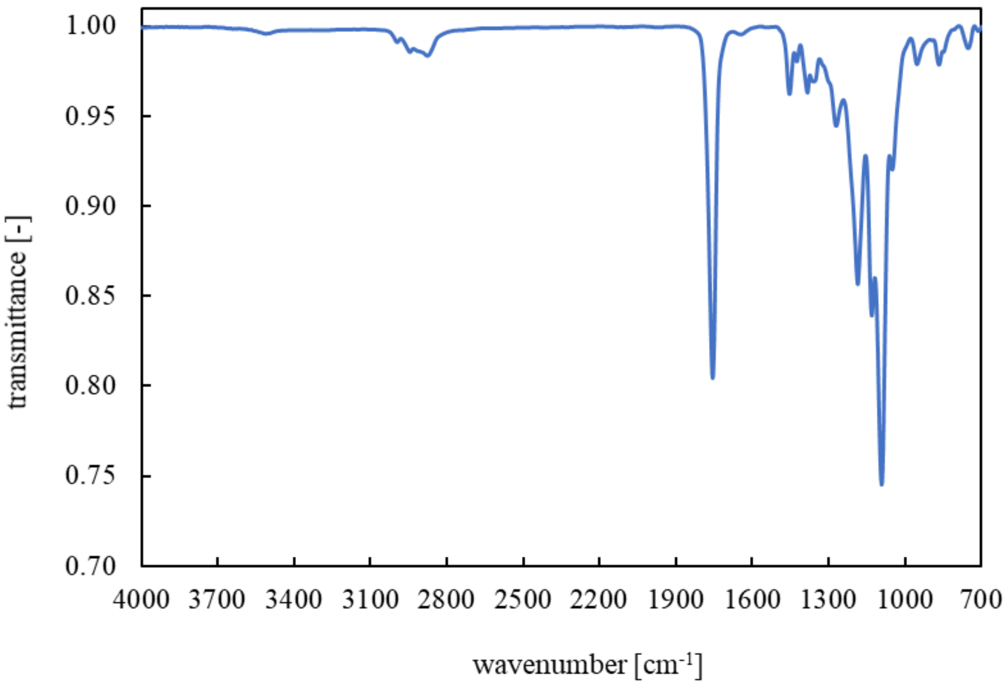

Figure 23: The IR spectrum of ABA/ITA.

From these results, a conclusion has been made that both Raman and IR spectroscopies are not suitable for determination of double bond conversion. To calculate and observe the reduction of double bonds, the ^{1}H NMR spectroscopy would be very helpful. However, it has been found out that the covalently crosslinked hydrogel is insoluble in chloroform. Furthermore, the same issue has occurred for tetrahydrofuran. Hence, GPC analysis of irradiated samples was precluded.

5.2.2.2 Thermogravimetric analysis (TGA)

When the copolymer is crosslinked and new covalent bonds are formed, the thermal stability of the sample is affected. The copolymer with higher crosslinking density should exhibit the highest thermal stability. This property can be analysed by TGA.

The temperature when the sample starts to degrade is called the onset temperature (T_{onset}). For comparison purposes, the T_{onset} was defined as a temperature of 10 % weight loss. The copolymer contains ester bonds that degrade at a maximum rate at the first inflection point of the curves (T_1). The T_1 shifted towards higher temperatures with increasing crosslinking time. The percentage weight loss of the sample did not vary among the samples, meaning that the ratio of ester bonds in the copolymer structure was not affected during crosslinking. The second inflection point (T_2) belongs to the temperature at which the ether bonds of the copolymer degrade at the highest rate. This temperature was measured to be around 395 °C. As we can see from the shift of the T_{onset} and of the curves, the copolymer gets more thermally stable after irradiation. The T_{onset} has shifted by 9.7 °C after irradiating the sample for 30 min. The inflection points and the T_{onset} of the samples are shown in Table 6.

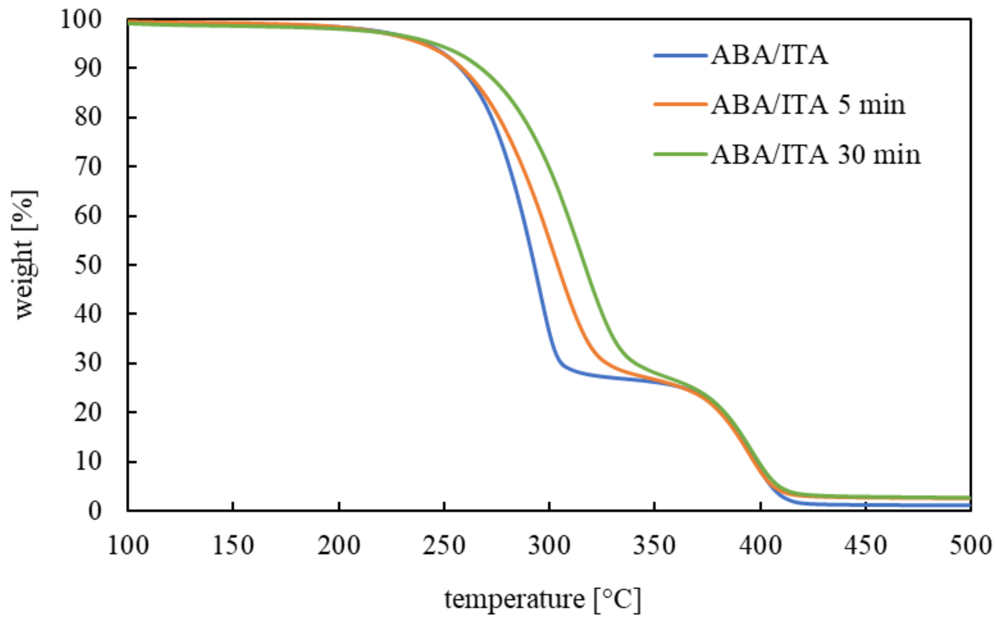

Figure 24: Thermal properties of non-irradiated and irradiated ABA/ITA.

Table 6: The temperatures of start of degradation (T_{onset}), degradation of ester bonds (T_1) and ether bonds (T_2) received from Figure 24.

	T_{onset} [°C]	T_1 [°C]	T_2 [°C]
ABA/ITA	257.8	295.3	396.3
ABA/ITA 5 min	258.4	303.2	394.8
ABA/ITA 30 min	267.4	316.1	395.8

5.2.2.3 Hydrolytic stability in physiological solution

When chemical crosslinking is employed to the hydrogel network, the structure stabilizes and should exhibit longer life-time. The hydrolytic stability was studied in inserts with membrane enabling the transfer of molecules smaller than 0.4 µm. The hydrogel samples were immersed in physiological solution and left at physiological temperature. The hydrogel absorbed water, swelled, thus triggering the hydrolytic cleavage of ester bonds. The hydrolytic stability of physical hydrogel and hybrid hydrogels irradiated for different times are shown in Figure 25. During the first 11 days of the experiment, an increase of mass of the hydrogel is observed. The swelling reached 40 % in the inserts. Afterwards, the hydrogel structure collapsed and a fast decrease in mass was observed. From this measurement, a bulk degradation can be concluded as the diffusion of water is faster than degradation. The hydrogels irradiated for two and four minutes do not exhibit observable prolonged stability. The stability of the hybrid hydrogel irradiated for six minutes was extended to 12 days.

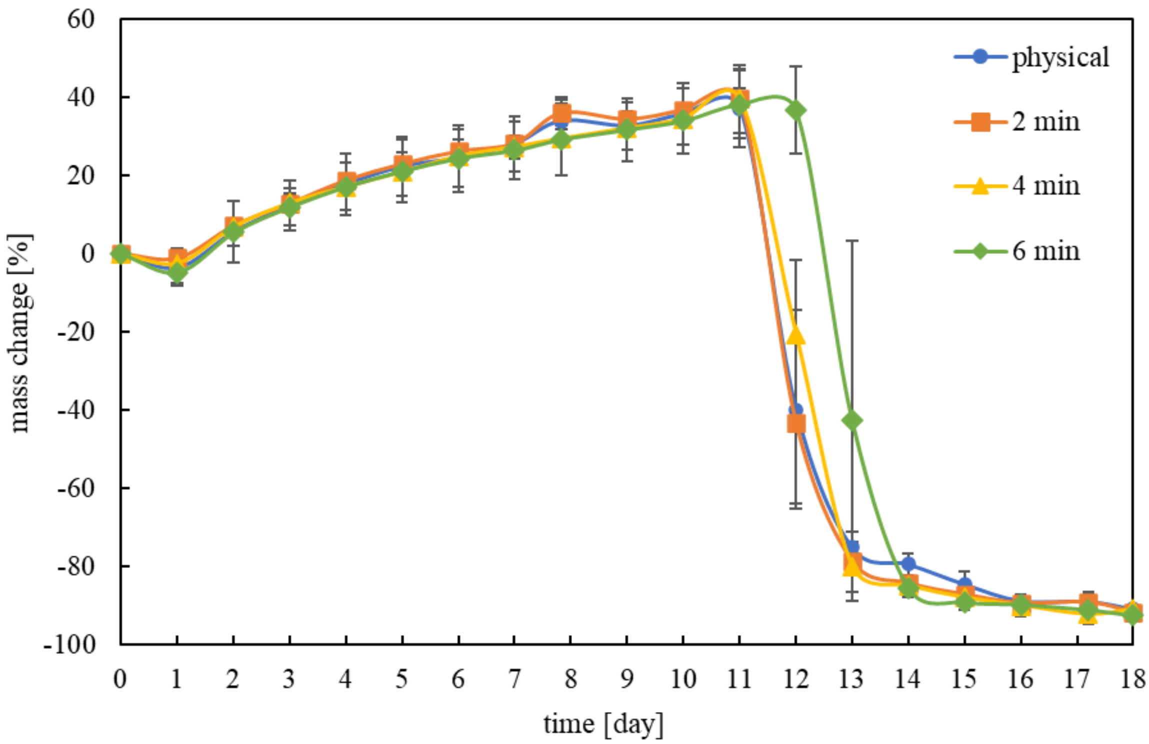

Figure 25: Comparison of the hydrolytic stability in physiological solution of physical and hybrid hydrogels irradiated for 2, 4, and 6 min.

During the experiment, the immersion solutions were changed at each time interval. pH values were measured and can be seen in Figure 26. The copolymer is of an acidic nature. The degradation products are lactic, glycolic acid and PEG. The acids cause a decrease in the pH of the physiological solution. During the first 12 days, there is a slight decrease in pH due to the degradation. Once most of the hydrogel degraded, the pH rose up to 4.75. Interestingly, the physical hydrogel exhibited in general the highest pH values during the experiment. However, the difference is quite insignificant.

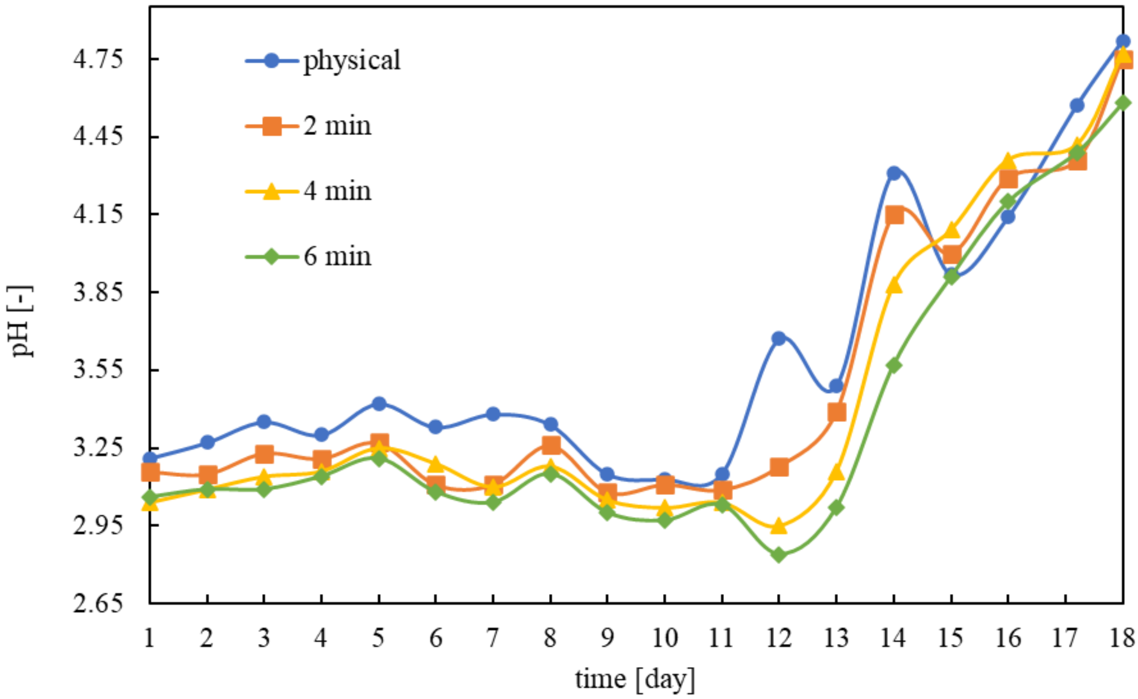

Figure 26: pH values of the immersion solution (physiological solution) during a hydrolytic stability experiment of physical and hybrid hydrogels irradiated for 2, 4, and 6 min.

The hybrid hydrogel irradiated for six minutes exhibited the longest stability as it can be observed in Figure 25. In order to determine whether even longer irradiation time would result in a denser chemical network and more stable hydrogels, another experiment was performed with samples irradiated for 5, 10, 20 and 30 min (Figure 27). The hydrolytic stability increased with increasing irradiation time from 11 to 14 days.

Usually with a denser hydrogel network, the hydrogel is capable of absorbing less water. In the case of ABA/ITA hybrid hydrogels, the swelling is increased with longer irradiation time. Therefore, it is behaving in an opposite manner. As the hybrid hydrogel network consists of core-crosslinked micelles, more covalent bonds linking the micellar core might cause size reduction of micelles. Smaller micelles result in a larger inter-micellar spaces allowing the absorption of more water. The hydrogel irradiated for five minutes swelled up to 46 % compared to the hydrogel irradiated for 30 min that swelled up to 72 % in maximum.

The photos of the hybrid hydrogel irradiated for 30 min after 8, 14 and 15 days in the physiological solution are shown in Figure 28. There is a visible decrease in hydrogel volume after 14 days due to degradation however the hydrogel network is intact. Whereas the disruption in the hydrogel network can be observed after 15 days.

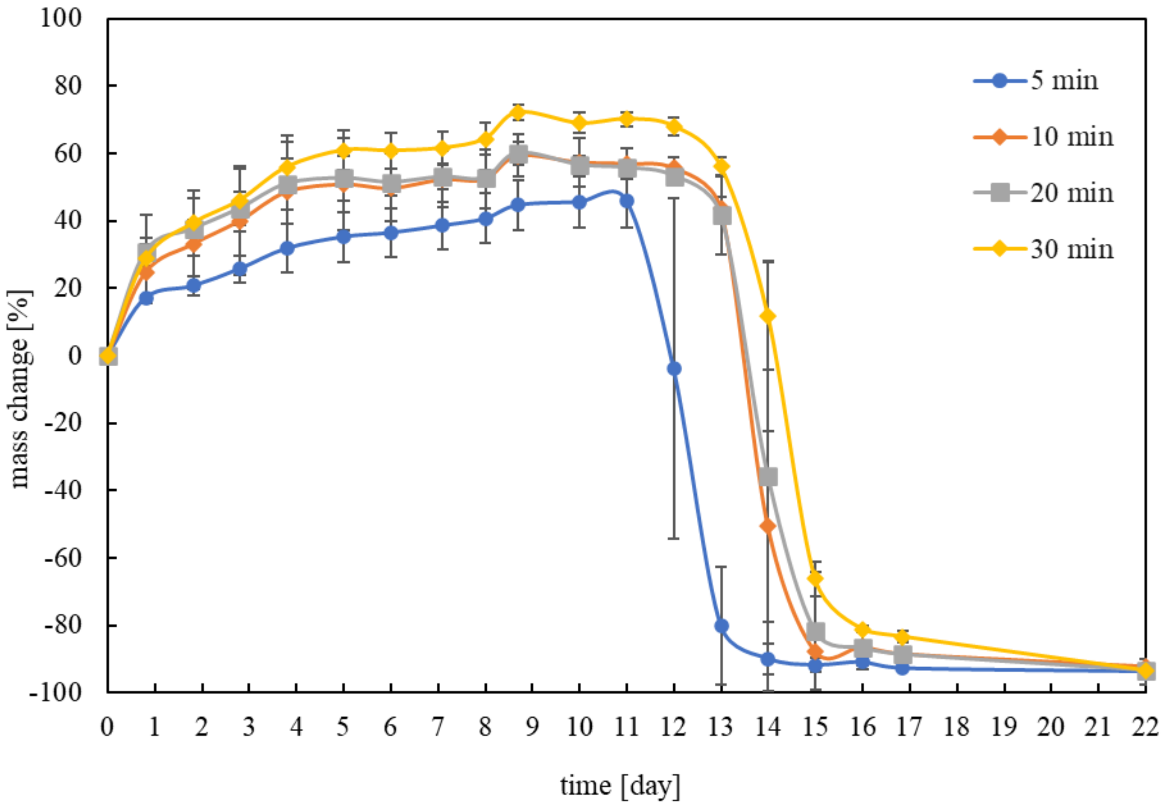

Figure 27: Hydrolytic stability of hybrid hydrogels irradiated for 5, 10, 20, and 30 min in physiological solution at 37 C.

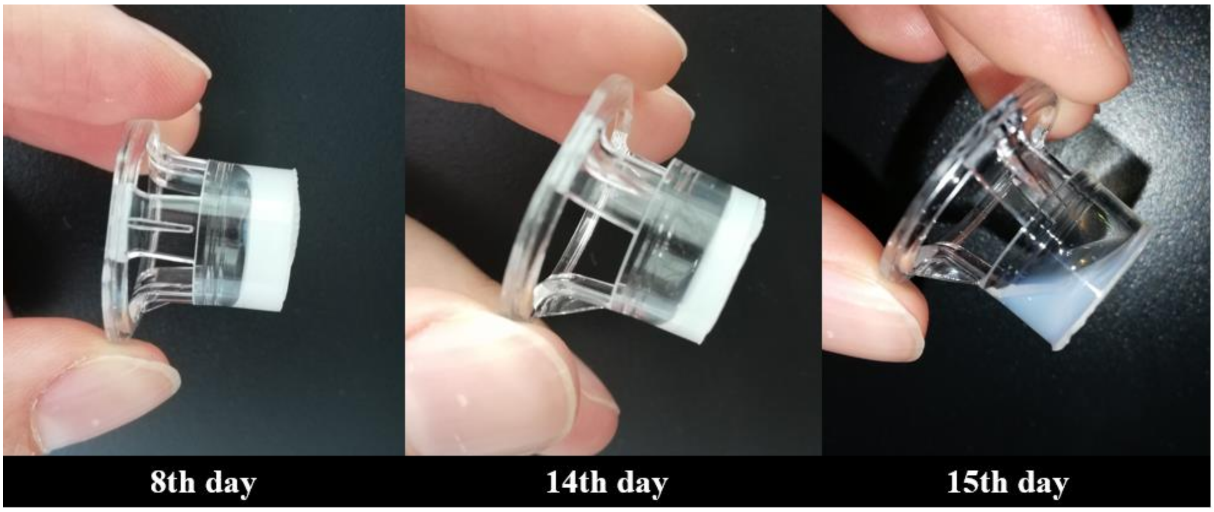

Figure 28: The hybrid hydrogel irradiated for 30 min in an insert during the hydrolytic stability experiment in physiological solution at 37 °C.

pH values of the removed physiological solution at each time interval were measured. The solutions exhibited acidic pH due to the presence of degradation products of the hydrogel. As it can be seen in Figure 29, the pH increased after 15 days when most of the hydrogel had already degraded.

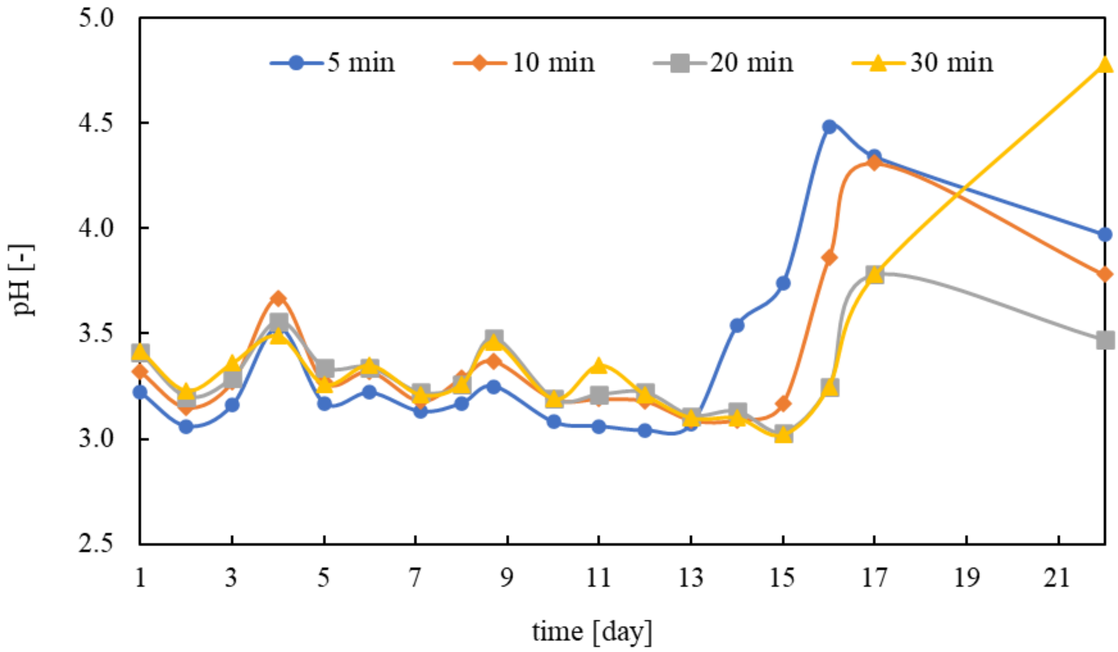

Figure 29: pH values of the immersion solutions at each time interval during hydrolytic stability experiment of hybrid hydrogels irradiated for 5, 10, 20, and 30 min.

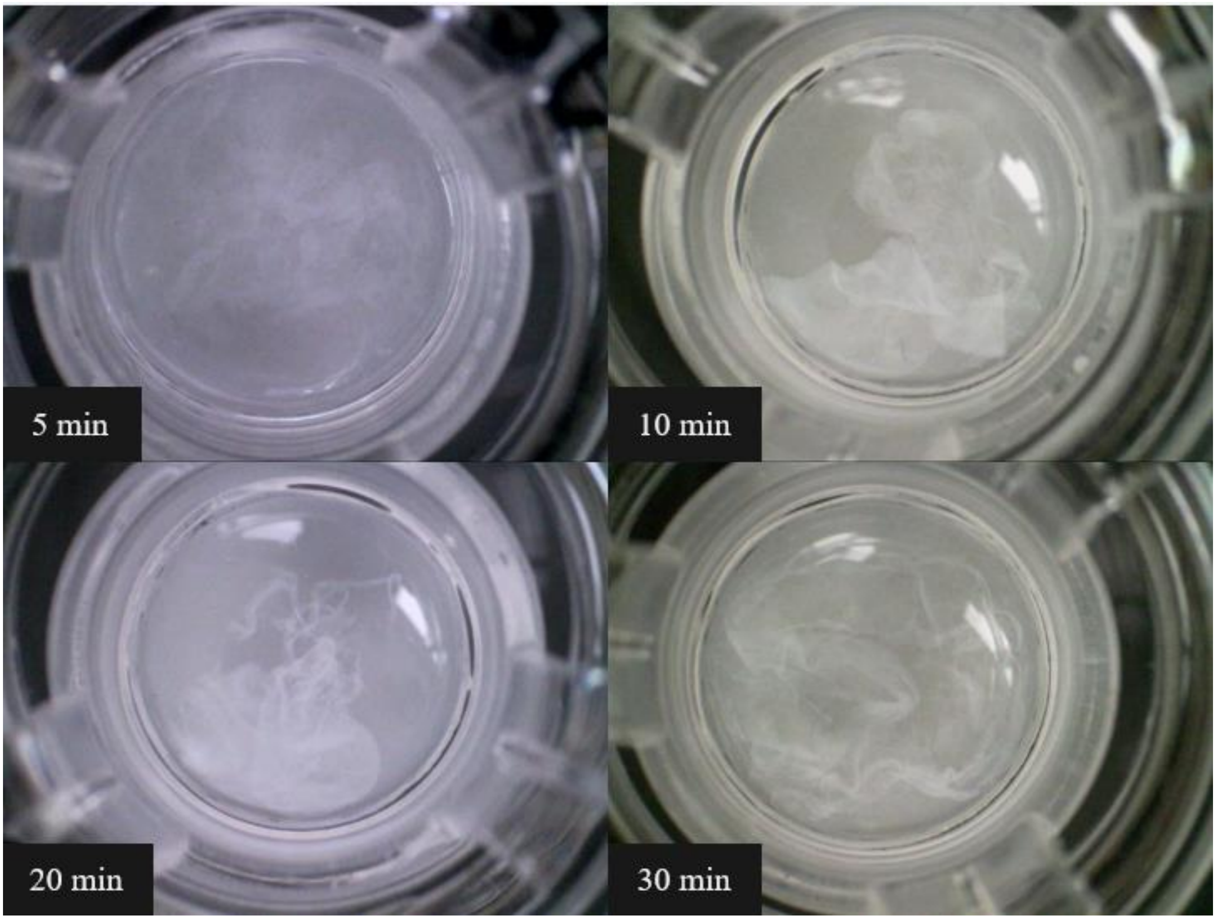

Figure 30: The residual fractions of hybrid hydrogels irradiated for different times after 18 days in physiological solution at 37 °C.

Even after 17 days in the physiological solution, there was still some hydrogel left in the inserts. The amount of residual hydrogel in the inserts increased with increasing irradiation time. For the hydrogel irradiated for five minutes 7.2 % of the mass stayed. In the case of 10 min irradiation, 11.5 % did not degrade yet. For the 20 min irradiated hydrogel, 11.4 % of hydrogel was weighed in the insert and for 30 min hybrid hydrogel, even 16.6 % did not migrate through the membrane. This could be the chemically crosslinked fraction of the hybrid hydrogel. The non-degraded parts of the hybrid hydrogels are shown in Figure 30.

5.2.2.4 Hydrolytic stability in PBS

The pH values of the immersion solutions were very acidic, therefore the use of buffer was considered instead of the physiological solution. Buffers are used to reduce the changes in pH. Moreover, when the pH of the hydrogel was measured, it was determined to be 2.35. This value is very low. Several bioactive compounds, especially those based on protein structure, would denature and lose their bioactive properties. In order to solve these problems, the ABA/ITA copolymer was dissolved in phosphate buffer solution (PBS) of pH 7.5 to form a hydrogel and such hydrogel was immersed in the same PBS solution. The 20wt.% PBS hydrogel had a pH of 4.05. This value is very much more acceptable.

Samples of PBS hydrogels were prepared and immersed in PBS and left at 37 °C. After one day in the buffer solution, the hydrogel structure of the samples was disrupted. In order to determine whether the problem was the more neutral pH, hydrogels were prepared and half of them were immersed in PBS of pH 4 and the other half in PBS with pH 7. The result can be seen on Figure 31. The hydrogels in the inserts are prepared in the same way, the only difference is the pH of the immersion solution.

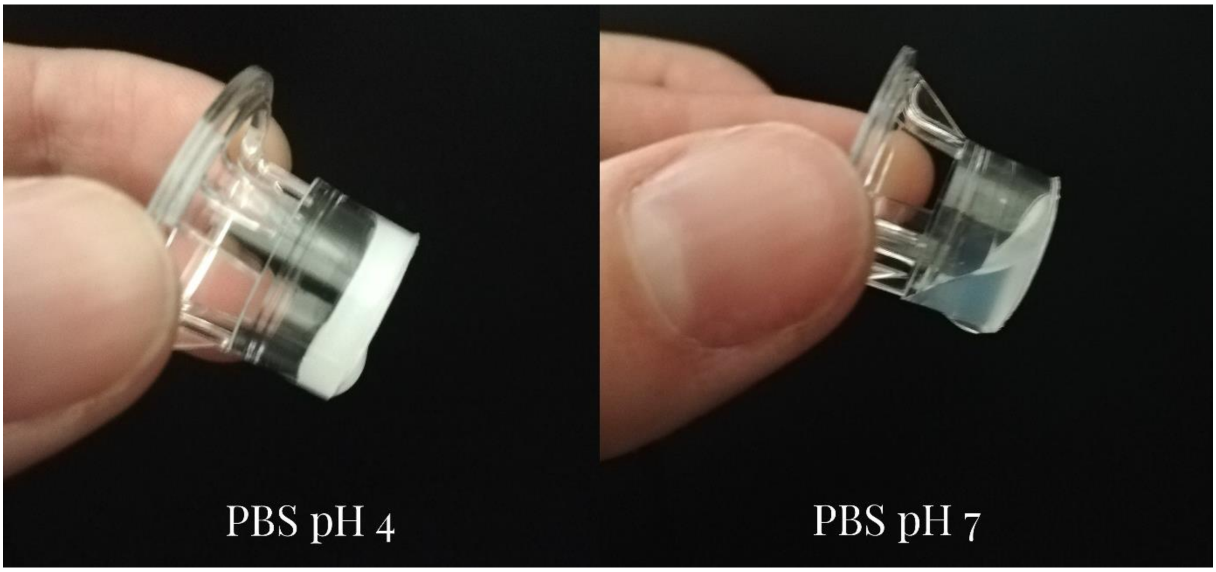

Figure 31: Physically crosslinked hydrogels of 20 wt.% ABA/ITA immersed in PBS either with pH 4 or 7 and left overnight at 37 °C.

At acidic pH, the carboxyl groups at the ends of the copolymer chains form hydrogen bonds that help to hold the micellar structure. However, when the pH is increased, the carboxyl groups dissociate causing the disruption of micellar structures due to electrostatic repulsion [8]. The pH of human blood equals to 7.4. As in this work, the application of the hydrogel is aimed towards wound dressings, the stability of the hydrogel at neutral pH is crucial. Carboxyl groups cause the disruption of the structure therefore to solve this problem, we chose to mask the carboxyl groups to prevent it from dissociation.

5.3 Synthesis and characterization of *α,ω-N*-butylitaconamide-PLGA-PEG-PLGA

To mask the carboxyl groups and prevent their dissociation at neutral pH, a small molecule of butylamine was bonded to the functional groups. The carboxyl groups were firstly activated by EDC and stabilized by NHS before the addition of butylamine. The reaction is very simple as it can take place in an aqueous solution at room temperature. The modification was carried out after copolymer purification and lyophilization in order to determine the exact mass of the product after synthesis. The copolymer batch was then again dissolved in UPW and the butylamine modification was performed. The butylamine is linked to the copolymer chain via an amide bond. As urea is produced during the reaction as a side product and the EDC is cytotoxic, the copolymer solution was again purified to get rid of them. The copolymer was precipitated from the solution at 80 °C and decanted. Both EDC and urea are very soluble in water therefore they are washed out during decantation. The modified copolymer *α,ω-N*-butylitaconamide-PLGA-PEG-PLGA (butyl-ABA/ITA) was freeze-dried.

GPC and ^{1}H NMR analyses were performed on three batches of masked copolymers to confirm the modification. The received average values are shown in Table 7.

Table 7: Average values of butyl-ABA/ITA received from GPC (^{a}) and NMR (^{b}) compared to the measured values of ABA/ITA.

	M_n [g/mol]		PDI	PLGA/PEG [wt./wt.]	LA/GA [mol/mol]	butyl [mol.%]
ABA/ITA	5 878 ± 88^{a}	5473 ± 52^{b}	1.12 ± 0.01^{a}	2.64 ± 0.04^{b}	2.92 ± 0.04^{b}	-
butyl-ABA/ITA	5 638 ± 97^{a}	5678 ± 43^{b}	1.13 ± 0.03^{a}	2.78 ± 0.04^{b}	3.07 ± 0.04^{b}	54.3 ± 1.3^{b}

According to the data from GPC and ^{1}H NMR, the structure of the copolymer was not affected by the EDC/NHS activation and subsequent butylamine modification. The degree of copolymer modification by butylamine was calculated from the ^{1}H NMR spectrum to 54.3 mol.%. When compared to the amount of ITA, approximately 85 % of carboxyl groups were masked.

The ^{1}H NMR spectrum of butyl-ABA/ITA compared to ABA/ITA with assigned peaks to the protons in the structure is shown on Figure 32. The peaks belonging to the protons on butylamide are coloured in red. The proton on nitrogen of the amide bond is represented by a singlet at 7.83 ppm. The chemical shifts of protons on butyl decrease with further position from the amide group. The degree of modification was calculated from the peaks coloured in red. At the range from 6.5 to 5.5 ppm the protons on double bonds are visible (Figure 32, no.6). As the modification by butylamine did not undergo at 100 %, the peaks at the 6.31 and 5.73 ppm are still present however with lower intensity. New peaks at this area have formed. These represent protons on the double bond influenced by the amide group. With butyl bonded through the amide bond to the carboxyl group, the chemical shift of protons marked with no. 6 decreases to 6.15 and 5.52 ppm.

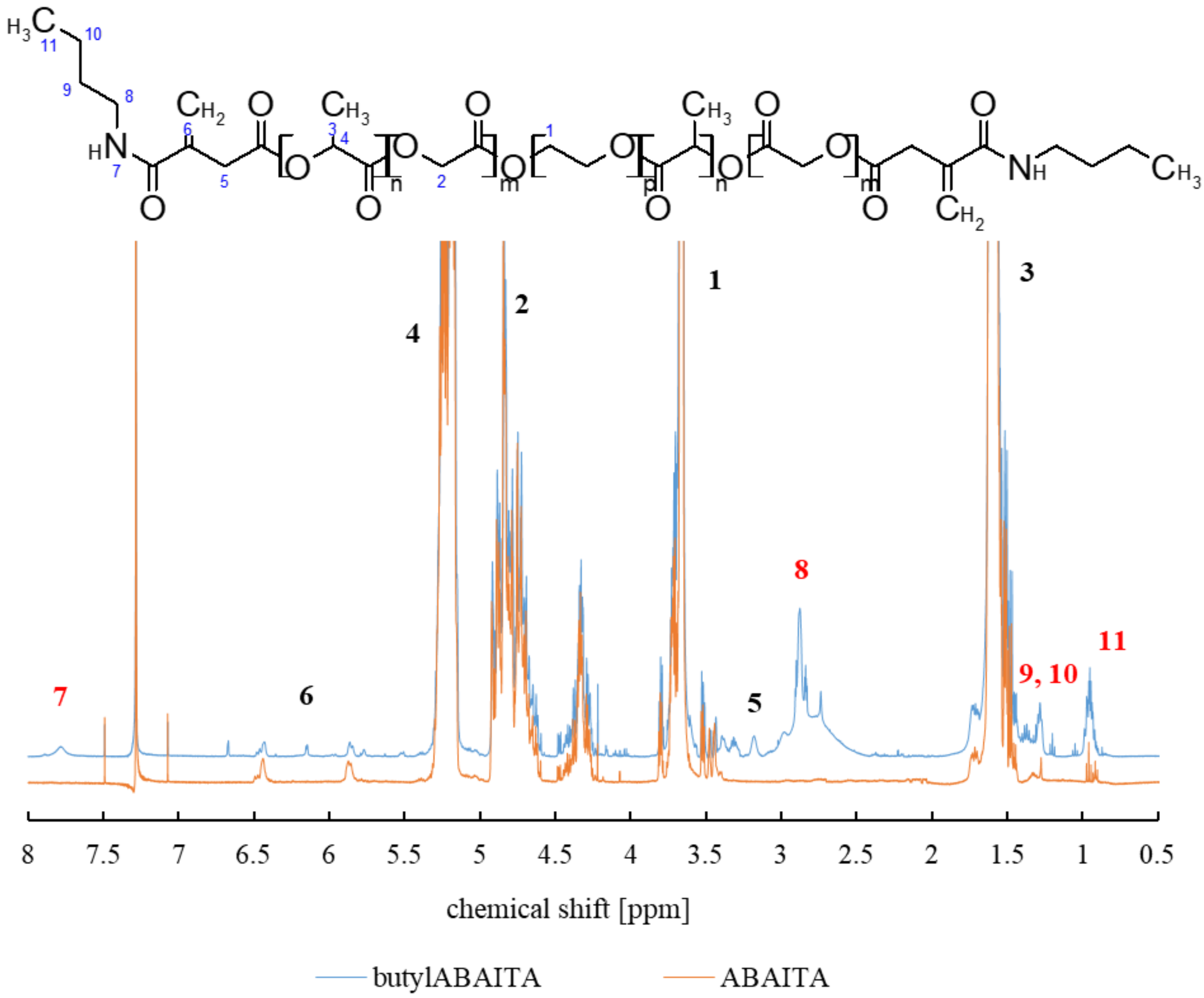

Figure 32: [1]H NMR spectrum of butyl-ABA/ITA compared to ABA/ITA.

To prove the butylamine modification, FTIR analysis was performed on the ABA/ITA and butyl-ABA/ITA copolymers as well. The spectrum is shown in Figure 33. According to the literature, the bands specific for amides are around 3 300 cm^{-1} and 1 570 cm^{-1}. The 3 300 cm^{-1} band is shownion Figure 34 and stands for an NH stretch in monosubstituted amides. The CN stretch is demonstrated by the 1 570 cm^{-1} band in Figure 35.

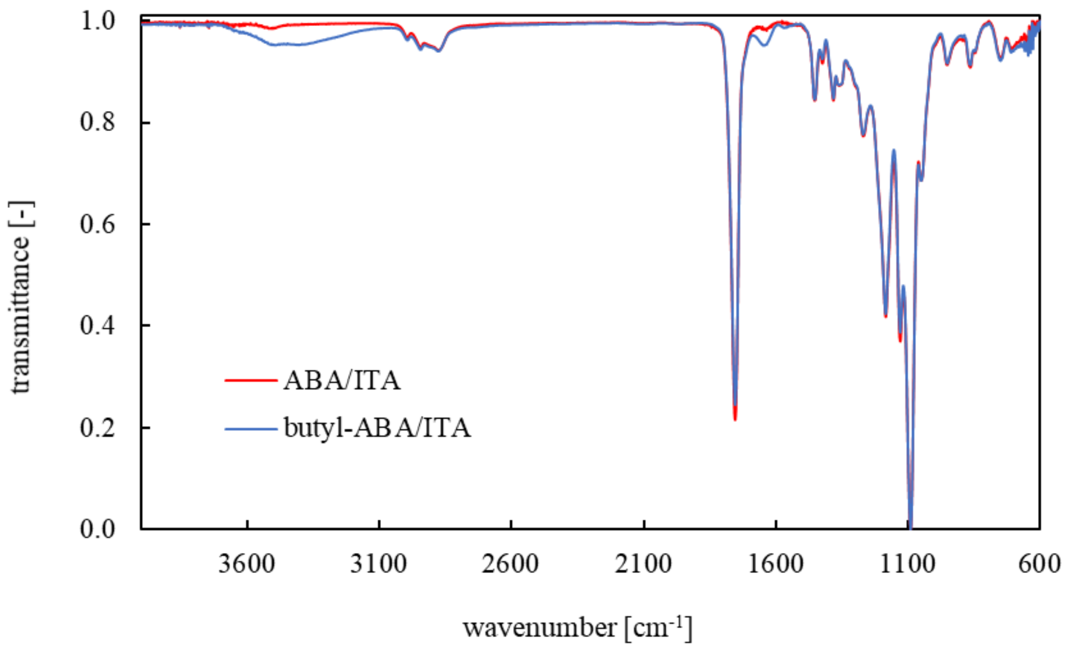

Figure 33: FTIR spectrum of butyl-ABA/ITA and ABA/ITA.

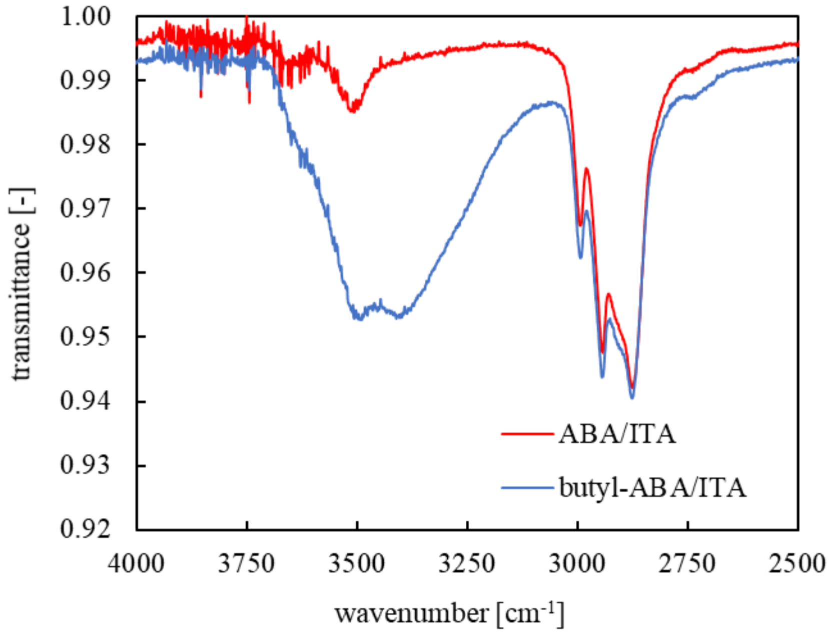

Figure 34: Zoom of the FTIR spectra of ABA/ITA and butyl-ABA/ITA on NH stretch.

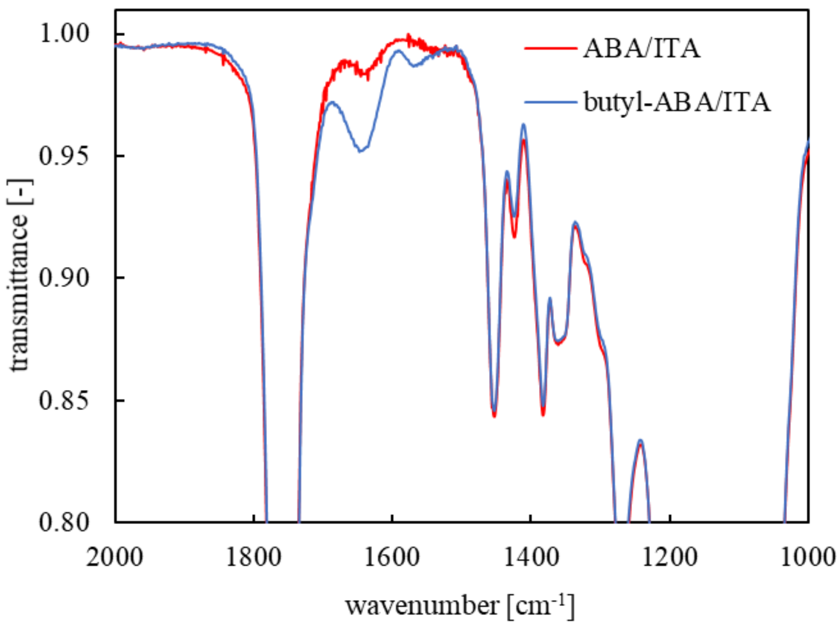

Figure 35: Zoom of the FTIR spectra of ABA/ITA and butyl-ABA/ITA on CN stretch band.

5.4 Crosslinking of *α*,*ω*-*N*-butylitaconamide-PLGA-PEG-PLGA

5.4.1 Physical network

The modified structure of the copolymer would affect the thermogelling properties of the copolymer. In order to determine how much, the viscoelastic properties of the butyl-ABA/ITA hydrogel were analysed. The rheological properties of 20wt.% solutions of ABA/ITA and butyl-ABA/ITA in UPW are compared in Figure 36. After butyl modification, the temperature window when the solution is in the form of a gel has shifted towards higher temperatures. The sol-gel transition has moved to 35.3 °C, the gel to suspension transition to 41.2 °C and the temperature at which the gel exhibits the highest stiffness to 39.8 °C. However, the solution is still capable of forming a hydrogel at the physiological temperature.

For application purposes, a different solution was considered. The rheological properties of the 20wt.% copolymer solutions in UPW and PBS are shown in Figure 37. The influence of the different solvents is apparent. The copolymer in PBS exhibited higher stiffness compared to the one in UPW. Moreover, the transition temperatures shifted closer to the original values of ABA/ITA. PBS contains phosphate salts as well as sodium chloride. Salts can be divided into kosmotropes and chaotropes according to their influence on the hydrophobic effect. Kosmotropes, such as sodium chloride or phosphate, enhance the hydrophobic effect by tightening the structure of water molecules around. [69]

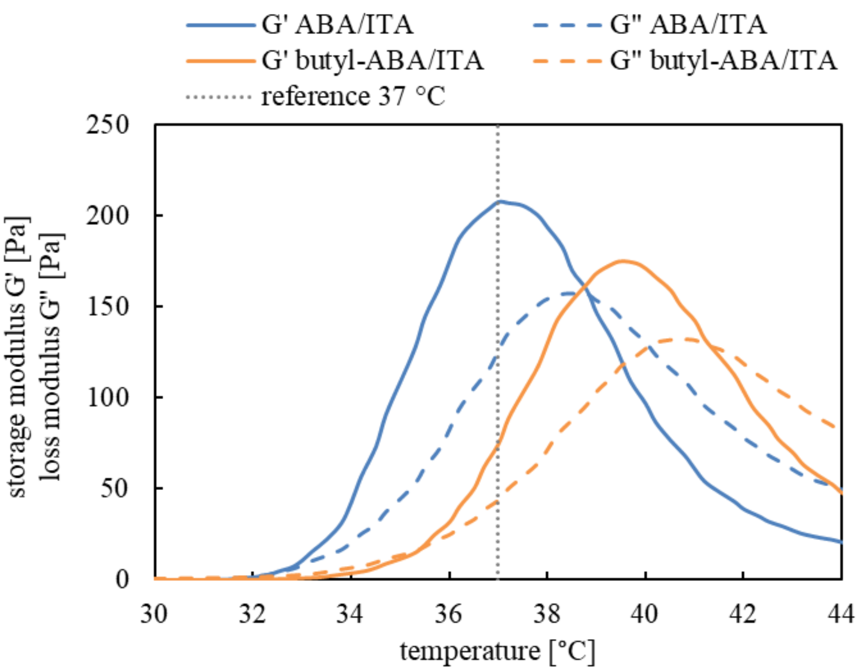

Figure 36: Rheological properties of 20wt.% aqueous solutions of ABA/ITA and butyl-ABA/ITA.

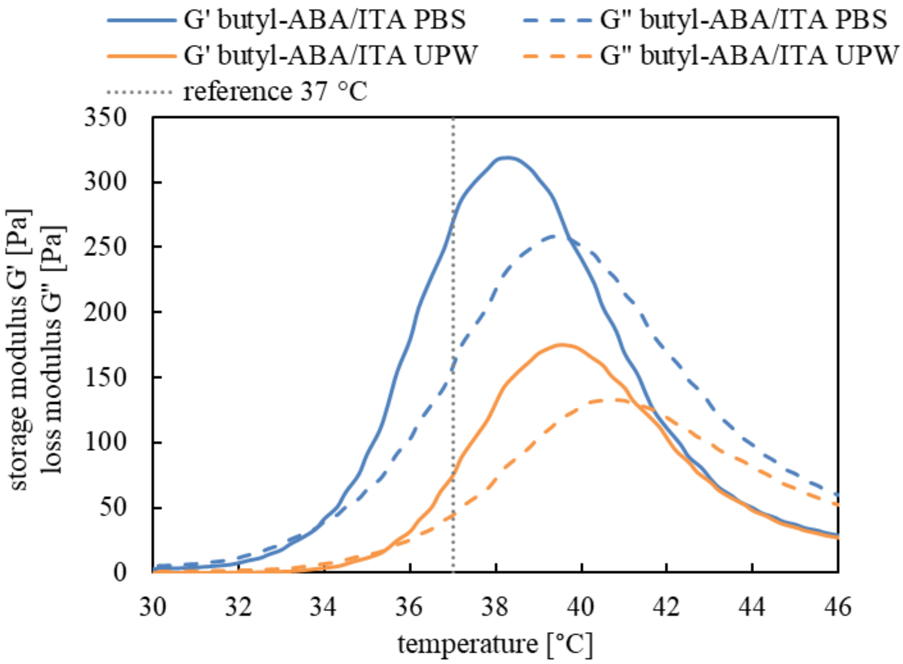

Figure 37: The influence of solution on the rheological properties of 20wt.% solutions of butyl-ABA/ITA.

5.4.2 Chemical network

The influence of photocrosslinking on the hydrogel and copolymer was studied. As Raman and FTIR spectroscopy could not detect the double bonds and therefore were unable to determine the degree of crosslinking, they were no longer applied to butyl-ABA/ITA.

5.4.2.1 Rheological analyses

The effect of photocrosslinking on the mechanical properties of 20wt.% solution of butyl-ABA/ITA was studied. The viscoelastic curves under oscillation stress of 20wt.% aqueous solutions are shown in Figure 38. After the addition of the photoinitiator LiTPO, the storage and loss moduli decreased. The decrease of viscosity of the hydrogels in the presence of LiTPO was observed by Habánková (2017) [70]. The mechanical properties of the hydrogel improved after photocrosslinking for 30 min.

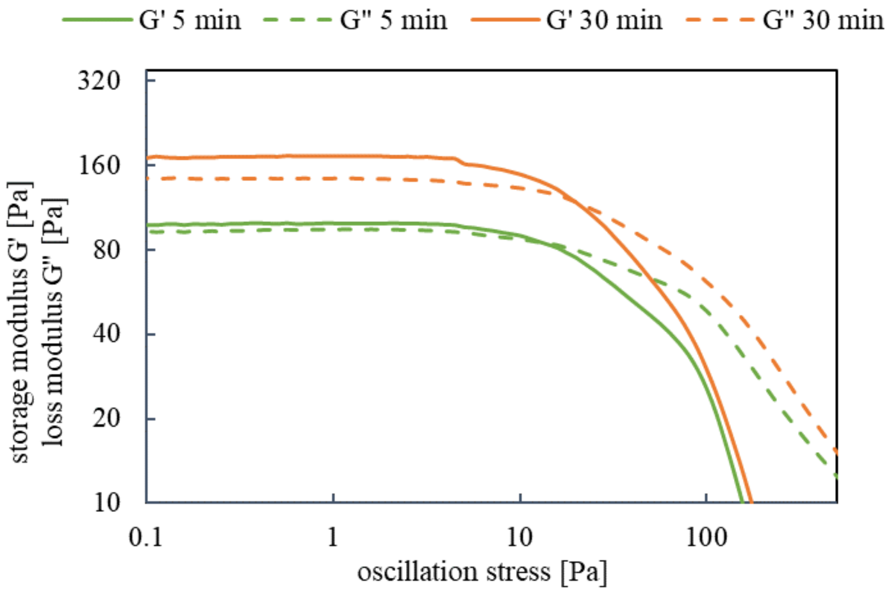

Figure 38: The influence of chemical crosslinking on the viscoelastic properties of 20wt.% butyl-ABA/ITA solutions in UPW.

The same measurement was performed also on hydrogel prepared in PBS. The stiffness of the hydrogels is improved at both irradiation times compared to the hydrogels in UPW. The hybrid hydrogel irradiated for 30 min exhibited higher G’ than physically stabilized hydrogel.

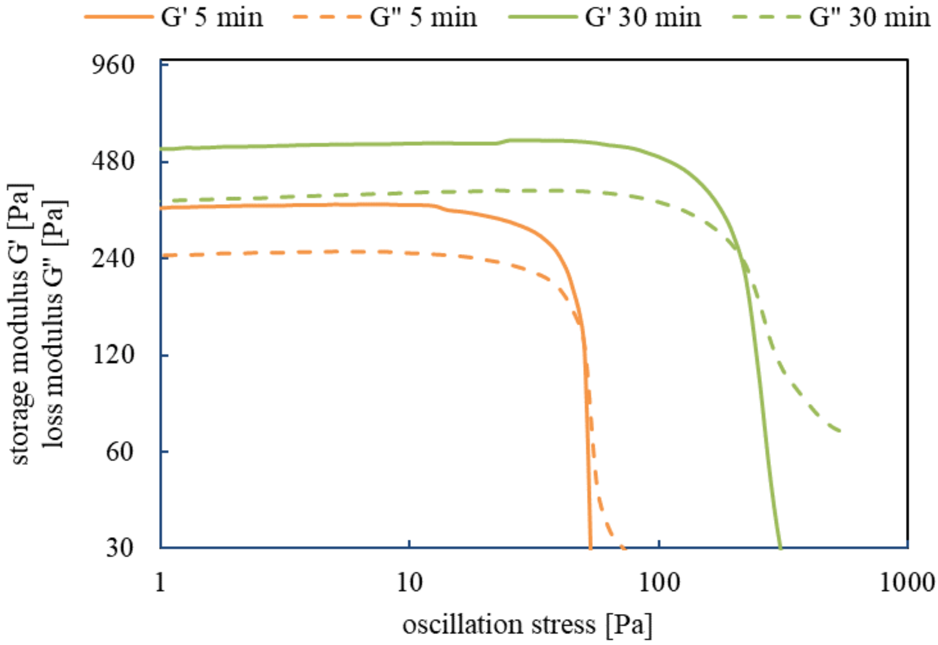

Figure 39: The effect of chemical crosslinking on the viscoelastic properties of 20wt.% butyl-ABA/ITA solutions in PBS.

5.4.2.2 Thermogravimetric analysis

The influence of photocrosslinking on thermal stability of freeze-dried butyl-ABA/ITA copolymer was determined as well. The TGA curves are shown on Figure 40. A shift of the degradation curves is observable in the case of the copolymer irradiated for 30 min. The difference between non-irradiated and irradiated for 5 min is not quite distinguishable. More measurements would have to be performed to diminish the deviation caused by sample preparation. For now, it cannot be concluded for sure whether the issue was that 5 min irradiation is not long enough for covalent crosslinks to form and to be visible on the TGA curve or whether a mistake had occurred during a sample preparation.

The difference in the TGA curves of ABA/ITA and butyl-ABA/ITA is noticeable between 200 and 250 °C. An additional weight decrease appeared. The first derivative of weight was calculated, and the curves are shown in Figure 41. The new inflection point is more apparent on this graph. The first inflection point belongs to amide bonds and has a value of around 212 °C. Ester bonds in the copolymer structure degrade the fastest at the next inflection point of around 284.0 to 302.2 °C. The last inflection point stands for the degradation of ether bonds and is around 394.0 to 395.9 °C.

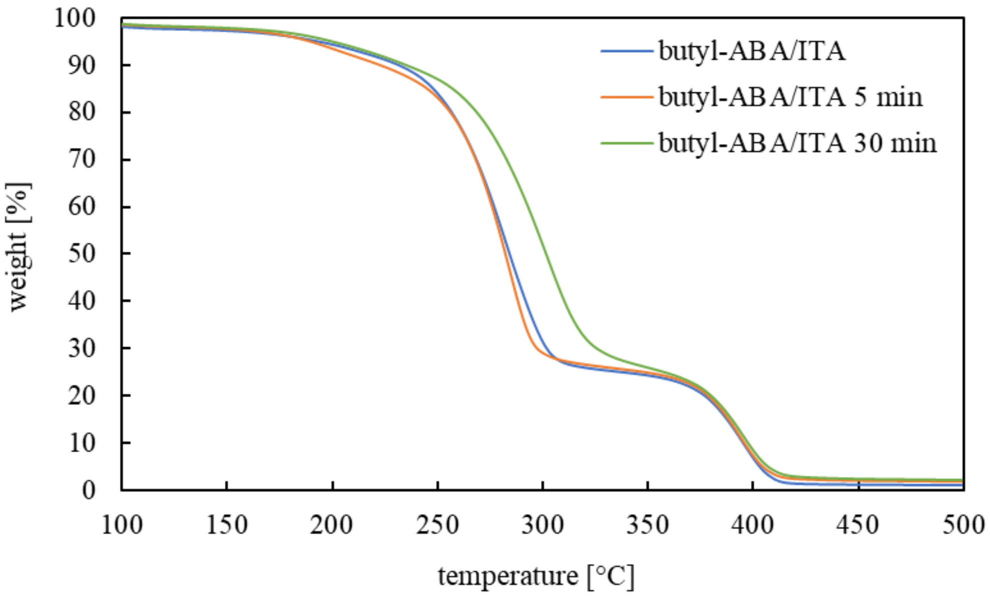

Figure 40: TGA curves of irradiated and non-irradiated butyl-ABA/ITA.

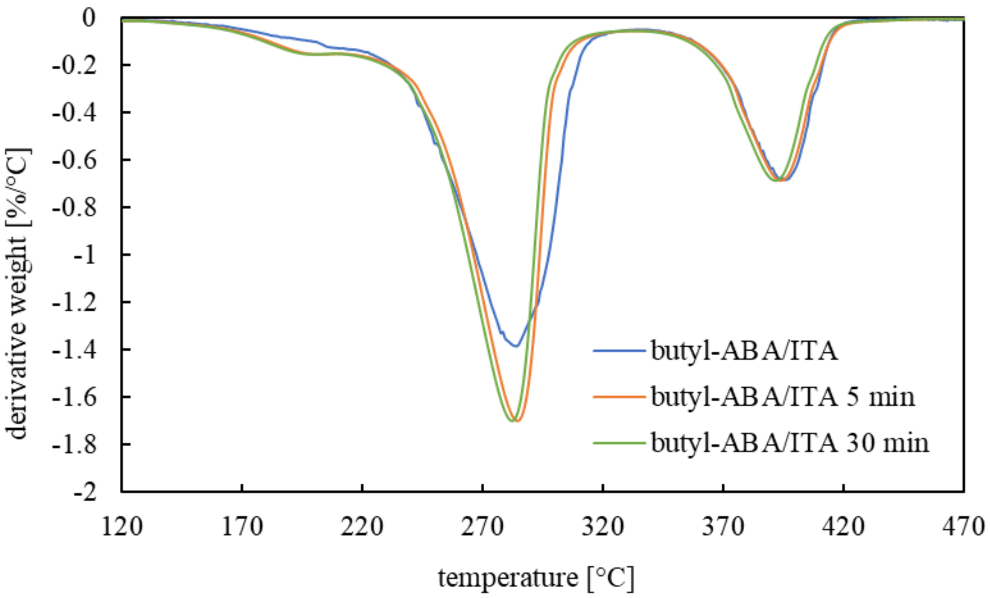

Figure 41: First derivative of weight of TGA curves.

5.4.2.3 Hydrolytic stability in PBS

The hydrolytic stability of hydrogels prepared from 20wt.% solution of butyl-ABA/ITA was determined only in PBS. The butyl modification was solely done to improve the hydrogel stability in PBS at 37 °C.

Firstly, 20wt.% solutions of butyl-ABA/ITA were prepared in PBS. Physical network was formed at 37 °C and several samples were irradiated for 5, 10, 20, and 30 min to form hybrid hydrogels. These samples were then immersed in PBS and left at 37 °C. The inserts were weighed at appropriate time intervals and the immersion solution was exchanged. The hydrolytic stability of these PBS hydrogels is shown in Figure 42. The stability of the hydrogels was improved after masking the carboxyl groups by butylamine however the hydrogels still degraded very fast. Surprisingly, the non-irradiated physical hydrogel exhibited the best stability. The stability of the hybrid hydrogels could have been affected by the presence of the photoinitiator that decreased the viscosity of the samples and could have influenced the micelle formation.

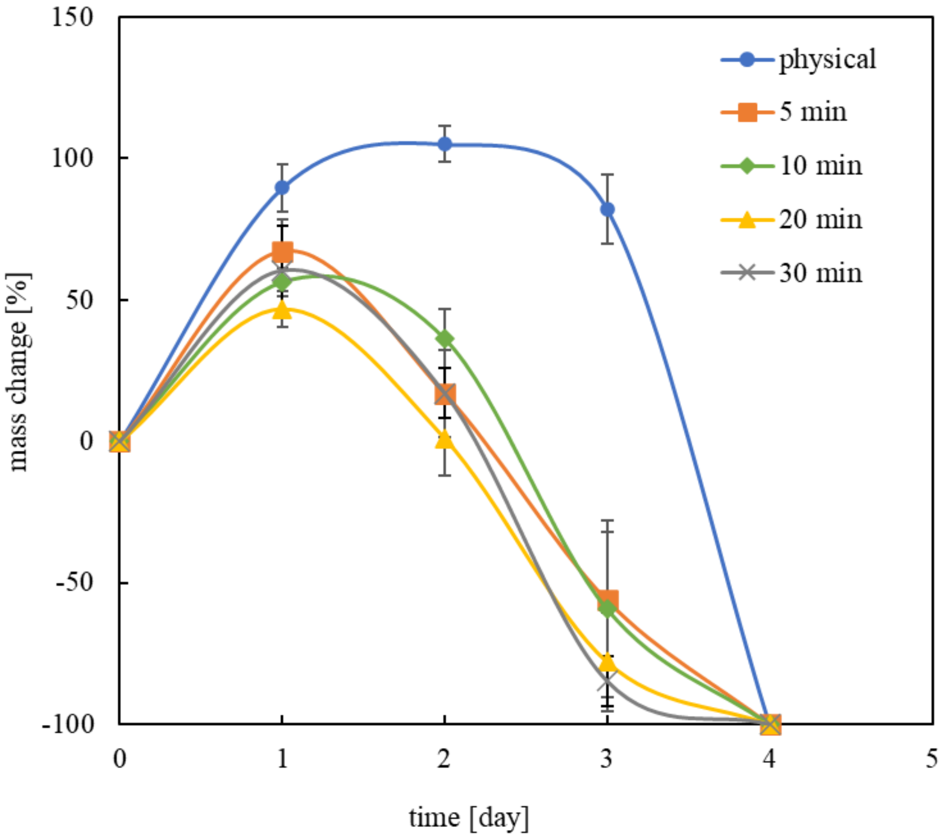

Figure 42: Hydrolytic stability of PBS 20wt.% butyl-ABA/ITA hydrogels in PBS at 37 °C.

The hydrolytic stability of the PBS hydrogels was quite insufficient, therefore UPW hydrogels were prepared. The hydrogels were probably supersaturated with ions. The hydrolytic stability of UPW hydrogels is shown in Figure 43. The stability has improved for all samples. The physically stabilized hydrogel proved to be the most stable again. Unexpectedly, the hybrid hydrogel irradiated for 15 min exhibited longer stability than the one irradiated for 30 min. The photos of the UPW samples after two and four days in PBS at 37 °C are shown in Figure 44. pH values of removed immersion solutions were at all intervals above 5.5. This is an essential improvement as in the next step a protein was incorporated. Acidic pH would cause denaturation of the protein.

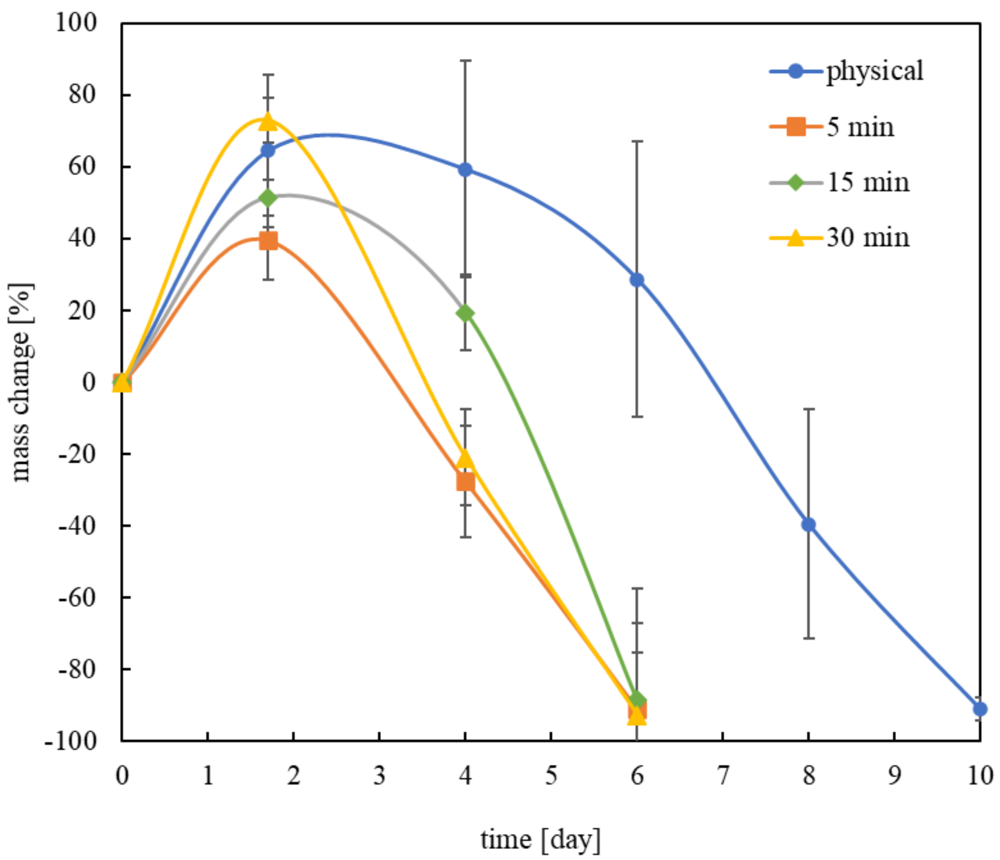

Figure 43: Hydrolytic stability of UPW butyl-ABA/ITA hydrogels in PBS at 37 °C.

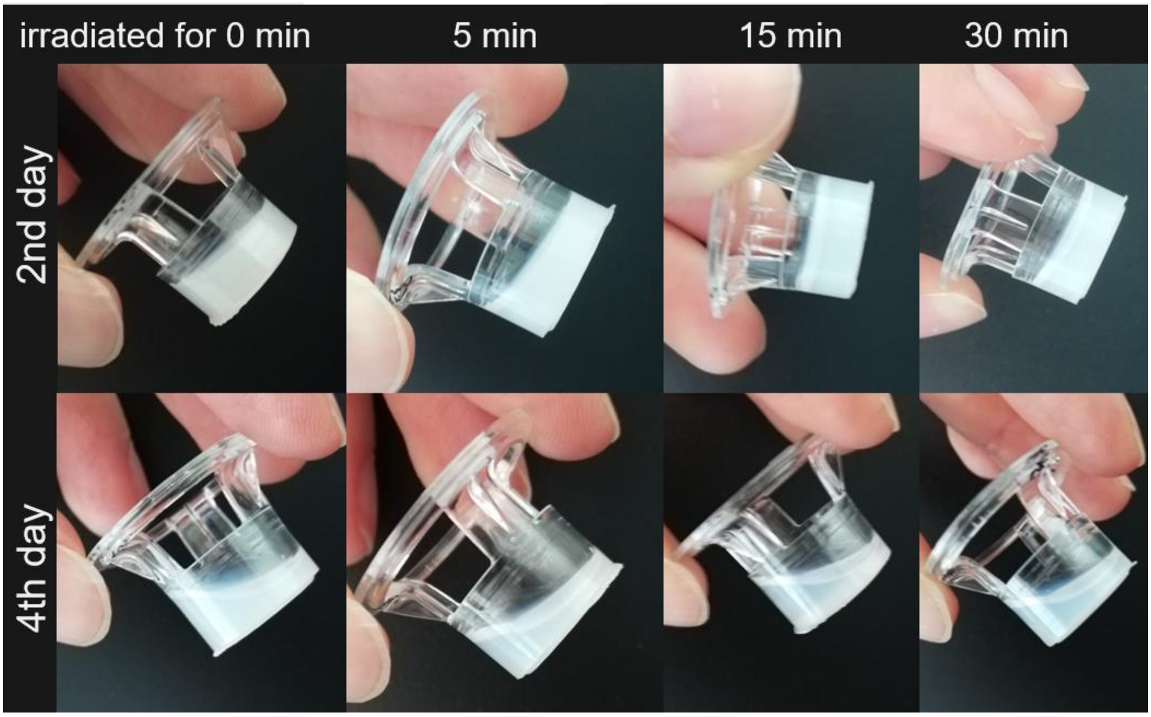

Figure 44: Visual comparison of irradiated and non-irradiated UPW hydrogels during the hydrolytic stability experiment after two and four days in PBS at 37 °C.

The UPW hydrogels exhibited better stability results even though, when measured on a rheometer, they demonstrated worse viscoelastic properties. For the subsequent release experiments, the hydrolytic stability results were more decisive. As proteins would be included in the next step, the pH of the hydrogels was measured as well. The PBS hydrogels possessed the pH of 4.85 whereas the UPW hydrogels demonstrated pH 4.08. According to previous experiments with the FGF2-STAB®, the growth factor retained its biological activity above pH 4. As the UPW hydrogels exhibited better hydrolytic stability and satisfactory pH, they were chosen for the release experiments.

5.5 Release of FGF2-STAB® from hydrogel networks

As a result of the characterisation experiments with butyl-ABA/ITA, UPW hydrogels were selected for release studies. The FGF2-STAB® growth factor was incorporated into the hydrogel network and its release was observed. Prolonged release would be beneficial for wound treatment as repeated application or dosing of the protein would not be needed. Three types of hydrogel networks were prepared in order to compare the different release kinetics. The growth factor was incorporated into a physical, chemical, and hybrid hydrogel network.

Two types of samples were prepared. To the first one, protein solution was added in the resulting concentration of 100 μg/ml. Instead of the protein solution, the same volume of PBS was pipetted to hydrogel, in the second type of samples. These were marked as blanks. During the experiment, the hydrogel weight change and pH of the immersion solution were measured. Moreover, a certain part of the immersion solution was used for UV-Vis spectrophotometric detection of released proteins. Another detection method applied in this thesis was SDS-PAGE electrophoresis. The methods were taken from Lysáková (2019) [64]. The samples in the inserts are shown in Figure 45.

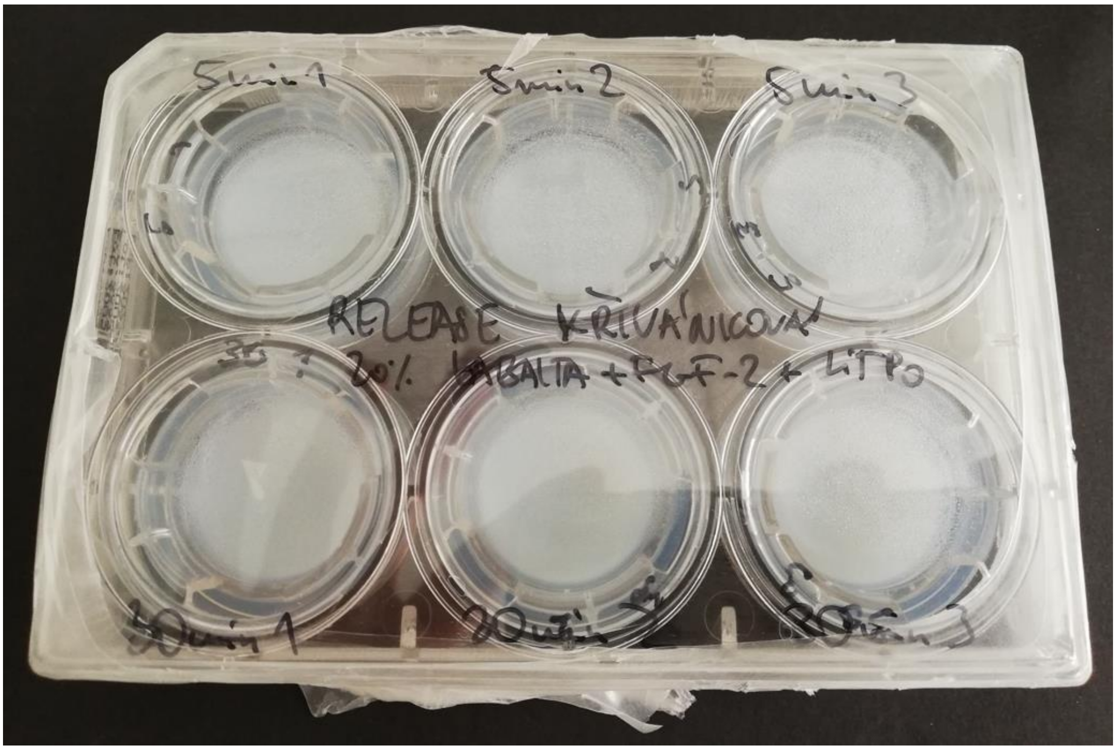

Figure 45: Samples in inserts prepared for the release of FGF2-STAB®.

5.5.1 Colorimetric detection on UV-Vis spectrophotometer

At each time interval, the amount of released protein was measured by the Bradford assay on UV-Vis spectrophotometer. According to the expected amount of released protein, the ratio of Bradford dye and the sample was selected as stated in the experimental part (4.4.9). The appropriate calibration curve was used for calculating the protein concentration. The equations of the calibration curves are stated in Table 8.

Table 8: Calibration equations for different expected amounts of released protein.

	equation
lower concentration (10 – 100 µg/ml)	$y = 0.00664x + 0.07002$
higher concentration (50 – 750 µg/ml)	$y = 0.00071x + 0.00604$

The Bradford dye changes colour when in the presence of a protein from brown to blue (Figure 46). Absorbance of the samples was determined on UV-Vis spectrophotometer at 595 nm. From the received values of absorbance, the absorbance of blank samples was deducted. A blank sample was prepared for each type of hydrogel network and each irradiation time.

Figure 46: The change in colour of the Bradford dye: pure Bradford dye (left) and the dye in the presence of a protein (right).

The curve of the FGF2-STAB® release from the physical hydrogel network is shown in Figure 47. According to the data received from the Bradford assay, it seems as if 25 % of the protein was either on the surface or very close to the surface of the hydrogel due to the very fast release. During the experiment, the overall released concentration was determined to be only 39 %.

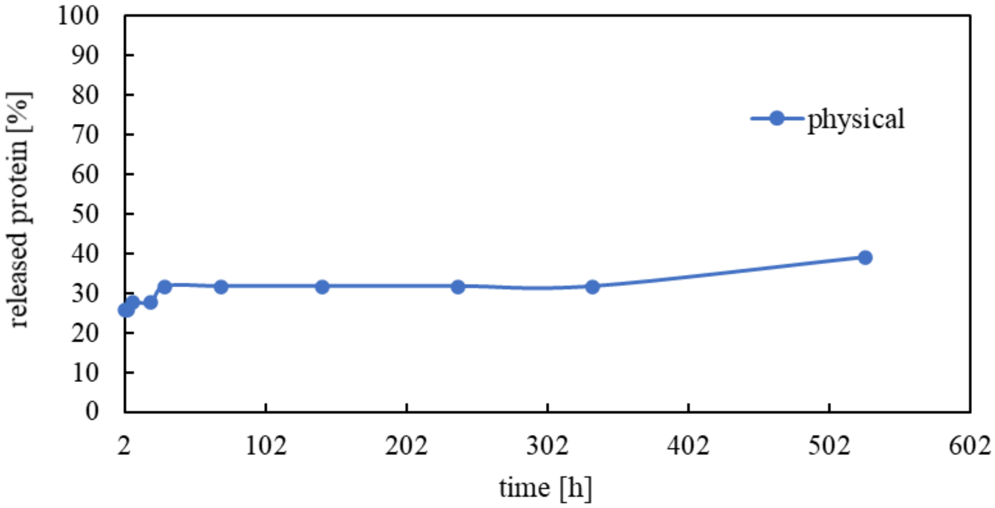

Figure 47: The release curve of FGF2-STAB® from the physical hydrogel network.

The release from the hybrid network is shown on Figure 48. A two-step release is visible from the curves. The first release could be diffusion-controlled whereas the second phase happened due to hydrogel degradation. This could be confirmed from the hydrolytic stability studies mentioned in 5.4.2.3. The second release phase occurred after two days in PBS while the hydrogel underwent degradation (Figure 43).

The growth factor was released faster from the hybrid hydrogel samples irradiated for 30 min than from the ones irradiated for 5 min. This behaviour could be since, when irradiated for longer time, more intra-micellar covalent crosslinks are formed, resulting in bigger inter-micellar space. The growth factor FGF2-STAB® is of rather hydrophilic nature. Therefore, it does not encapsulate inside micelles and the release is then simpler. This effect is in accordance with the hydrolytic study of ABA/ITA (5.2.2.3).

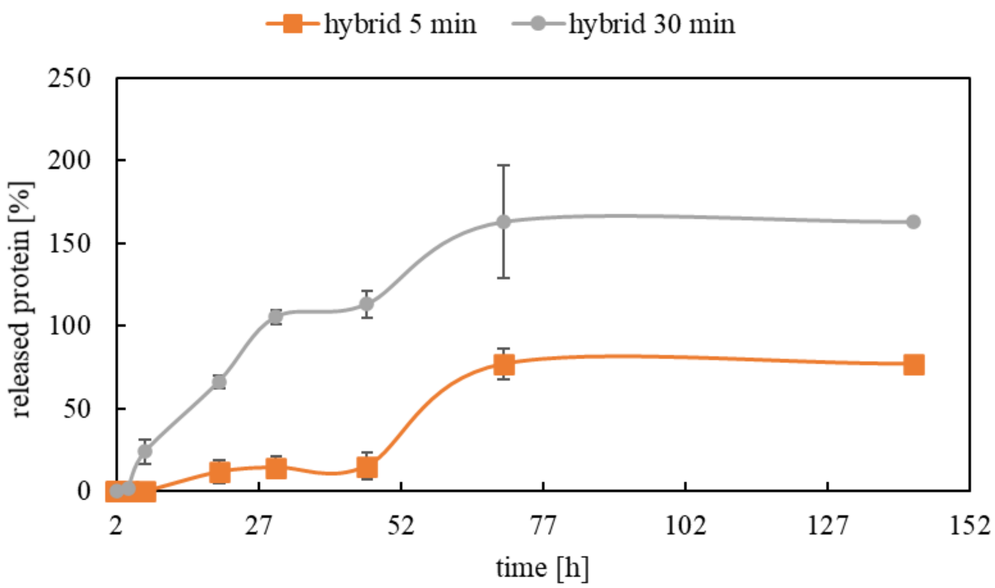

Figure 48: The release of FGF2-STAB® from hybrid hydrogel networks.

The growth factor FGF2-STAB® was incorporated to the chemical hydrogel network as well. The release curves are shown in Figure 49. The release from chemical networks is of different nature compared to the previous hydrogel networks. The release is delayed. In the case of hydrogel irradiated for 5 min, the release started after six days. The first detected growth factor was detected after nearly 14 days in the sample irradiated for 30 min. This result was quite unexpected as the hydrogel's structure did not stay intact after such a long time and seemed as if it already underwent a degradation. The hydrogel did not form micellar network before photocrosslinking. The structure is therefore of a different nature. The covalent links did not form inside the micelles but produced a well-defined hydrogel network. As the growth factor is of a hydrophilic nature, the chemical network prevented the diffusion of the protein from the structure. The release was degradation-controlled. When irradiated for 30 min, a denser chemical network is formed explaining the later release compared to the hydrogel irradiated for 5 min.

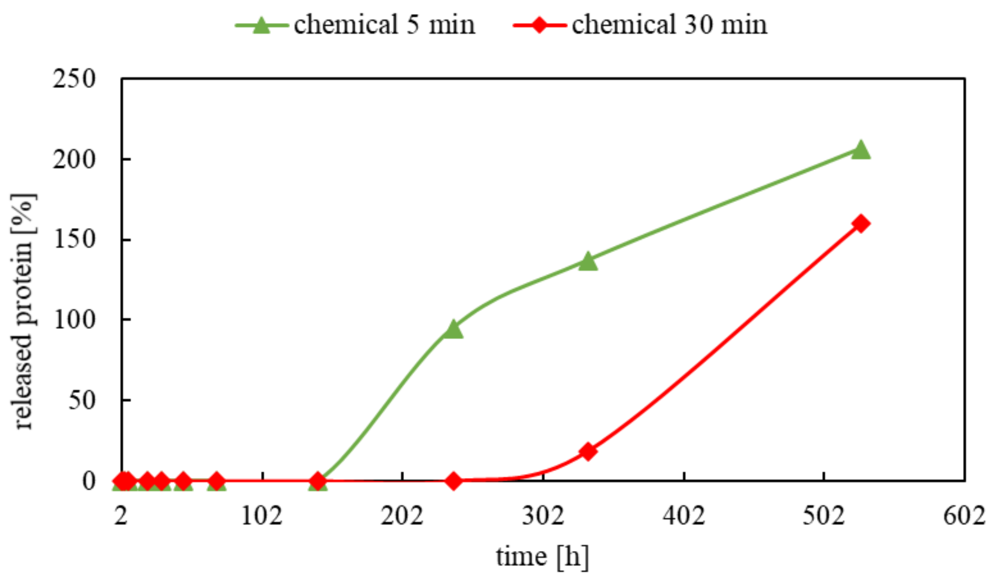

Figure 49: The release of FGF2-STAB® from chemical hydrogel networks.

The Bradford assay is quite sensitive to contaminants. As the measured sample contained copolymer degradation products (lactic and glycolic acid, PEG) as well as phosphate salts from PBS, the concentration of the contaminants could have been high. At some time intervals, the blank sample even exhibited higher absorbance than the protein-containing sample (Figure 50). Even though the only difference between the blanks and samples is the presence of the protein, it apparently also influenced the hydrogel stability. The samples containing proteins exhibited higher stability. The mass change of the samples during the experiment is shown in the FiguresFigure 51Figure 52Figure 53. The blank samples are highlighted with dashed line. The protein contains charged amino acids. The residues may interact with the copolymer structure thus increasing the hydrogel stability.

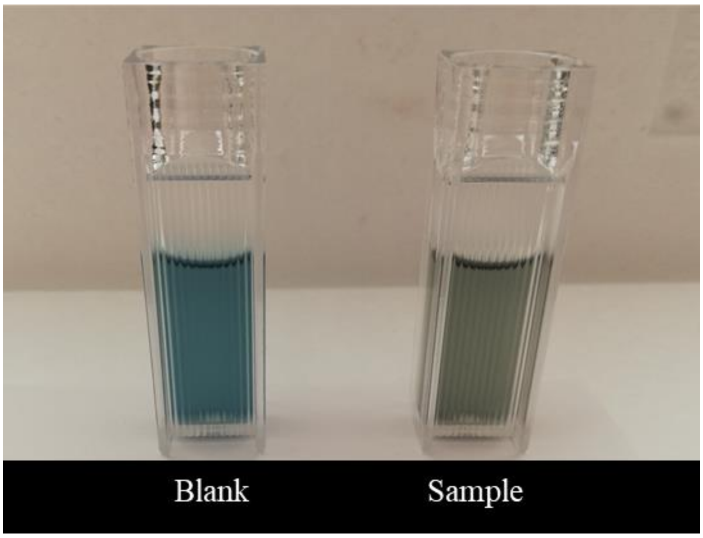

Figure 50: The visual colour comparison of blank vs. sample.

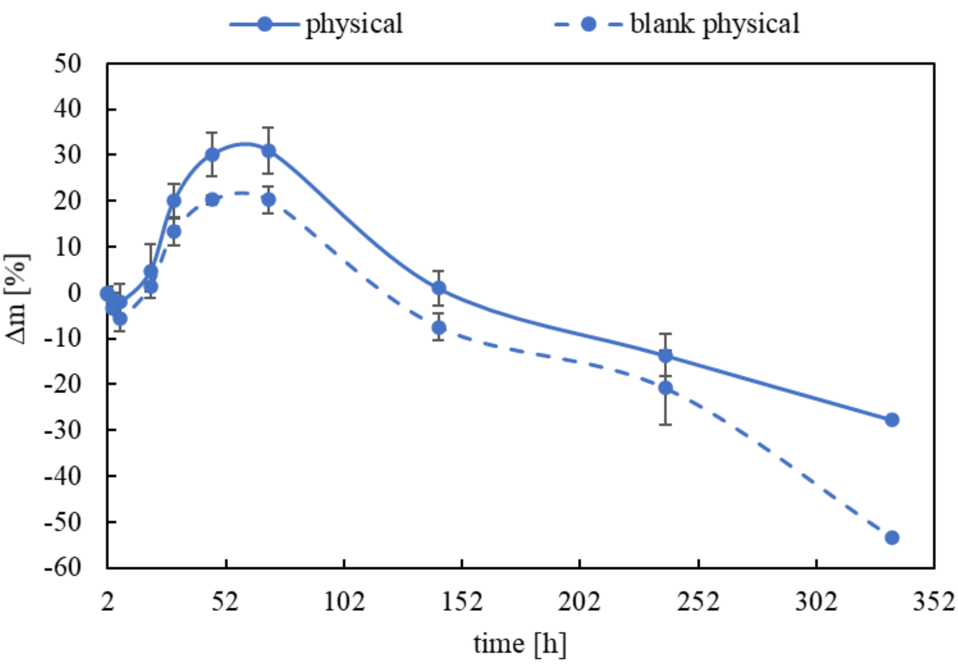

Figure 51: The comparison of hydrolytic stability of physically crosslinked hydrogels with and without FGF2-STAB®.

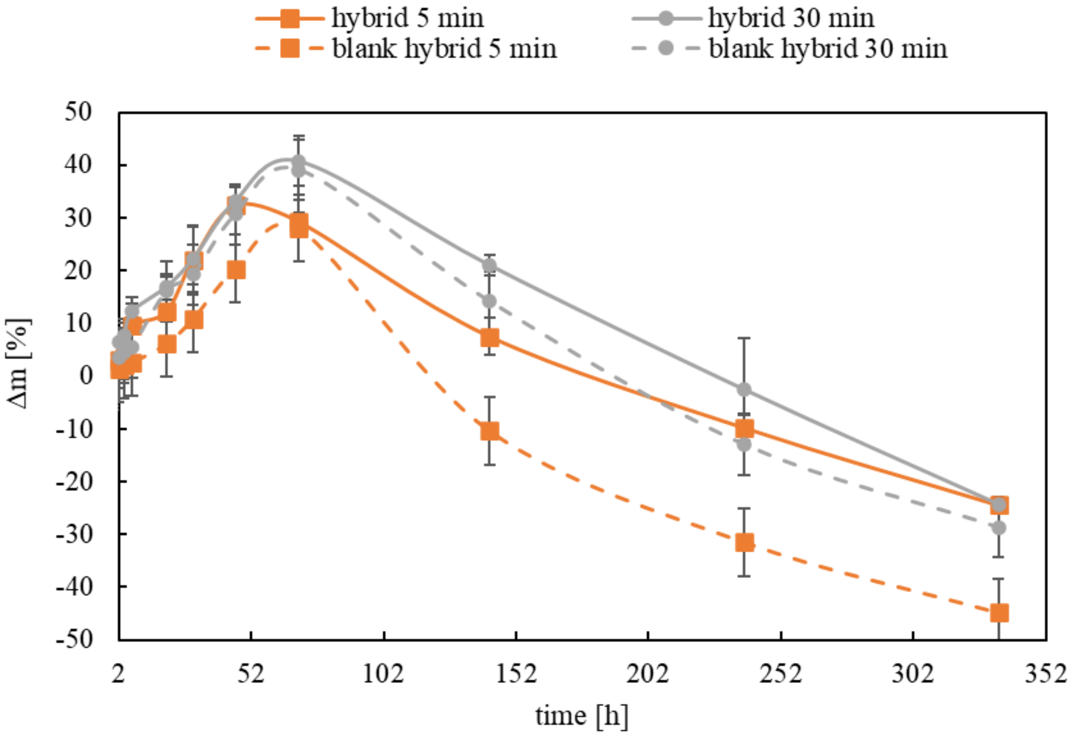

Figure 52: The comparison of hydrolytic stability of hybrid hydrogel samples with and without FGF2-STAB®.

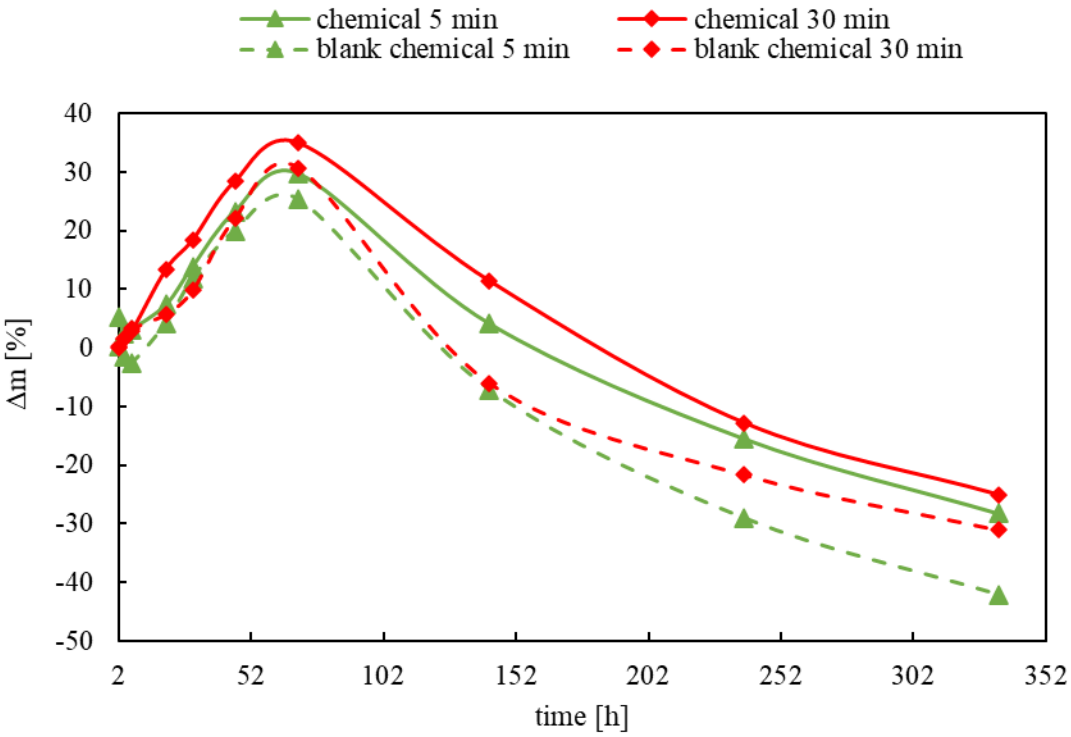

Figure 53: The comparison of hydrolytic stability of chemically crosslinked hydrogels with and without FGF2-STAB®.

5.5.2 SDS-PAGE method

As the degree of contaminant interference was quite high, another protein detection method was applied. SDS-PAGE is an electrophoretic method for protein analysis (Figure 54). Samples combined with the SDS surfactant are dosed to the polyacrylamide gel. SDS denatures the protein molecules and assigns them a uniform negative charge. The samples are then separated only according to their size. The samples were separated on a 15% polyacrylamide gel.

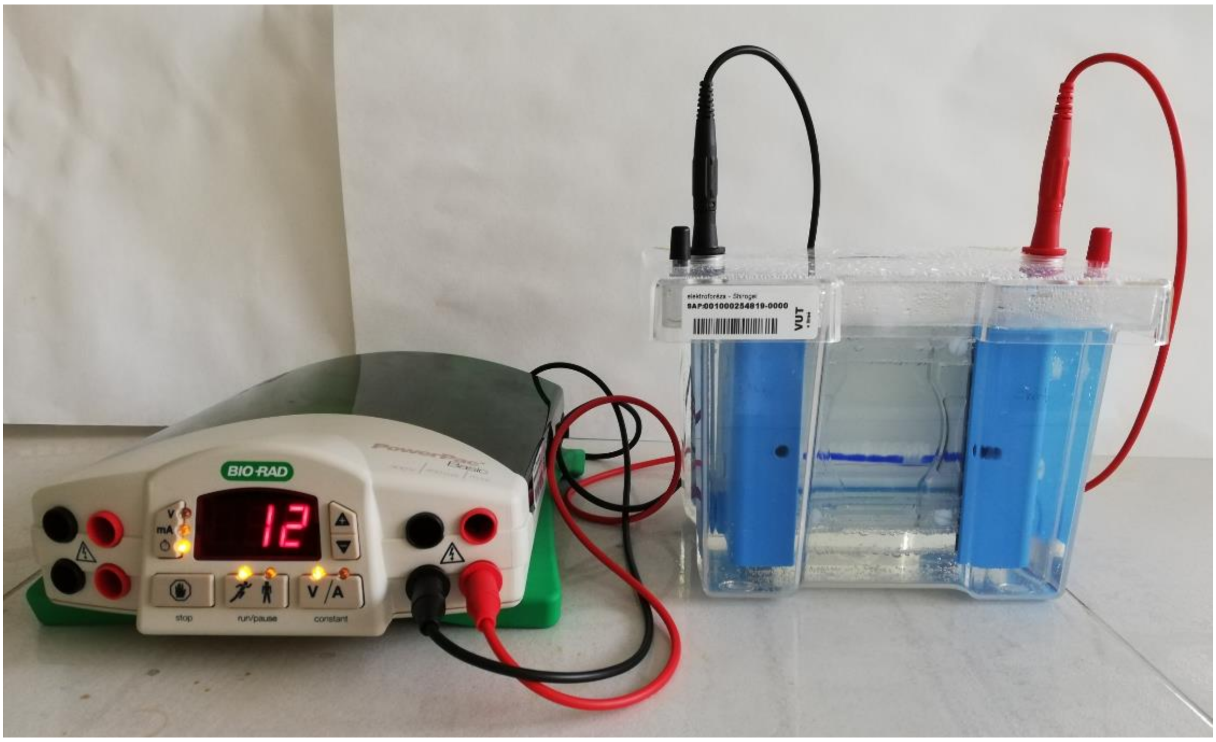

Figure 54: The apparatus of SDS-PAGE.

The result of one SDS-PAGE experiment is shown in Figure 55. The calibration samples and the marker have nicely separated however the samples have clearly stayed in the beginning of the gel. The marker consists of bands of 116.0, 66.2, 45.0, 35.0, 25.0, 18.4 and 14.4 kDa. The calibration bands are slightly above the 18.4 kDa marker thus confirming the size of FGF2-STAB® of 21 kDa. However, the growth factor in the samples may have formed agglomerates with the copolymer chain and the overall size may be too large to migrate through the 15% gel, therefore a less dense gel (10%) was prepared.

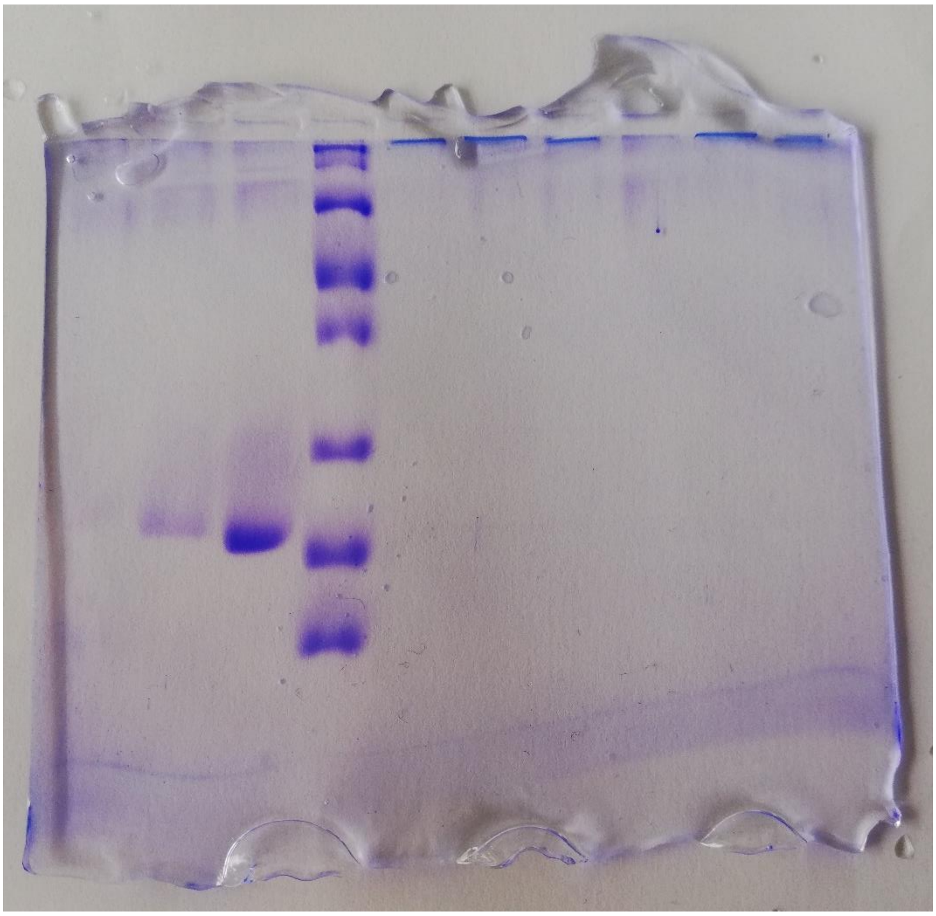

Figure 55: SDS-PAGE with 15% gel. From left to right: calibration 5, 20, 50 µg/ml, protein marker, physical hydrogel after 2 h, hybrid (5 min) after 2 h, hybrid (30 min) after 2 h, physical after 4, hybrid (5 min) after 4 h and hybrid (30 min) after 4 h.

The result obtained from 10% gel is shown on Figure 56. The FGF2-STAB® calibration did not separate properly as the size of the growth factor was too small and migrated through the whole gel. In this case none of the samples can be observed. At the top of the gel there are still blue stripes indicating the position of the dosed sample.

The detection of the released growth factors by SDS-PAGE was unsuccessful. Reverse-phase high performance liquid chromatography enables protein detection as well as it can answer the question whether the protein forms an agglomerate together with the copolymer. For a more specific spectrophotometric detection of the growth factor, a fluorescent dye may be used.

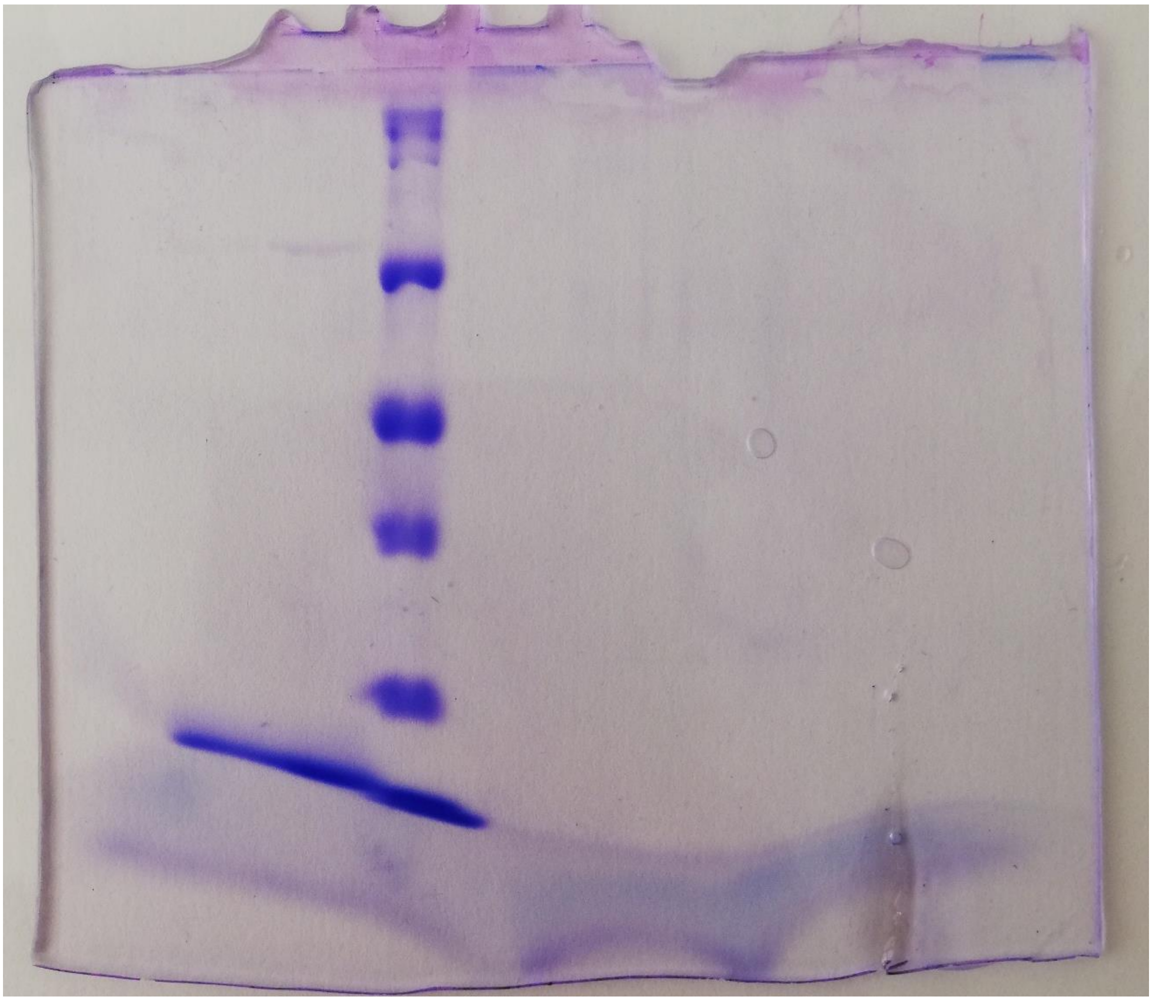

Figure 56: SDS-PAGE with 10% polyacrylamide gel.

6 CONCLUSION

The goal of this work was to synthesize a light and temperature-sensitive *α,ω*-itaconyl-PLGA-PEG-PLGA copolymer from which a hybrid hydrogel may be prepared. A stabilized growth factor FGF2-STAB® was incorporated into the hydrogel structure and its release was observed by UV-Vis via the Bradford assay and by SDS-PAGE.

The ABA/ITA copolymer was successfully synthesized and characterized by GPC and ^{1}H NMR. The formation of physical hydrogel network of a 20wt.% aqueous solution at physiological temperature was confirmed by rheometer. Moreover, Raman and IR spectroscopy was applied to determine the double bond conversion after irradiation by light (395 – 405 nm) in the presence of a LiTPO photoinitiator. However, these methods were unable to detect the double bonds in the copolymer chain. The thermal stability of the copolymer should increase after crosslinking. This behaviour was confirmed on TGA. The start of the degradation of the copolymer was delayed by 9.7 °C after 30 min irradiation.

Hydrolytic stability of physical and hybrid ABA/ITA hydrogels were studied in physiological solution at 37 °C. It has been proven that photocrosslinking enhances the hydrogel stability in physiological solution. The physically stabilized hydrogel degraded after 11 days, whereas the hybrid hydrogel irradiated for 30 min stayed intact for 14 days. Interestingly, the swelling properties increased with increasing photocrosslinking time. The covalent crosslinks produced during irradiation link the micellar cores, causing micellar size reduction. With smaller micelles, a larger inter-micellar space is formed allowing more solution diffusion into the hydrogel structure. It has been found out that the copolymer causes a decrease in pH of the immersion solution. The pH values stayed at approximately 3.3 during the experiment. Such an acidic environment would cause protein denaturation. Therefore, instead of a physiological solution, a phosphate buffer solution was used. However, when the hydrogel was immersed in neutral pH, the carboxyl groups were dissociated, leading to a hydrogel network disruption.

The ABA/ITA copolymer was modified by butylamine via EDC/NHS activation. The butylamine was bonded to the carboxyl groups, thus preventing their dissociation. In average, 85 % of the carboxyl groups were masked by butylamine in the resulting *α,ω-N*-butylitaconamide-PLGA-PEG-PLGA. The M_{n}, PDI, PLGA/PEG, and LA/GA were not affected by the modification according to the data obtained from GPC and ^{1}H NMR. The formation of a physical network at physiological temperature was confirmed. The viscoelastic properties of the formed physical and hybrid hydrogels in different solutions were studied. Even though the hydrogels formed in PBS exhibited better rheological properties, UPW hydrogels were chosen for the release experiment as they exhibited better hydrolytic stability. The pH of the UPW hydrogels as well as of the immersion solution (PBS) during the hydrolytic stability stayed above 4 thus not endangering the protein biological activity.

Release of FGF2-STAB® was observed via Bradford assay and SDS-PAGE from physical, hybrid, and chemical hydrogel networks. In the case of physical network, the Bradford assay detected only overall 39 % of the growth factor released after 22 days while most of it (25 %) was released already after 2 hours. The hybrid hydrogel exhibited a two-phase release. During the first phase, the release was diffusion-controlled whereas the second phase occurred due to hydrogel degradation. The release proceeded faster with the denser crosslinking network. The FGF2-STAB® is of a hydrophilic nature, therefore a larger inter-micellar space eases its release. The release from chemical network was delayed as the first protein detected by the Bradford assay of 6 or 14 days for 5 and 30 min irradiation time, respectively.

The Bradford assay is quite sensitive to the presence of contaminants. The dye interacted with the degraded copolymer, probably resulting in distorted data. Hence, the samples were analysed by the SDS-PAGE method as well. However, the FGF2-STAB® probably formed agglomerates with the copolymer or due to photocrosslinking. These agglomerates were too large to migrate through the separation gel. Even after the use of a gel with lower crosslinking density, no results were obtained.

The protein detection methods in this thesis did not prove to be ideal. The spectroscopic detection with the use of fluorescent dye could diminish the interference of contaminants due to its high specificity. Unfortunately, fluorescent dyes are generally of high cost. Another possible method is a reverse-phase high performance liquid chromatography. Moreover, the protein activity after its release from the hydrogel structure should be determined.

In this thesis, the issue with carboxyl group dissociation was resolved with butylamine masking, however other molecules could be bonded to the functional groups. For example, a bioactive compound could be bonded to the copolymer structure, preventing the carboxyl group dissociation as well as prolonging the drug release.

7 REFERENCES

[1] RAGHUWANSHI, Vikram Singh and Gil GARNIER. Characterisation of hydrogels: Linking the nano to the microscale. *Advances in Colloid and Interface Science* [online]. 2019, **274** [cit. 2021-7-25]. ISSN 00018686. Accessible on: doi:10.1016/j.cis.2019.102044

[2] GUPTA, B., R. AGARWAL and M.S. ALAM. Hydrogels for wound healing applications. *Biomedical Hydrogels* [online]. Elsevier, 2011, 2011, s. 184-227 [cit. 2021-7-25]. ISBN 9781845695903. Accessible on: doi:10.1533/9780857091383.2.184

[3] MONTEIRO, Nelson, Greeshma THRIVIKRAMAN, Avathamsa ATHIRASALA, Anthony TAHAYERI, Cristiane M. FRANÇA, Jack L. FERRACANE and Luiz E. BERTASSONI. Photopolymerization of cell-laden gelatin methacryloyl hydrogels using a dental curing light for regenerative dentistry. *Dental Materials* [online]. 2018, **34**(3), 389-399 [cit. 2021-7-25]. ISSN 01095641. Accessible on: doi:10.1016/j.dental.2017.11.020

[4] ZENTNER, Gaylen M, Ramesh RATHI, Chung SHIH, et al. Biodegradable block copolymers for delivery of proteins and water-insoluble drugs. *Journal of Controlled Release* [online]. 2001, **72**(1-3), 203-215 [cit. 2021-7-25]. ISSN 01683659. Accessible on: doi:10.1016/S0168-3659(01)00276-0

[5] YU, Lin and Jiandong DING. Injectable hydrogels as unique biomedical materials. *Chemical Society Reviews* [online]. 2008, **37**(8) [cit. 2021-7-25]. ISSN 0306-0012. Accessible on: doi:10.1039/b713009k

[6] CHEN, Liang, Tianyuan CI, Lin YU and Jiandong DING. Effects of Molecular Weight and Its Distribution of PEG Block on Micellization and Thermogellability of PLGA–PEG–PLGA Copolymer Aqueous Solutions. *Macromolecules* [online]. 2015, **48**(11), 3662-3671 [cit. 2021-7-25]. ISSN 0024-9297. Accessible on: doi:10.1021/acs.macromol.5b00168

[7] OBORNA, J., L. MRAVCOVA, L. MICHLOVSKA, L. VOJTOVA and M. VAVROVA. The effect of PLGA-PEG-PLGA modification on the sol-gel transition and degradation properties. *Express Polymer Letters* [online]. 2016, **10**(5), 361-372 [cit. 2021-7-25]. ISSN 1788618X. Accessible on: doi:10.3144/expresspolymlett.2016.34

[8] CESPI, Marco, Giulia BONACUCINA, Mattia TIBONI, Luca CASETTARI, Alessandra CAMBRIANI, Francesco FINI, Diego Romano PERINELLI and Giovanni Filippo PALMIERI. Insights in the rheological properties of PLGA-PEG-PLGA aqueous dispersions: Structural properties and temperature-dependent behaviour. *Polymer* [online]. 2021, **213** [cit. 2021-7-25]. ISSN 00323861. Accessible on: doi:10.1016/j.polymer.2020.123216

[9] LIOW, Sing Shy, Qingqing DOU, Dan KAI, Anis Abdul KARIM, Kangyi ZHANG, Fujian XU and Xian Jun LOH. Thermogels: In Situ Gelling Biomaterial. *ACS Biomaterials Science & Engineering* [online]. 2016, **2**(3), 295-316 [cit. 2021-7-25]. ISSN 2373-9878. Accessible on: doi:10.1021/acsbiomaterials.5b00515

[10] GUO, Zhong, Sha LI, Changyong WANG, Jiake XU, Brett KIRK, Jianping WU, Zonghua LIU and Wei XUE. Biocompatibility and cellular uptake mechanisms of poly(N -isopropylacrylamide) in different cells. *Journal of Bioactive and Compatible Polymers* [online]. 2017, **32**(1), 17-31 [cit. 2021-7-25]. ISSN 0883-9115. Accessible on: doi:10.1177/0883911516648969

[11] ZHOU, Qing, Li ZHANG, Tiehong YANG and Hong WU. Stimuli-responsive polymeric micelles for drug delivery and cancer therapy. *International Journal of Nanomedicine* [online]. 2018, **13**, 2921-2942 [cit. 2021-7-25]. ISSN 1178-2013. Accessible on: doi:10.2147/IJN.S158696

[12] KITAGAWA, Midori, Tomoki MAEDA and Atsushi HOTTA. PEG-based nanocomposite hydrogel: Thermo-responsive sol-gel transition and degradation behavior controlled by the LA/GA ratio of PLGA-PEG-PLGA. *Polymer Degradation and Stability* [online]. 2018, **147**, 222-228 [cit. 2021-7-25]. ISSN 01413910. Accessible on: doi:10.1016/j.polymdegradstab.2017.11.024

[13] CHANG, Xiaohua, Dengwen HU, Liangren CHEN, Yaping WANG and Yutian ZHU. Synthesis, self-assembly and thermoresponsive behavior of Poly(lactide-co-glycolide)-b-Poly(ethylene glycol)-b-Poly(lactide-co-glycolide) copolymer in aqueous solution. *Polymer* [online]. 2021, **223** [cit. 2021-7-25]. ISSN 00323861. Accessible on: doi:10.1016/j.polymer.2021.123673

[14] KHORSHID, Neda Khameh, Kaizheng ZHU, Kenneth D. KNUDSEN, Sara BEKHRADNIA, Sverre Arne SANDE and Bo NYSTRÖM. Novel Structural Changes during Temperature-Induced Self-Assembling and Gelation of PLGA-PEG-PLGA Triblock Copolymer in Aqueous Solutions. *Macromolecular Bioscience* [online]. 2016, **16**(12), 1838-1852 [cit. 2021-7-25]. ISSN 16165187. Accessible on: doi:10.1002/mabi.201600277

[15] JAIN, Rajeev A. The manufacturing techniques of various drug loaded biodegradable poly(lactide-co-glycolide) (PLGA) devices. *Biomaterials* [online]. 2000, **21**(23), 2475-2490 [cit. 2021-7-25]. ISSN 01429612. Accessible on: doi:10.1016/S0142-9612(00)00115-0

[16] SU, Chong, Yingze LIU, Runzhi LI, Wei WU, John Paul FAWCETT and Jingkai GU. Absorption, distribution, metabolism and excretion of the biomaterials used in Nanocarrier drug delivery systems. *Advanced Drug Delivery Reviews* [online]. 2019, **143**, 97-114 [cit. 2021-7-25]. ISSN 0169409X. Accessible on: doi:10.1016/j.addr.2019.06.008

[17] MAKADIA, Hirenkumar K. and Steven J. SIEGEL. Poly Lactic-co-Glycolic Acid (PLGA) as Biodegradable Controlled Drug Delivery Carrier. *Polymers* [online]. 2011, **3**(3), 1377-1397 [cit. 2021-7-25]. ISSN 2073-4360. Accessible on: doi:10.3390/polym3031377

[18] MICHLOVSKÁ, L.: *Functionalization of biodegradable polymers by itaconic anhydride*. Brno: Brno University of Technology, Faculty of Chemistry, 2009. 59 p. Supervisor Assoc. Prof. Lucy Vojtová.

[19] GERVAIS, KJ: *Evaluation of a biodegradable thermogel polymer for intraocular delivery of cyclosporine A to prevent posterior capsule opacification*. The Ohio State University, 2017. 91 p.

[20] QIAO, Mingxi, Dawei CHEN, Xichen MA and Yanjun LIU. Injectable biodegradable temperature-responsive PLGA–PEG–PLGA copolymers: Synthesis and effect of copolymer composition on the drug release from the copolymer-based hydrogels. *International Journal of Pharmaceutics* [online]. 2005, **294**(1-2), 103-112 [cit. 2021-7-25]. ISSN 03785173. Accessible on: doi:10.1016/j.ijpharm.2005.01.017

[21] CHOI, Suna and Sung Wan KIM. Controlled Release of Insulin from Injectable Biodegradable Triblock Copolymer Depot in ZDF Rats. *Pharmaceutical Research* [online]. 2003, **20**(12), 2008-2010 [cit. 2021-7-25]. ISSN 0724-8741. Accessible on: doi:10.1023/B:PHAM.0000008050.99985.5c

[22] ELSTAD, Nancy L. and Kirk D. FOWERS. OncoGel (ReGel/paclitaxel) — Clinical applications for a novel paclitaxel delivery system. *Advanced Drug Delivery Reviews* [online]. 2009, **61**(10), 785-794 [cit. 2021-7-25]. ISSN 0169409X. Accessible on: doi:10.1016/j.addr.2009.04.010

[23] YU, Lin, Kun LI, Xiaojun LIU, Chang CHEN, Yongchu BAO, Tianyuan CI, Qinghua CHEN and Jiandong DING. In Vitro and In Vivo Evaluation of a Once-weekly Formulation of an Antidiabetic Peptide Drug Exenatide in an Injectable Thermogel. *Journal of Pharmaceutical Sciences* [online]. 2013, **102**(11), 4140-4149 [cit. 2021-7-25]. ISSN 00223549. Accessible on: doi:10.1002/jps.23735

[24] YU, Lin, Zheng ZHANG, Huan ZHANG and Jiandong DING. Mixing a Sol and a Precipitate of Block Copolymers with Different Block Ratios Leads to an Injectable Hydrogel. *Biomacromolecules* [online]. 2009, **10**(6), 1547-1553 [cit. 2021-7-25]. ISSN 1525-7797. Accessible on: doi:10.1021/bm900145g

[25] YU, Lin, Tianyuan CI, Shuchun ZHOU and Jiandong DING. Sustained release of doxorubicin from a thermosensitive hydrogel. *Journal of Controlled Release* [online]. 2013, **172**(1) [cit. 2021-7-25]. ISSN 01683659. Accessible on: doi:10.1016/j.jconrel.2013.08.110

[26] GAO, Yuan, Fuzheng REN, Baoyue DING, Ningyun SUN, Xiang LIU, Xueying DING and Shen GAO. A thermo-sensitive PLGA-PEG-PLGA hydrogel for sustained release of docetaxel. *Journal of Drug Targeting* [online]. 2010, **19**(7), 516-527 [cit. 2021-7-25]. ISSN 1061-186X. Accessible on: doi:10.3109/1061186X.2010.519031

[27] WANG, Puxiu, Wei CHU, Xuezhi ZHUO, et al. Modified PLGA–PEG–PLGA thermosensitive hydrogels with suitable thermosensitivity and properties for use in a drug delivery system. *Journal of Materials Chemistry B* [online]. 2017, **5**(8), 1551-1565 [cit. 2021-7-25]. ISSN 2050-750X. Accessible on: doi:10.1039/C6TB02158A

[28] MICHLOVSKÁ, Lenka, Lucy VOJTOVÁ, Ludmila MRAVCOVÁ, Soňa HERMANOVÁ, Jiří KUČERÍK and Josef JANČÁŘ. Functionalization Conditions of PLGA-PEG-PLGA Copolymer with Itaconic Anhydride. *Macromolecular Symposia* [online]. 2010, **295**(1), 119-124 [cit. 2021-7-25]. ISSN 10221360. Accessible on: doi:10.1002/masy.200900071

[29] DA CRUZ, Juliana C., Eliana F. CAMPORESE SÉRVULO and Aline M. DE CASTRO. Microbial Production of Itaconic Acid. *Microbial Production of Food Ingredients and Additives* [online]. Elsevier, 2017, 2017, s. 291-316 [cit. 2021-7-25]. ISBN 9780128115206. Accessible on: doi:10.1016/B978-0-12-811520-6.00010-6

[30] CHAMRADOVÁ, I.: *Reologické vlastnosti biodegradabilních termocitlivých kopolymerů*. Brno: Brno University of Technology, Faculty of Chemistry, 2012. 63 p. Supervisor: Assoc. Prof. Lucy Vojtová.

[31] MICHLOVSKÁ, L.: *Synthesis and Characterization of Multifunctionalized Biodegradable Copolymers*. Brno: Brno University of Technology, Faculty of Chemistry, 2014. 92 p., Supervisor: Assoc. Prof. Lucy Vojtová.

[32] MICHLOVSKÁ, L., L. VOJTOVÁ, O. HUMPA, J. KUČERÍK, J. ŽÍDEK and J. JANČÁŘ. Hydrolytic stability of end-linked hydrogels from PLGA–PEG–PLGA macromonomers terminated by α,ω-itaconyl groups. *RSC Advances* [online]. 2016, **6**(20), 16808-16816 [cit. 2021-7-25]. ISSN 2046-2069. Accessible on: doi:10.1039/C5RA26222D

[33] SONTYANA, Adonijah Graham, Ansuja Pulickal MATHEW, Ki-Hyun CHO, Saji UTHAMAN and In-Kyu PARK. Biopolymeric In Situ Hydrogels for Tissue Engineering and Bioimaging Applications. *Tissue Engineering and Regenerative Medicine* [online]. 2018, **15**(5), 575-590 [cit. 2021-7-25]. ISSN 1738-2696. Accessible on: doi:10.1007/s13770-018-0159-1

[34] YANG, Jeong-A., Junseok YEOM, Byung Woo HWANG, Allan S. HOFFMAN and Sei Kwang HAHN. In situ-forming injectable hydrogels for regenerative medicine. *Progress in Polymer Science* [online]. 2014, **39**(12), 1973-1986 [cit. 2021-7-25]. ISSN 00796700. Accessible on: doi:10.1016/j.progpolymsci.2014.07.006

[35] ASWATHY, S.H., U. NARENDRAKUMAR and I. MANJUBALA. Commercial hydrogels for biomedical applications. *Heliyon* [online]. 2020, **6**(4) [cit. 2021-7-25]. ISSN 24058440. Accessible on: doi:10.1016/j.heliyon.2020.e03719

[36] TOMAL, Wiktoria and Joanna ORTYL. Water-Soluble Photoinitiators in Biomedical Applications. *Polymers* [online]. 2020, **12**(5) [cit. 2021-7-25]. ISSN 2073-4360. Accessible on: doi:10.3390/polym12051073

[37] PORTNOV, Tanya, Tiberiu R. SHULIMZON and Meital ZILBERMAN. Injectable hydrogel-based scaffolds for tissue engineering applications. *Reviews in Chemical Engineering* [online]. 2017, **33**(1) [cit. 2021-7-25]. ISSN 2191-0235. Accessible on: doi:10.1515/revce-2015-0074

[38] GOU, Maling, Xin QU, Wei ZHU, Mingli XIANG, Jun YANG, Kang ZHANG, Yuquan WEI and Shaochen CHEN. Bio-inspired detoxification using 3D-printed hydrogel nanocomposites. *Nature Communications* [online]. 2014, **5**(1) [cit. 2021-7-25]. ISSN 2041-1723. Accessible on: doi:10.1038/ncomms4774

[39] CALDERON, G. A., P. THAI, C. W. HSU, B. GRIGORYAN, S. M. GIBSON, M. E. DICKINSON and J. S. MILLER. Tubulogenesis of co-cultured human iPS-derived endothelial cells and human mesenchymal stem cells in fibrin and gelatin methacrylate gels. *Biomaterials Science* [online]. 2017, **5**(8), 1652-1660 [cit. 2021-7-25]. ISSN 2047-4830. Accessible on: doi:10.1039/C7BM00223H

[40] ZAHORANOVA, Anna, Lucy VOJTOVA, Eva DUSICKA, Lenka MICHLOVSKA, Nikola KRIVANKOVA and Stefan BAUDIS. Hybrid Hydrogel Networks by Photocrosslinking of Thermoresponsive α,ω-Itaconyl-PLGA-PEG-PLGA Micelles in Water: Influence of the Lithium Phenyl-2,4,6-Trimethylbenzoylphosphinate Photoinitinator. *Macromolecular Chemistry and Physics* [online]. [cit. 2021-7-25]. ISSN 1022-1352. Accessible on: doi:10.1002/macp.202000165

[41] HUANG, Hung-Jin, Yu-Liang TSAI, Shih-Ho LIN and Shan-hui HSU. Smart polymers for cell therapy and precision medicine. *Journal of Biomedical Science* [online]. 2019, **26**(1) [cit. 2021-7-25]. ISSN 1423-0127. Accessible on: doi:10.1186/s12929-019-0571-4

[42] HAO, Jinkun and R.A. WEISS. Mechanical behavior of hybrid hydrogels composed of a physical and a chemical network. *Polymer* [online]. 2013, **54**(8), 2174-2182 [cit. 2021-7-25]. ISSN 00323861. Accessible on: doi:10.1016/j.polymer.2013.01.052

[43] KONG, Hyun Joon, Emma WONG and David J. MOONEY. Independent Control of Rigidity and Toughness of Polymeric Hydrogels. *Macromolecules* [online]. 2003, **36**(12), 4582-4588 [cit. 2021-7-25]. ISSN 0024-9297. Accessible on: doi:10.1021/ma034137w

[44] LI, Jiangbo, Hanchao LIU, Chao WANG and Guangsu HUANG. A facile method to fabricate hybrid hydrogels with mechanical toughness using a novel multifunctional cross-linker. *RSC Advances* [online]. 2017, **7**(56), 35311-35319 [cit. 2021-7-25]. ISSN 2046-2069. Accessible on: doi:10.1039/C7RA05645A

[45] MAHOU, Redouan, Solène PASSEMARD, Michele CARVELLO, Alessandra PETRELLI, François NOVERRAZ, Sandrine GERBER-LEMAIRE and Christine WANDREY. Contribution of polymeric materials to progress in xenotransplantation of microencapsulated cells: a review. *Xenotransplantation* [online]. 2016, **23**(3), 179-201 [cit. 2021-7-25]. ISSN 0908665X. Accessible on: doi:10.1111/xen.12240

[46] CHE, Yunjiao, Stefan ZSCHOCHE, Franziska OBST, Dietmar APPELHANS and Brigitte VOIT. Double-crosslinked reversible redox-responsive hydrogels based on disulfide–thiol interchange. *Journal of Polymer Science Part A: Polymer Chemistry* [online]. 2019, **57**(24), 2590-2601 [cit. 2021-7-25]. ISSN 0887-624X. Accessible on: doi:10.1002/pola.29539

[47] SZABÓ, Luca, François NOVERRAZ and Sandrine GERBER-LEMAIRE. Multicomponent Alginate-Derived Hydrogel Microspheres Presenting Hybrid Ionic-Covalent Network and Drug Eluting Properties. *Helvetica Chimica Acta* [online]. 2020, **103**(9) [cit. 2021-7-25]. ISSN 0018-019X. Accessible on: doi:10.1002/hlca.202000115

[48] PASSEMARD, Solène, Luca SZABÓ, François NOVERRAZ, Elisa MONTANARI, Carmen GONELLE-GISPERT, Léo H. BÜHLER, Christine WANDREY and Sandrine GERBER-LEMAIRE. Synthesis Strategies to Extend the Variety of Alginate-Based Hybrid Hydrogels for Cell Microencapsulation. *Biomacromolecules* [online]. 2017, **18**(9), 2747-2755 [cit. 2021-7-25]. ISSN 1525-7797. Accessible on: doi:10.1021/acs.biomac.7b00665

[49] National Institute of Biomedical Imaging and Bioengineering [online]. NIBIB NIH [cit. 2021-7-25]. Accessible on: nibib.nih.gov

[50] PATRICK, Graham L. *An introduction to medicinal chemistry*. 5th ed. Oxford: Oxford University Press, c2013. ISBN isbn978-0-19-969739-7.

[51] CALÓ, Enrica and Vitaliy V. KHUTORYANSKIY. Biomedical applications of hydrogels: A review of patents and commercial products. *European Polymer Journal* [online]. 2015, **65**, 252-267 [cit. 2021-7-25]. ISSN 00143057. Accessible on: doi:10.1016/j.eurpolymj.2014.11.024

[52] HUANG, Xiao and Christopher S BRAZEL. On the importance and mechanisms of burst release in matrix-controlled drug delivery systems. *Journal of Controlled Release* [online]. 2001, **73**(2-3), 121-136 [cit. 2021-7-25]. ISSN 01683659. Accessible on: doi:10.1016/S0168-3659(01)00248-6

[53] PAOLINI, Marion S., Owen S. FENTON, Chandrabali BHATTACHARYA, Jason L. ANDRESEN and Robert LANGER. Polymers for extended-release administration. *Biomedical Microdevices* [online]. 2019, **21**(2) [cit. 2021-7-25]. ISSN 1387-2176. Accessible on: doi:10.1007/s10544-019-0386-9

[54] CHYZY, Adam, Monika TOMCZYKOWA and Marta E. PLONSKA-BRZEZINSKA. Hydrogels as Potential Nano-, Micro- and Macro-Scale Systems for Controlled Drug Delivery. *Materials* [online]. 2020, **13**(1) [cit. 2021-7-25]. ISSN 1996-1944. Accessible on: doi:10.3390/ma13010188

[55] LEE, Jinhyun Hannah and Yoon YEO. Controlled drug release from pharmaceutical nanocarriers. *Chemical Engineering Science* [online]. 2015, **125**, 75-84 [cit. 2021-7-25]. ISSN 00092509. Accessible on: doi:10.1016/j.ces.2014.08.046

[56] MISRA, Ambikanandan and Aliasgar SHAHIWALA, ed. *Applications of polymers in drug delivery*. Shawbury: Smithers Rapra, 2014. ISBN 978-1-84735-851-6.

[57] ZARZYCKI, Roman, Zofia MODRZEJEWSKA and Katarzyna NAWROTEK. Drug release from hydrogel matrices. *Ecological Chemistry and Engineering* [online]. 2010, **17**(2) [cit. 2021-7-25]. Accessible on: http://tchie.uni.opole.pl/freeECE/S_17_2/Zarzycki_17(S2).pdf

[58] OBORNÁ, J.: *Řízené uvolňování léčiv z biodegradabilních hydrogelů*. Brno: Brno University of Technology, Faculty of Chemistry, 2018. 118 p. Supervisor: prof. RNDr. Milada Vávrová, CSc.

[59] KARMEGAM, Vasanthy, Pooneh SOLTANTABAR, Erika Joy L. CALUBAQUIB, Ruvanthi N. KULARATNE and Mihaela C. STEFAN. Biodegradable Aliphatic Polyesters for Drug Delivery. *Material Matters* [online]. 2017, 12.2 [cit. 2021-7-25]

[60] FREDENBERG, Susanne, Marie WAHLGREN, Mats RESLOW and Anders AXELSSON. The mechanisms of drug release in poly(lactic-co-glycolic acid)-based drug delivery systems—A review. *International Journal of Pharmaceutics* [online]. 2011, **415**(1-2), 34-52 [cit. 2021-7-25]. ISSN 03785173. Accessible on: doi:10.1016/j.ijpharm.2011.05.049

[61] BARRIENTOS, Stephan, Olivera STOJADINOVIC, Michael S. GOLINKO, Harold BREM and Marjana TOMIC-CANIC. PERSPECTIVE ARTICLE: Growth factors and cytokines in wound healing. *Wound Repair and Regeneration* [online]. 2008, **16**(5), 585-601 [cit. 2021-7-25]. ISSN 10671927. Accessible on: doi:10.1111/j.1524-475X.2008.00410.x

[62] CARTER, Edward P., Abbie E. FEARON and Richard P. GROSE. Careless talk costs lives: fibroblast growth factor receptor signalling and the consequences of pathway malfunction. *Trends in Cell Biology* [online]. 2015, **25**(4), 221-233 [cit. 2021-7-25]. ISSN 09628924. Accessible on: doi:10.1016/j.tcb.2014.11.003

[63] NUGENT, Matthew A and Renato V IOZZO. Fibroblast growth factor-2. *The International Journal of Biochemistry & Cell Biology* [online]. 2000, **32**(2), 115-120 [cit. 2021-7-25]. ISSN 13572725. Accessible on: doi:10.1016/S1357-2725(99)00123-5

[64] LYSÁKOVÁ, K.: *Optimization of methods for protein analysis released from thermosensitive hydrogel*. Brno: Brno University of Technology, Faculty of Chemistry, 2019. 71 p. Supervisor: Assoc. Prof. Lucy Vojtová.

[65] OKADA-BAN, Mai, Jean Paul THIERY and Jacqueline JOUANNEAU. Fibroblast growth factor-2. *The International Journal of Biochemistry & Cell Biology* [online]. 2000, **32**(3), 263-267 [cit. 2021-7-25]. ISSN 13572725. Accessible on: doi:10.1016/S1357-2725(99)00133-8

[66] Enantis: Stable Fibroblast Growth Factor 2 FGF2-STAB®. 2017 [print]

[67] SILVERSTEIN, Robert M. *Spectrometric identification of organic compounds*. 8th ed. Hoboken: Wiley, c2015. ISBN 9780470616376.

[68] LARKIN, Peter. *Infrared and raman spectroscopy: principles and spectral interpretation*. [1st ed.]. Amsterdam: Elsevier, 2011. ISBN 978-0-12-386984-5.

[69] LAWAL, Olayide S. Kosmotropes and chaotropes as they affect functionality of a protein isolate. *Food Chemistry* [online]. 2006, **95**(1), 101-107 [cit. 2021-7-25]. ISSN 03088146. Accessible on: doi:10.1016/j.foodchem.2004.12.041

[70] HABÁNKOVÁ, E.: *Rheological evaluation of thermosensitive macromonomer photogelation in aqueous environment*. Brno: Brno University of Technology, Faculty of Chemistry. 2017. 82 p. Supervisor: Assoc. Prof. Lucy Vojtová.

8 LIST OF ABBREVIATIONS AND SYMBOLS

ABA/ITA	α,ω-itaconyl-PLGA-PEG-PLGA
ATR-FTIR	Attenuated Total Reflectance Fourier Transformed Infrared Spectroscopy
BAPO	bisacylphosphine oxide
butyl-ABA/ITA	α,ω-N-butylitaconamide-PLGA-PEG-PLGA
CMC	critical micelle concentration
EDC	*N*-(3-Dimethylaminopropyl)-*N*'-ethylcarbodiimide hydrochloride
EGF	epidermal growth factor
FDA	Food and Drug administration
FGF	fibroblast growth factor
FGF2-STAB®	stabilized fibroblast growth factor 2
GA	glycolide
GelMA	gelatin-methacryloyl
GPC	gel permeation chromatography
1H NMR	proton nuclear magnetic resonance
IR	infrared
ITA	itaconic anhydride
LA	D,L-lactide
LCST	lower critical solution temperature
LiTPO	lithium phenyl-2,4,6-trimethylbenzoylphosphinate
MAPO	monoacylphosphine oxide
Mn	number average molecular weight
NHS	*N*-Hydroxysuccinimide
PBS	phosphate buffer saline
PDFG	platelet-derived growth factor
PDI	polydispersity index

PEG	poly(ethylene glycol)
PEGDA	poly(ethylene glycol) diacrylate
PLGA	poly(D,L-lactic acid-*co*-glycolic acid)
PLGA-PEG-PLGA	poly(D,L-lactic acid-*co*-glycolic acid)-b-poly(ethylene glycol)-b-poly(D,L-lactic acid-*co*-glycolic acid)
SDS	sodium dodecyl sulfate
SDS-PAGE	sodium dodecyl sulphate poly(acrylamide) gel electrophoresis
TEMED	*N,N,N',N*'-Tetramethylethylenediamine
TGA	thermogravimetric analysis
TGF-β	transforming growth factor-beta
THF	tetrahydrofuran
UPW	ultra-pure water
UV	ultraviolet
Vis	visible